CAPABILITY OF THE TOTAL IN-FLIGHT SIMULATOR (TIFS)

Philip A. Reynolds, et al

Cornell Aeronautical Laboratory, Incorporated

February 1972

AFFDL-TR-72-39

CAPABILITY OF THE TOTAL IN-FLIGHT SIMULATOR (TIFS)

P. A. REYNOLDS
R. WASSERMAN
G. J. FABIAN
P. R. MOTYKA

CORNELL AERONAUTICAL LABORATORY, INC.

TECHNICAL REPORT AFFDL-TR-72-39

JULY 1972

AIR FORCE FLIGHT DYNAMICS LABORATORY
AIR FORCE SYSTEMS COMMAND
WRIGHT-PATTERSON AIR FORCE BASE, OHIO 45433

Unclassified

Security Classification

DOCUMENT CONTROL DATA - R&D

(Security classification of title, body of abstract and indexing annotation must be entered when the overall report is classified)

1. ORIGINATING ACTIVITY (Corporate author) Cornell Aeronautical Laboratory, Inc. 4455 Genesee Street Buffalo, New York 14221	2a. REPORT SECURITY CLASSIFICATION Unclassified 2b. GROUP

3. REPORT TITLE

CAPABILITY OF THE TOTAL IN-FLIGHT SIMULATOR (TIFS)

4. DESCRIPTIVE NOTES (Type of report and inclusive dates)

FINAL REPORT

5. AUTHOR(S) (Last name, first name, initial)

Reynolds, Philip A.; Wasserman, Richard, Fabian, Gardner, J.; Motyka, Paul, R.

6. REPORT DATE	7a. TOTAL NO. OF PAGES	7b. NO. OF REFS
February 1972	147	22

8a. CONTRACT OR GRANT NO. F33615-71-C-1110 b. PROJECT NO. 684B c. d.	9a. ORIGINATOR'S REPORT NUMBER(S) CAL Report No. TB-3020-F-4 9b. OTHER REPORT NO(S) (Any other numbers that may be assigned this report) AFFDL-TR-72-

10. AVAILABILITY/LIMITATION NOTICES

11. SUPPLEMENTARY NOTES	12. SPONSORING MILITARY ACTIVITY
	Air Force Flight Dynamics Laboratory Wright-Patterson Air Force Base, Ohio

13. ABSTRACT

TIFS is a newly developed, variable stability C-131 aircraft with the unique capability to vary its flying qualities in all six degrees of freedom. It also surpasses the utility of past variable stability aircraft through the realism possible in its separate, new evaluation cockpit. The capabilities and features of this in-flight simulator considerably broaden the ability of the aircraft designer to deal with difficult trade-offs in flying qualities problems. A base configuration can be set up and then its stability and control characteristics can be systematically varied for investigations to gain research knowledge pertinent to flight vehicle and flight control system design. This report describes the theoretical basis for in-flight motion reproduction and how this theory can be applied to determine the TIFS capability to simulate a given aircraft. Physical characteristics as determined in flight and examples of simulation are given. Flight test records of model-following performance are also included. The objective of this report is to give the reader the basic information for planning a TIFS experiment.

DD FORM 1 JAN 64 1473

Ia

Unclassified

Security Classification

Unclassified
Security Classification

14. KEY WORDS	LINK A		LINK B		LINK C	
	ROLE	WT	ROLE	WT	ROLE	WT
Total In-Flight Simulator (TIFS) Motion Simulation Capability Model-Following Capability Turbulence Alleviation Feel System Capability						

INSTRUCTIONS

1. ORIGINATING ACTIVITY: Enter the name and address of the contractor, subcontractor, grantee, Department of Defense activity or other organization *(corporate author)* issuing the report.

2a. REPORT SECURITY CLASSIFICATION: Enter the overall security classification of the report. Indicate whether "Restricted Data" is included. Marking is to be in accordance with appropriate security regulations.

2b. GROUP: Automatic downgrading is specified in DoD Directive 5200.10 and Armed Forces Industrial Manual. Enter the group number. Also, when applicable, show that optional markings have been used for Group 3 and Group 4 as authorized.

3. REPORT TITLE: Enter the complete report title in all capital letters. Titles in all cases should be unclassified. If a meaningful title cannot be selected without classification, show title classification in all capitals in parenthesis immediately following the title.

4. DESCRIPTIVE NOTES: If appropriate, enter the type of report, e.g., interim, progress, summary, annual, or final. Give the inclusive dates when a specific reporting period is covered.

5. AUTHOR(S): Enter the name(s) of author(s) as shown on or in the report. Enter last name, first name, middle initial. If military, show rank and branch of service. The name of the principal author is an absolute minimum requirement.

6. REPORT DATE: Enter the date of the report as day, month, year, or month, year. If more than one date appears on the report, use date of publication.

7a. TOTAL NUMBER OF PAGES: The total page count should follow normal pagination procedures, i.e., enter the number of pages containing information.

7b. NUMBER OF REFERENCES: Enter the total number of references cited in the report.

8a. CONTRACT OR GRANT NUMBER: If appropriate, enter the applicable number of the contract or grant under which the report was written.

8b, 8c, & 8d. PROJECT NUMBER: Enter the appropriate military department identification, such as project number, subproject number, system numbers, task number, etc.

9a. ORIGINATOR'S REPORT NUMBER(S): Enter the official report number by which the document will be identified and controlled by the originating activity. This number must be unique to this report.

9b. OTHER REPORT NUMBER(S): If the report has been assigned any other report numbers *(either by the originator or by the sponsor)*, also enter this number(s).

10. AVAILABILITY/LIMITATION NOTICES: Enter any limitations on further dissemination of the report, other than those imposed by security classification, using standard statements such as:

(1) "Qualified requesters may obtain copies of this report from DDC."

(2) "Foreign announcement and dissemination of this report by DDC is not authorized."

(3) "U. S. Government agencies may obtain copies of this report directly from DDC. Other qualified DDC users shall request through _____."

(4) "U. S. military agencies may obtain copies of this report directly from DDC. Other qualified users shall request through _____."

(5) "All distribution of this report is controlled. Qualified DDC users shall request through _____."

If the report has been furnished to the Office of Technical Services, Department of Commerce, for sale to the public, indicate this fact and enter the price, if known.

11. SUPPLEMENTARY NOTES: Use for additional explanatory notes.

12. SPONSORING MILITARY ACTIVITY: Enter the name of the departmental project office or laboratory sponsoring *(paying for)* the research and development. Include address.

13. ABSTRACT: Enter an abstract giving a brief and factual summary of the document indicative of the report, even though it may also appear elsewhere in the body of the technical report. If additional space is required, a continuation sheet shall be attached.

It is highly desirable that the abstract of classified reports be unclassified. Each paragraph of the abstract shall end with an indication of the military security classification of the information in the paragraph, represented as *(TS), (S), (C), or (U)*

There is no limitation on the length of the abstract. However, the suggested length is from 150 to 225 words.

14. KEY WORDS: Key words are technically meaningful terms or short phrases that characterize a report and may be used as index entries for cataloging the report. Key words must be selected so that no security classification is required. Identifiers, such as equipment model designation, trade name, military project code name, geographic location, may be used as key words but will be followed by an indication of technical context. The assignment of links, rules, and weights is optional.

*U.S.Government Printing Office: 1972 — 759-486/157

Unclassified
Security Classification

I 6

CAPABILITY OF THE TOTAL IN-FLIGHT SIMULATOR (TIFS)

FINAL TECHNICAL REPORT

P. A. REYNOLDS
R. WASSERMAN
G. J. FABIAN
P. R. MOTYKA

CAL REPORT NO. TB-3020-F-4
(AFFDL-TR-72-39)

CONTRACT F33615-71-C-1110

JULY 1972

IC

FOREWORD

This technical report concerning the Total In-Flight Simulator (TIFS) was prepared by the Cornell Aeronautical Laboratory, Inc., (CAL), Buffalo, New York, in partial fulfillment of the reporting requirements of USAF Contract No. F33615-71-C-1110. The work was performed under the Advanced Development Program, Project 684B entitled "Extensive Checkout of the Variable Stability System in the TIFS Airplane" and was administered under the direction of the Air Force Flight Dynamics Laboratory, Air Force Systems Command, Wright-Patterson Air Force Base, Ohio with J. R. Pruner (AFFDL/FGC) as Project Engineer.

This report was submitted by the authors for Air Force approval in February 1972, and is being published simultaneously as CAL Report No. TB-3020-F-4.

This technical report has been reviewed and is approved.

C. B. WESTBROOK
Chief, Control Criteria Branch
Flight Control Division
Air Force Flight Dynamics Laboratory

ABSTRACT

TIFS is a newly developed, variable stability C-131 aircraft with the unique capability to vary its flying qualities in all six degrees of freedom. It also surpasses the utility of past variable stability aircraft through the realism possible in its separate, new evaluation cockpit. The capabilities and features of this in-flight simulator considerably broaden the ability of the aircraft designer to deal with difficult trade-offs in flying qualities problems. A base configuration can be set up and then its stability and control characteristics can be systematically varied for investigations to gain research knowledge pertinent to flight vehicle and flight control system design. This report describes the theoretical basis for in-flight motion reproduction and how this theory can be applied to determine the TIFS capability to simulate a given aircraft. Physical characteristics as determined in flight and examples of simulation are given. Flight test records of model-following performance are also included. The objective of this report is to give the reader the basic information for planning a TIFS experiment.

TABLE OF CONTENTS

LIST OF ILLUSTRATIONS

LIST OF TABLES

LIST OF SYMBOLS

b	wing span
$\bar{c}$	reference chord
e	error
g	gravity constant (32.2 ft/sec^2)
h_p	pressure altitude
m	airplane mass
n_x, n_y, n_z	body axis components of accelerometer signals in g units
p, q, r	body axis components of angular velocity
$\bar{q}$	dynamic pressure
s	Laplace operator
u, v, w	body axis components of linear velocity
u	control vector
v	gust vector
x, y, z	body axis system
$\bar{x}, \bar{y}, \bar{z}$	position of TIFS center of gravity in the model body axis system
C_x, C_y, C_z	body axis components of force coefficient, $C_x = F_x/\bar{q}S$, etc.
C_ℓ, C_m, C_n	body axis components of moment coefficient, $C_\ell = L/\bar{q}S$, etc.
$-C_D, C_Y, -C_L$	wind axis components of aerodynamic force coefficient excluding thrust
F	matrix of dimensional stability derivatives
G	matrix of dimensional control derivatives
I	identity matrix
$I_{xx}, I_{yy}, I_{zz}, I_{xz}$	moments of inertia in the x, y, z body axis
J	matrix of dimensional turbulence input derivatives
S	wing area

T	thrust (T_x , T_y , T_z are body axis components)
V	true airspeed
V_e	equivalent airspeed $(\sqrt{\rho/\rho_{SL}}\,/V)$
W	airplane weight
$Z_\alpha, Z_{\delta_e}, Z_{\delta_x}, Z_{\delta_y}$	dimensional derivatives in body axis $\left(Z_{\delta_e} = \bar{q}SC_{Z_{\delta_e}}\Big/mV, etc.\right)$
α	angle of attack
β	angle of sideslip
$\delta_e, \delta_a, \delta_r, \delta_x,$ $\delta_y, \delta_z, \delta_c, \delta_T$	Control deflections of the TIFS elevator, aileron, rudder, throttle, side force surface, direct lift flap, and Fowler flap, and the model throttle respectively
ϵ	error
ρ	air density
ω	frequency
ν, γ, μ	Euler angles in a wind axis system (see Figure 3.1)
Φ	power spectral density
ψ, θ, ϕ	Euler angles in a body axis system
$[\alpha]$	the transformation matrix $\begin{bmatrix} \cos\alpha & 0 & -\sin\alpha \\ 0 & 1 & 0 \\ \sin\alpha & 0 & \cos\alpha \end{bmatrix}$
$[\beta]$	the transformation matrix $\begin{bmatrix} \cos\beta & \sin\beta & 0 \\ -\sin\beta & \cos\beta & 0 \\ 0 & 0 & 1 \end{bmatrix}$
$[\gamma]$	same as $[\alpha]$ with γ replacing α
$[\theta]$	same as $[\alpha]$ with θ replacing α

$[\mu]$	the transformation matrix $\begin{bmatrix} 1 & 0 & 0 \\ 0 & \cos\mu & \sin\mu \\ 0 & -\sin\mu & \cos\mu \end{bmatrix}$
$[\phi]$	same as $[\mu]$ with ϕ replacing μ
$[\chi]$	same as $[\mu]$ with χ replacing μ
$[\psi]$	same as $[\mu]$ with ψ replacing μ
$[\ ]'$	transpose of $[\ ]$
$(\ )_c$	command to ( ) controller
$(\ )_{Ext}$	extremal value - either positive or negative
$(\ )_g$	gust component of ( )
$(\ )_I$	inertial component of ( )
$(\ )_m$	model quantity
$(\ )_p$	plant or TIFS quantity (when comparing TIFS and model quantities the absence of any subscript also signifies a TIFS quantity)
$(\ )_{DYN}$	components of ( ) dependent on rates of motion
$(\ )_{ST}$	components of ( ) dependent on instantaneous positions or angles
$(\ )_t$, $(\ )_{TRIM}$, or $(\ )_0$	value of ( ) at trim or reference condition at the start of a transient
$(\ )_T$	total aerodynamic value of ( ) ($V_T = V_I + V_g$, etc.) or part of ( ) due to thrust
$(\ )_{TCG}$	value of ( ) in an axis system with origin at the TIFS center of gravity

$( )_W$	wind axis component
$\dot{( )}$	time derivative of ( )
$\Delta( )$	increment in ( ) (usually measured from the trim value)

SECTION I

INTRODUCTION

The Total In-Flight Simulator (TIFS) is a variable stability airplane which has been developed by modifying a C-131 twin-engine transport. It has been designed to reproduce in actual flight the flying qualities of a wide range of large airplanes. There are several basic features which provide this capability. An evaluation cockpit has been added which is entirely separate from the normal airplane command cockpit. With the addition of direct lift flaps and aerodynamic side force surfaces, there is control not only of the moments about all three axes but also the forces acting along the three axes. An elaborate and versatile automatic flight control system has been installed to generate the required motions of the aircraft in all six degrees of freedom.

The TIFS airplane pictured in the frontispiece is a modified C-131H, which is the military counterpart of the Convair 580. This version of the C-131 is equipped with Allison 501-D13 turboprop power plants of 4000 horsepower each. The zero fuel weight is in the range 47,000 to 49,000 pounds with a takeoff maximum gross weight of 54,600. An isometric cutaway drawing of TIFS is shown in Figure 1.1. The simulation cockpit is removable, so that it can be replaced by other cockpits of different configurations. The direct lift flaps extend from the inboard end of the ailerons to the engine nacelle and in that region replace the normal landing flap. Inboard of the direct lift flaps, the normal Fowler flaps for landing have been retained. The direct lift flaps are plain flaps with a total area of 108 sq ft (11.7% of wing area) and can be deflected ± 40°. The surfaces for generating aerodynamic side forces extend above and below the wing and are pivoted about an axis normal to the wing plane. Their total area is 100 sq ft (50 sq ft on each side of the aircraft), and they can be deflected ± 30°. The installations in the aircraft include sensors, computers, control actuators, displays and flight data recording equipment.

There are a variety of purposes and applications for in-flight simulation. Flight evaluations of the flying qualities of new airplane configurations can be accomplished, such as investigation of the behavior of extremely large

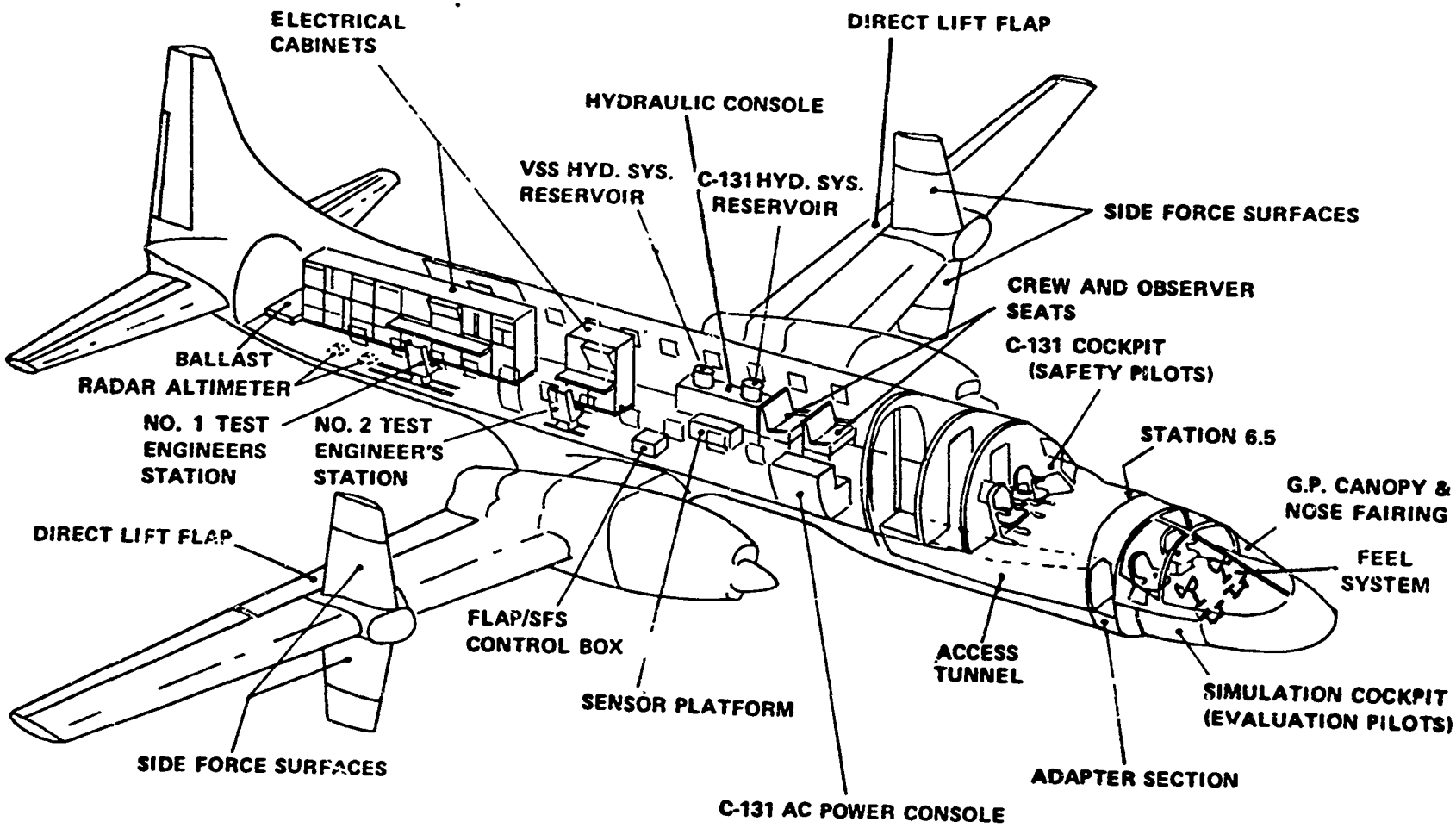

Figure 1.1 Total In-Flight Simulator

airplanes. This can be extended to investigating the flight control characteristics of entirely new types of designs, as for example, reproducing the landing approach flight characteristics of a large re-entry vehicle. The simulator can be used as a conventional variable stability airplane. A base configuration can be set up and then its stability and control characteristics can be systematically varied to gain research knowledge pertinent to flight vehicle and flight control system design. The flight characteristics of specific aircraft can be simulated in great detail, both to evaluate flying qualities in advance of the first flight of the actual airplane and to investigate difficulties that may arise during the airplane's flight test program. This purpose is applicable to problems arising in the areas of stability and control, flight control system behavior, cockpit controller characteristics and cockpit displays. Finally, a well established and highly valuable use of in-flight simulation is pilot training. In-flight simulation of emergency conditions can be conducted safely because, if the evaluation pilot is having control problems, the safety pilot can switch the system off and resume control of the normal base airplane.

Simulation in the TIFS vehicle has the fundamental advantage of being accomplished in actual flight. The evaluation cockpit is fitted out to duplicate the vision, displays, controls and control feel of the airplane being simulated. Furthermore, through the action of the variable stability system, the responses of the vehicle to the pilot's control actions, as experienced and felt by the evaluation pilot, duplicate the flight behavior of the airplane being simulated. Thus complete simulation in actual flight is achieved in regard to stability and control, flying qualities, flight control system characteristics, cockpit controls and displays.

1.1 POINTS CONCERNING TOTAL IN-FLIGHT SIMULATION AND TIFS

Let us consider in a little further detail the principles by which in-flight simulation is accomplished. The concept of providing a correct reproduction of the cockpit environment is clear enough. The TIFS airplane is

presently equipped with a general purpose cockpit providing greater than usual visibility for the pilot. By proper masking, the window configuration of any particular airplane can be reproduced. Then the cockpit displays, controls and instruments can be duplicated in as great detail as desired.

In considering the reproduction of cockpit motions, it is important to realize that the pilot senses linear accelerations at his location in the cockpit and the angular motions of the cockpit. If the TIFS cockpit reproduces these accelerations and motions, the simulation is accomplished. With the duplication of both cockpit environment and cockpit motions, total in-flight simulation is achieved.

If the TIFS cockpit is to be made to move as required to duplicate the motions of another airplane, it is necessary to control all six degrees of freedom, that is, to have control over moments about, and forces along, all three axes. Through proper control of all six degrees of freedom, it is possible to simulate, for example, the motions of a large airplane's cockpit which is located a great distance ahead of the airplane's center of gravity. The low lift curve slope of a delta wing airplane can be reproduced. The troublesome task of controlling sideslip in turn entries and recoveries for very large airplanes can be studied through use of the variable stability system.

Why was a C-131 chosen as the basic airframe instead of a more modern, high performance airplane? The point here is that in simulating another airplane, the basic vehicle characteristics should not show through and intrude upon the simulation. For example, if an airplane with flexible, swept wings had been chosen, the structural response to gusts would be that of the base airplane. It would be most difficult to suppress these natural response characteristics, let alone to try to simulate the structural response of another airplane. In general, the best simulation of other airplanes can be produced if the base airplane has fundamentally simple and straightforward characteristics. Specifically, it is highly desirable that it be relatively

rigid and that it have uncomplicated stability and control characteristics.

Next it should be noted that there is no advantage to choosing an airplane that is larger than necessary. In using variable stability to alter the airplane's response characteristics, it is generally a great deal easier to slow down the motions of a relatively small airplane than it is to speed up the responses of a big one. Also, the good control surface servo frequency response so vital to high performance variable stability is harder to obtain with large control surfaces on a large airplane. Finally, the consideration of maintenance and operating costs is always important, and here the Convair shows up very well.

What is the advantage of TIFS over a ground-based simulation? Ground-based simulation is of great use to be sure, for purposes such as design, training, and practice in cockpit procedures, systems management, and navigation. But when it comes to the dynamics and feel of the airplane interacting with its controls, displays, flight control system, and view of the outside world, in-flight simulation is a great deal closer to the real thing. Sometimes the person asking this question does not understand that the C-131 characteristics do not show through. Perhaps he is accustomed to sitting in a ground-based simulator, pretending he is flying a C-5A, for example, and he is really asking what is so much better about sitting in a C-131 pretending he is flying a C-5A. What he fails to realize is that the in-flight simulation system really transforms the C-131's flying characteristics into those of the C-5A so that he has no feel at all of flying a C-131. Thus he is not in the least subject to any need to pretend that the C-131 is something else. He has the direct, complete and natural feel of the airplane being simulated.

How can an airplane of limited speed capability simulate high speed airplanes? There are several points to be made here. First, many problems of interest and importance are ones that arise in the landing approach condition. In this condition, TIFS can match the speed of the airplane being simulated and so the question does not arise. Next consider the simulation

of small amplitude maneuvers about a reference condition of high speed, straight and level flight. Such maneuvers will involve certain time histories of increments in cockpit translation and rotation about the steady condition. With control of all six degrees of freedom, TIFS can duplicate these time histories and provide correct simulation even if speed is not matched. This is true, however, only to the point where one or another of the controls reaches the limits of its authority. The limits of control authority are primarily reflected in limits on change in heading and rates of climb and descent. In many situations these limits are not serious. An important example is aerial refueling. This is inherently a small disturbance task, and TIFS can provide excellent simulation regardless of speed mismatch.

Even in simulation with speed mismatch there are possibilities for compromise which still produce a high quality approximation of the true situation. Consider the case of a sustained steady turn at altitude. Here let us suppose that TIFS flying at 240 knots is being used to simulate another airplane flying at 480 knots. Now the fact that force equals mass times acceleration tells us that in this situation a match between TIFS and simulated aircraft acceleration in a turn will produce a rate of change of heading that is twice too large. The consequences of this effect may not be serious however. The pilot observes that the scenery will be moving past the windshield too fast. However, he may not have any important sensation of the steady turn rate being in error. Turn entry and recovery dynamics can still be reproduced correctly and the computer can drive the cockpit instruments so that they display the simulated flight variables correctly.

1.2 DOCUMENTATION OF TIFS CAPABILITIES

The capabilities of a new system such as the TIFS which represents a significant advance in the state of the simulation art are difficult to define fully at this early stage. The ways TIFS will and can be used are not entirely predictable. Also there has been no flight test program specifically designed to determine all the capabilities although many areas have been explored in

accomplishing the objectives of the present contract. The gust alleviation capability has not been fully optimized; the response-feedback method of motion simulation has not yet been investigated; there have been no simulations with speed mismatch; and at the time of this writing as yet no simulations had been conducted at speeds above 200 knots. The list of new areas to explore is extensive, and, in a real sense, this report, as the previous report, Reference 2, should also be labeled "preliminary".

However, it is reasonable to document the capabilities as they are known at the present time so that potential users and other interested people in the technical community can understand and evaluate the simulator. It is probable that as the TIFS is used, further reports updating this one will be desirable to keep these people informed.

This report begins with Section II explaining, in theory, specifically how the desired motion is reproduced in flight. It amplifies the discussion in Section 1.1 above and sets the groundwork for the definition of TIFS capabilities. Sections III through VI deal with motion reproduction capability. Sections III and IV describe the general bounds on unaccelerated and accelerated motion. These are always present whether model-following or response-feedback control techniques are used. In Section IV the TIFS controller dynamics which are basic to the question of motion bandwidth are documented. Section V deals with the model-following performance achieved. Section VI presents the current results with the gust environment.

Sections VII, VIII and IX deal with capabilities aside from motion reproduction. These include the very important cockpit feel systems, cockpit displays, vision, navigation, communication, audio environment, data gathering and processing, and the TIFS airplane flight operational factors affecting simulation capability.

The TIFS program documentation outside of this report is composed of five formal reports, several hundred TIFS Memos and CTIFS Memos,

and more than fourteen hundred mechanical and electrical drawings. The formal reports are References 1 through 5 plus this report.

The TIFS Memos range from informal brief documents dealing with the technical details of the system design and operation to voluminous structural analysis. They were generated in the normal daily course of the program and fully document the technical effort aside from the mechanical and electrical drawings.

The CTIFS Memos are the equivalent documents generated under the Air Transport TIFS (AT/TIFS) program. Many of these are applicable to the Air Force TIFS. That program was accomplished in parallel with the Air Force development from February 1968 to January 1970 under contract to TIFS, Inc. The effort was aimed at producing a prototype of a production flight simulation vehicle for training airline pilots for large advanced jet aircraft. The prototype is a Convair 580 fitted with an actual Boeing 707 nose so that a familiar aircraft could be simulated for demonstration purposes. The fuselage modification, computer mounting in the aft cabin, hydraulic system, evaluation cockpit feel system, and a few other system details differ substantially from the Air Force TIFS. However, the direct lift flaps and side force surfaces together with their structural mounting and actuation systems are essentially identical. The electrohydraulic and mechanical logic controlling the direct lift flaps and side force surfaces are the same and were designed and documented on the AT/TIFS program. Several system studies and aerodynamic analyses were performed on the AT/TIFS program which have applicability to both programs.

The TIFS and CTIFS memos are listed in Reference 4 and can be requested from the Air Force Flight Dynamics Laboratory.

The "Preliminary Design" Report (Reference 1) documents the program from its beginning in November of 1966 to June of 1967. At that point

the first series of wind tunnel tests had been completed, the basic aerodynamic configuration and loads had been defined, and structural design work was under way. Preliminary design of the hydraulic system and the electronics had been completed, and control loop studies were in progress.

The "Installation, Operation, and Maintenance Instructions" (Reference 3) and the "Final Report" (Reference 4) document the development through October 1970. This includes the second series of wind tunnel tests, the design, fabrication, installation, and checkout of all systems and structures, and the first series of flight tests. These tests demonstrated the proper functioning of the systems and carried the model-following development through simulation of a linear Boeing 707 model at 150 knots. The "Instructions" Report contains detailed material as the title implies. It also contains a list of all drawings describing the TIFS. The "Final Report" describes the final system in more general terms.

The "Preliminary Simulation Capabilities" Report (Reference 2) was published before actual flight tests and therefore deals with wind tunnel estimates and theoretical analyses. The effort on this study was not extensive because of the lack of firm data, but the results on maneuvering capability have been generally substantiated and are, for the most part, included in this report. That report treats maneuvering capability, terrain-following simulation, and includes some material on visual and motion cues.

The "Propeller Blade Stress Survey" Report (Reference 5) is a brief document produced by the Detroit Diesel Allison Division of General Motors - the turboprop engine manufacturer - describing the results of flight tests clearing the propellers for TIFS operations. The results are summarized in Section 9.2 in this report.

SECTION II
MOTION SIMULATION IN FLIGHT

The theoretical basis for determining the TIFS capability to simulate a given airplane starts with the equations of rigid body motion describing both TIFS and the given airplane, which will be referred to as the model. The equations are essentially the same for both model and TIFS and differ only in aerodynamic or minor kinematic detail. Section 2.1 below will serve as a review of these equations, notation, sign corrections, simplification, and axis systems used in TIFS simulation work for those readers who are already generally familiar with the subject of airplane dynamics. For other readers, appropriate references are recommended.

Once the equations are presented, the TIFS capabilities can be defined because capabilities are determined by comparing the TIFS control time histories as determined in turn from these equations with the control deflection, rate, or frequency response limits. Section 2.2 discusses this step from equations to control time histories.

Section 2.3 briefly treats the problem of how to produce the desired TIFS control deflections in real time as the computed motion of the model takes place in response to evaluation pilot input. Sections 2.4, 2.5, 2.6 and 2.7 mention other detailed points which are important to motion simulation.

2.1 EQUATIONS OF MOTION

The derivation of the equations of motion of an aircraft and the assumptions utilized in the derivation of these equations will not be presented in this section. Several excellent treatments regarding this derivation and application to the motion of an aircraft are available in many references (e.g., 6 and 7). The TIFS Preliminary Design Report (Reference 1) presents the exact nonlinear equations of motion. Approximate nonlinear equations of motion and linearized equations of motion of an aircraft, based upon additional simplifying approximations, are also discussed in Reference 1. The equations of motion used in TIFS simulation are described by a non-orthogonal

axis system selected for simplification in the determination of velocity. Thus, while the moment equations and the y and z-axis force equations are written in a body axis system, the sum of forces along the x-axis is written with respect to the wind axis rather than a body axis. Figure 2.1 illustrates the axis system and sign conventions used for TIFS simulations while Figure 2.2 illustrates the relationship between body axes and the non-orthogonal axis system used. Figure 2.3 illustrates the relationships between the Euler angles and angular velocity components in the body axis system.

Once the equations of motion are defined, it becomes desirable for efficient computation to examine the equations in an attempt to introduce simplifications for a particular simulation. For example, several inertial coupling terms in the moment equations may have little significant effect on the aircraft response in the landing approach flight phase. Once such higher-order effects are determined to be inconsequential, they can be neglected without compromising the response of the aircraft. In addition, small angle assumptions can usually be made. The simplifications that should be introduced into the "exact" nonlinear equations of motion for an aircraft are dependent not only upon the physical characteristics of the aircraft, but also upon the particular task to be investigated and the limitations imposed by equipment available for simulation.

In most developments of the equations of motion of an aircraft, the relative motion between the earth-fixed inertial axis system and the atmosphere is initially assumed to be zero. Thus to account for the effects of relative atmospheric motion (e.g., gusts) it is necessary to distinguish between the inertial components of aircraft motion, and the relative motion effects due to motion of the air mass. This is accomplished by expressing the aerodynamic forces and moments in the equations of motion as functions of the total local flow effects caused by the relative motion of the aircraft with respect to the air mass.

The following discussion illustrates the simplifications introduced into the "exact" nonlinear equations of motion that were used to model the

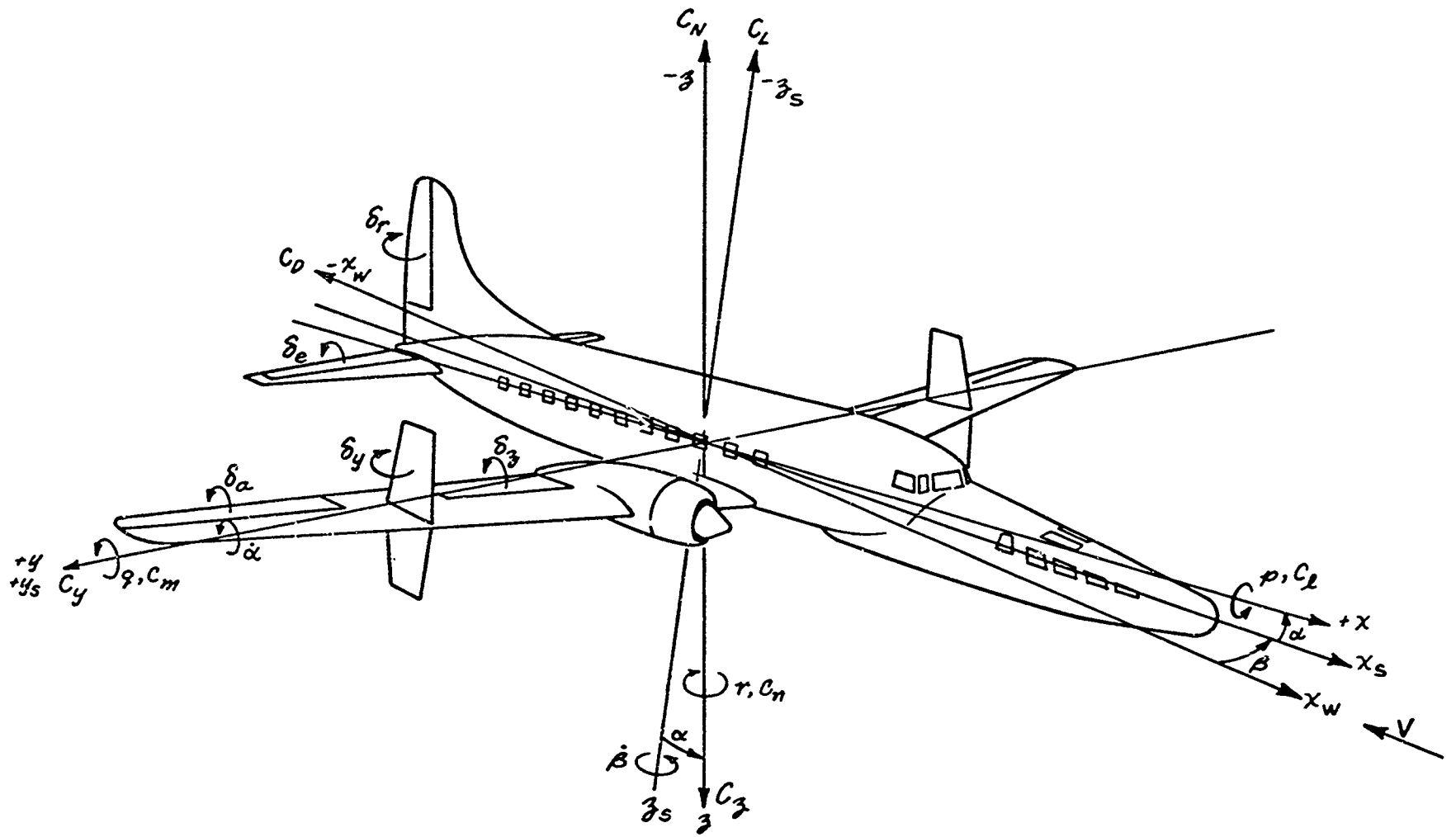

Figure 2.1 Axes and Sign Conventions for TIFS

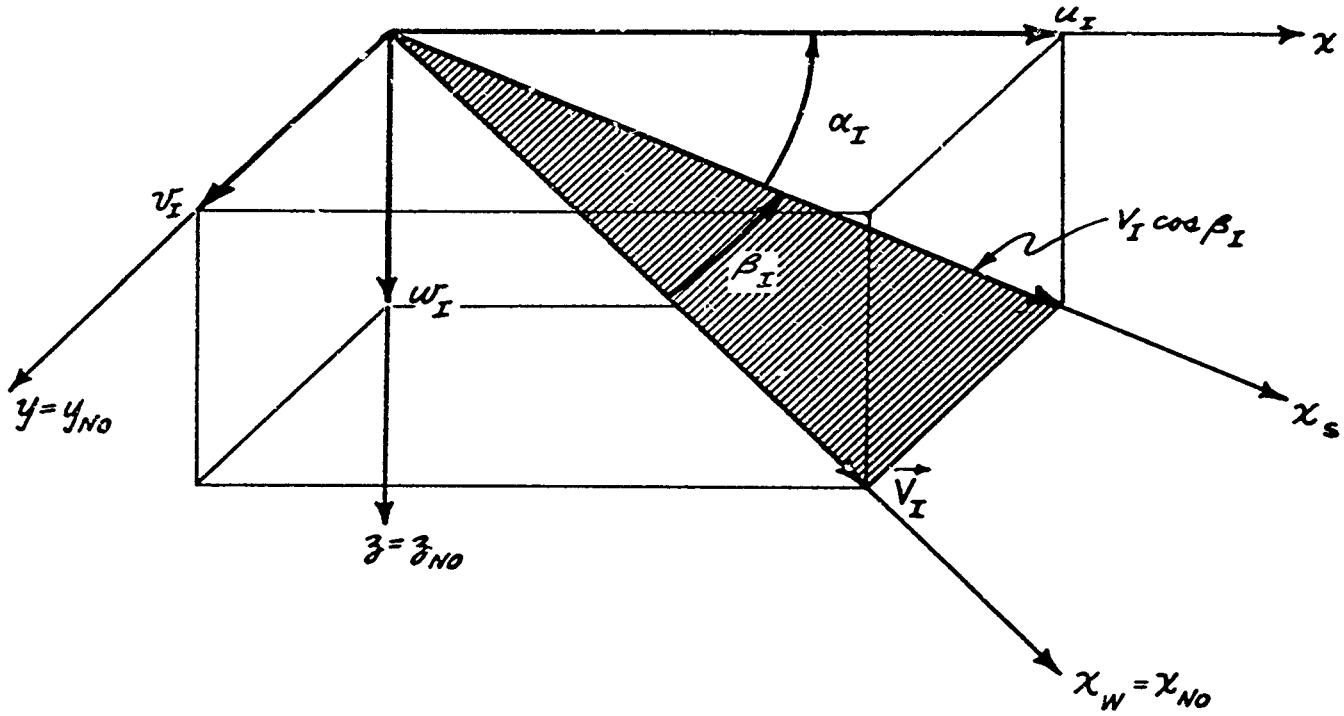

Figure 2.2 The Relation Between Body Axes and the Nonorthogonal Axes

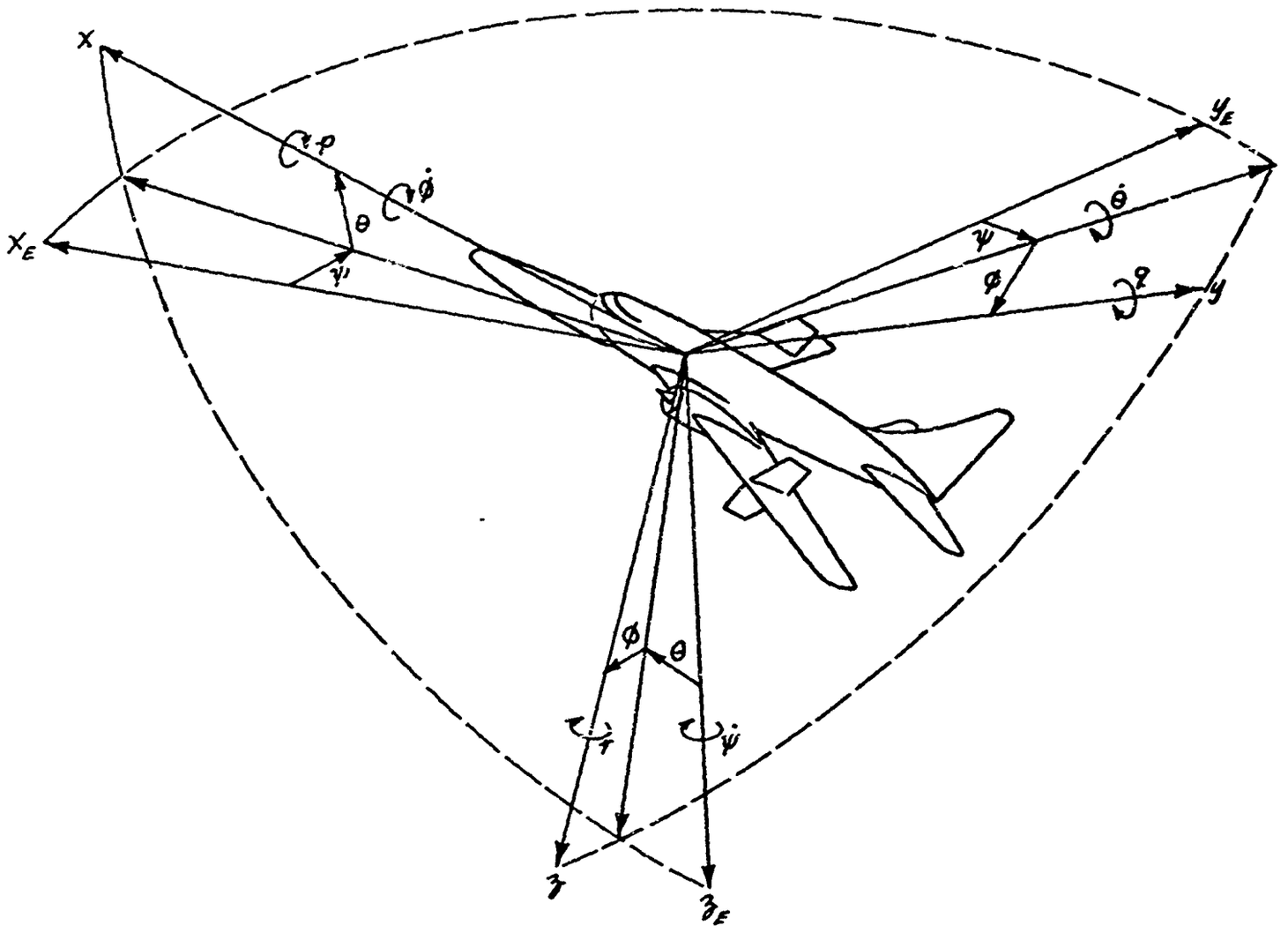

Figure 2.3 Euler Angles, Euler Angle Rates and Angular Velocity Components

equations of motion of a Class III aircraft in the landing approach flight phase reported in References 8 and 9.

The X force equation of motion in the wind axis system was written

$$m\dot{V}_I = -mg\sin\gamma - \tfrac{1}{2}\rho V_T^2 S C_D + T_x \cos\alpha_I \cos\beta_I + T_z \sin\alpha_I \cos\beta_I \qquad (2.1)$$

The thrust was assumed to be parallel to the x body reference axis thus $T_x \cong T$, $T_z = 0$. In addition, it was assumed that α_I and β_I would be sufficiently small that small angle assumptions (to the first order) could be introduced (i.e., $\cos\alpha_I \cong 1$, $\sin\alpha_I \cong \alpha_I$, etc.). Thus the previous equation becomes

$$\dot{V}_I = -g\sin\gamma - \frac{1}{2m}\rho V_T^2 S C_D + \frac{T}{m} \qquad (2.2)$$

where $\sin\gamma$ is $\dot{h}_I / V_I$ and can be expressed using the small angle assumption

$$\sin\gamma = \sin\theta - \beta_I \sin\phi\cos\theta - \alpha_I \cos\theta\cos\phi \qquad (2.3)$$

The Z force equation in a body axis system is

$$\dot{w}_I + (-q_I u_I + p_I v_I) = g\cos\phi\cos\theta + \frac{1}{2m}\rho V_T^2 S C_Z + \frac{T_z}{m} \qquad (2.4)$$

The body axis components of linear velocity are related to α_I, β_I, and V_I by

$$w_I = V_I \sin\alpha_I \cos\beta_I$$
$$u_I = V_I \cos\alpha_I \cos\beta_I$$
$$v_I = V_I \sin\beta_I$$

illustrated in Figure 2.2.

Thus, $$\dot{w}_I = V_I \sin\alpha_I \left(-\dot{\beta}_I \sin\beta_I\right) + \cos\beta_I \left(V_I \dot{\alpha}_I \cos\alpha_I + \dot{V}_I \sin\alpha_I\right) \qquad (2.5$$

Introducing the small angle assumptions yields

$$\frac{\dot{w}_I}{V_I} \approx -\alpha_I \beta_I \dot{\beta}_I + \dot{\alpha}_I + \alpha_I \frac{\dot{V}_I}{V_I} \qquad (2.6)$$

The expression ($\alpha_I \beta_I \dot{\beta}_I$) in Equation (2.6) can be considered as a higher order term and neglected with the same accuracy as replacing $\cos \beta_I$ by 1.0, giving

$$\frac{\dot{w}_I}{V_I} = \dot{\alpha}_I + \frac{\alpha_I \dot{V}_I}{V_I} \tag{2.7}$$

Introducing the small angle approximations for the ($- q_I u_I + p_I v_I$) term and assuming $T_z \cong 0$ yields

$$\dot{\alpha}_s = \frac{S}{2m} \rho \frac{V_T^2}{V_I} C_z + \frac{g}{V_I} \cos\phi \cos\theta + q_I - p_I \beta_I - \frac{\alpha_I \dot{V}_I}{V_I} \tag{2.8}$$

where
$$V_T = V_I + V_g \tag{2.9}$$

$$C_z = C_{z_{ST}} + \frac{\bar{c}}{2V_T} C_{z_{DYN}} \approx -C_L$$

$$C_{z_{ST}} \approx -\left(C_{L_0} + C_{L_\alpha} \alpha_T + C_{L_{\delta_e}} \delta_e + \ldots\right) \tag{2.10}$$

and
$$C_{z_{DYN}} \approx -\left(C_{L_{\dot{\alpha}}} \dot{\alpha}_T + C_{L_q} q_T\right) \tag{2.11}$$

The pitching moment equation in a body axis system can be expressed as (neglecting any engine gyroscopic terms)

$$M_{aero} + z_T T_x - x_T T_z = I_{yy} \dot{q}_I + \left(I_{xx} - I_{zz}\right) p_I r_I + I_{xz}\left(p_I^2 - r_I^2\right) \tag{2.12}$$

If the inertial coupling terms are neglected, and the thrust assumed to act through the c.g. thus producing zero pitching moment then

$$\dot{q}_I = \frac{1}{I_{yy}} \left(\frac{\rho V_T^2 S \bar{c}}{2} C_{m_{ST}} + \frac{\rho V_T S \bar{c}^2}{4} C_{m_{DYN}} \right) \tag{2.13}$$

where

$$C_{m_{ST}} = C_{m_0} + C_{m_\alpha} \alpha_T + C_{m_{\delta_e}} \delta_e + \ldots \tag{2.14}$$

$$C_{m_{DYN}} = C_{m_q} q_T + C_{m_{\dot{\alpha}}} \dot{\alpha}_T \; ^* \tag{2.15}$$

---

* Although the notation used for the aerodynamic coefficients appears to imply a linear dependency on the motion of the aircraft and the controls, in general for a simulation the data can be programmed as nonlinear functions of the variables if such are to be examined. Thus, in general C_m, C_L, etc. can have the form $f(\alpha_T, \dot{\alpha}_T, \delta_e, q_T, M, \ldots)$.

The Y force equation of motion in a body axis system can be written as

$$g \sin\phi \cos\theta + \frac{S}{2m} \rho V_T^2 C_y = \dot{v}_I + (r_I u_I - p_I w_I) \tag{2.16}$$

Using small angle assumptions

$$\frac{\dot{v}_I}{V_I} = \dot{\beta}_I + \beta_I \frac{\dot{V}_I}{V_I} \tag{2.17}$$

and Equation (2.16) can be written as

$$\dot{\beta}_I = \frac{S}{2m} \rho \frac{V_T^2}{V_I} C_y + \frac{g}{V_I} \sin\phi \cos\theta - \frac{\beta_I \dot{V}_I}{V_I} - r_I + p_I \alpha_I \tag{2.18}$$

where

$$C_y = C_{y_{ST}} + \frac{b}{2V_T} C_{y_{DYN}} \tag{2.19}$$

with definitions of $C_{y_{s.}}$ and $C_{y_{DYN}}$ similar to (2.10) and (2.11). The rolling and yawing moment equations written in a body axis system for symmetrical thrust conditions are (neglecting any engine gyroscopic effects)

$$L_{aero} = I_{xx} \dot{p}_I + q_I r_I (I_{zz} - I_{yy}) - (\dot{r}_I + p_I q_I) I_{xz} \tag{2.20}$$

$$N_{aero} = I_{zz} \dot{r}_I + p_I q_I (I_{yy} - I_{xx}) + (q_I r_I - \dot{p}_I) I_{xz} \tag{2.21}$$

For the landing approach simulation, it was assumed that the higher order angular velocity coupling terms could be neglected. In addition, the notation of the nondimensional coefficients was modified such that the product of inertia (I_{xz}) appeared in the definition of the aerodynamic moment coefficients and not explicitly in the equations of motion. Thus the form of the equations used in the landing approach investigation in References 8 and 9 was

$$\dot{p}_I = \frac{1}{2} \frac{\rho V_T^2 Sb}{I_{xx}} (C'_\ell) \tag{2.22}$$

$$\dot{r}_I = \frac{1}{2} \frac{\rho V_T^2 Sb}{I_{zz}} (C'_n) \tag{2.23}$$

where $$C'_{\ell} = \left[\frac{I_{xx}I_{zz}}{I_{xx}I_{zz}-I_{xz}^2}\right]\left[C_{\ell} + \frac{I_{xz}}{I_{zz}} C_n\right]$$

and $$C'_n = \left[\frac{I_{xx}I_{zz}}{I_{xx}I_{zz}-I_{xz}^2}\right]\left[C_n + \frac{I_{xz}}{I_{zz}} C_{\ell}\right]$$

Additional details on the development of the equations used for the landing approach programs recently performed on the TIFS aircraft appear in the appendices of References 8 and 9.

2.2 THE EXISTENCE AND UNIQUENESS OF CONTROL INPUT APPLICABLE TO IN-FLIGHT SIMULATION

Given the equations of the model and the TIFS, the first basic question concerning capability to match motion is, "Is there any at all?". This is the question of existence of control time histories to produce solutions of the TIFS equations which match the given time histories. Clearly there are variable stability airplanes without the capability to match certain motions; for example, one without side force capability trying to match yawing motion about a point aft of its empennage. The second basic question is that of uniqueness. Having found one set of control time histories producing a given motion, is there another set which will produce the same motion? If there is, then the task of determining motion amplitude limits becomes more complex. One might, for example, use the TIFS engines differentially for yaw control to augment the rudder capability or in turn indirectly provide more side force capability by taking advantage of the side force capability of the rudder. Now the control time history to match a given Dutch roll oscillation is no longer unique and sideslip limits based on side force surface stall limits must be redefined.

The preceding section examined the equations of motion of an aircraft. These equations can be classified as ordinary nonlinear differential equations, with six degrees of freedom. These degrees of freedom can be identified

with the six independent coordinates required to specify the position and orientation of a rigid body in space. Three degrees of freedom are required to specify the origin of the body-fixed axis system (i.e., c.g. position) and three degrees of freedom are required to specify the orientation of this body-fixed axis system (i.e., Euler angles). Thus while there are many choices possible for the six generalized coordinates, once a choice is made, the body-fixed axis system is uniquely determined by specifying the time history of the six degrees of freedom of the body. The equations of motion relate the forces amd moments acting on the aircraft to the time history of the six degrees of freedom.

The equations of motion for a rigid aircraft can be expressed in a first order form:

$$f(\dot{x}, x, u) = 0 \tag{2.24}$$

where x is a 12 x 1 state vector (3 position coordinates, 3 Euler angles 3 linear velocity components, and 3 body angular rates)

u is an m x 1 control vector, where for a normal aircraft m is 4 and for TIFS m is 6 (elevator, aileron, rudder, throttle, side force surface, and direct lift flap)

f is 12 x 1 vector of functions.

From the theory of nonlinear ordinary differential equations, there are many general results concerning the existence and uniqueness of solutions to equations like (2.24). The authors know of no completely general existence and uniqueness conditions applying to the simulation problem, however. But general physical statements can be made. The problem can be informally stated as follows:

> Given two systems described by $f_p[\dot{x}_p(t)\ ,\ x_p(t)\ ,\ u_p(t)] = 0$ and $f_m[\dot{x}_m(t), x_m(t), u_m(t)] = 0$ where $x_p(t)$ and $x_m(t)$ are both n x 1 vectors, is there a control time history $u_p(t)$, $(t \geq 0)$ which will produce $x_p(t) = x_m(t)$ given that $x_p(0) = x_m(0)$? Also from the point of view of determining simulation capability, if such a $u_p(t)$ exists, is it unique?

Drawing on a knowledge of the physics of rigid body motion, it can be argued informally and heuristically that for the aircraft equations of motion (2.24),

1) given $x_p(0)$ and $u_p(t)$, a solution $x_p(t)$ exists and is unique,

2) if $u_p(t)$ has six independent components, each of which exerts control over at least one of the degrees of freedom, then disregarding the limits on u_p, there exists a unique $u_p(t)$ for each given $x_p(t)$ which will produce that $x_p(t)$.

and 3) therefore, if, in particular, the specified $x_p(t)$ is a solution of $f_m\left[\dot{x}_m(t),\ x_m(t),\ u_m(t)\right] = 0$ then under the conditions of 2) complete simulation is possible and the region of allowable $x_m(t)$ can be determined from the region of allowable $u_p(t)$ because there is a one-to-one relationship.

Thus, it is possible to talk about perfect model following in TIFS and, in addition, convenient to define capability in terms of the control effectiveness and the control actuator dynamics. Note that uniqueness is not necessary for in-flight simulation to work. But it is necessary in determining capability to recognize non-uniqueness.

A simulation with speed or attitude not matched (and thus the actual path through space not matched) but with the deviations from that flight condition matched, also fits into the statements above: the problem is merely changed from one where $x_p(t) = x_m(t)$ to one where particular components of $x_m(t)$ and/or perturbations in x_m (i.e., $x_m(t) - x_m(0)$) are matched.

Some of these physical arguments are developed mathematically in Reference 1 for the linearized equations of motion.

2.3 CONTROL SYSTEM CONCEPTS FOR MOTION SIMULATION

The idea of using a yaw damper to improve the Dutch roll stability of an airplane is well established. In effect, the yaw damper changes the value of the airplane's damping-in-yaw stability derivative. The principle can be readily applied to altering the values of all the other stability derivatives of an airplane. Thus the terms in the equations of motion of the variable stability airplane can be adjusted to match the corresponding terms in the equations of motion of the airplane being simulated. This is the original variable stability concept, and it is known as the "response-feedback" approach. A response-feedback variable stability system can be described as a generalized stability augmentation system which has wide ranges of adjustment so that large variations in airplane response characteristics can be produced.

A response-feedback system operates by adding to or subtracting from the airplane's natural stability and control characteristics. Thus it is necessary to know accurately the stability and control characteristics of the base airplane at whatever flight test condition is being used. Also, it is difficult to calculate exactly in advance the variable stability system gain settings which will produce correct values all at once of the many parameters which define the aircraft dynamics. Thus, in-flight calibration of the configurations that are to be evaluated is generally necessary. The use of this type of variable stability system implies a substantial task of identifying the characteristics in detail of the base airplane and of the variable stability configurations that are to be tested.

A different and newer approach to variable stability uses the idea of "model following". In this type of system, the electrical signals that come from the evaluation pilot's use of his cockpit controls are fed as inputs to a computer which has in it the equations of motion of the airplane to be simulated. The output of this computer is the set of time histories of motion variables which describe the response of the simulated airplane to the inputs applied by the pilot. The task then is automatic operation of the controls of

the variable stability airplane in such a way that its motions follow or duplicate the motions defined by the model outputs. In other words, the job of the flight control system is to make the airplane follow the pitch, roll and yaw motions that come from the model computer, and likewise to follow the indicated changes in speed components along the three axes, or equivalent variables such as angle of attack and angle of sideslip. It should be noted that if there are fewer controls available than there are degrees of freedom in the equations of motion, some compromises will be necessary. Four or five controls are simply not sufficient to follow six independently varying quantities. It is a fundamental feature of TIFS that controls are provided for all six degrees of freedom, so that it will be possible to follow the model outputs simultaneously and accurately.

The model-following approach permits the computer that defines the aircraft being simulated to be set up and checked out on the ground prior to flight. Then if the variable stability airplane in flight can, without further adjustment, reproduce exactly the computer outputs, the problem of in-flight calibration is avoided. To be a little more realistic though, it must be remarked that the model following will surely not be perfect and that, to some degree, it will be necessary to know what the variable stability airplane characteristics are to improve the model following. This means a certain amount of in-flight calibration work is necessary to set control system gains even in the model-following mode. However, once the gains are set changing from one set of dynamics to another in a handling qualities experiment becomes the simple and accurate task of setting pots in the model computer.

A variable stability system must be designed with constant attention to the achievement of excellent dynamic performance, all the way from the sensors through the entire system to the control actuators. If time lags are large in the various channels of a response-feedback system, the task of trying to compensate for the lags in all the channels can become complex and even entirely unmanageable. Clearly also, one key point to success of a model-following system is the ability to accomplish the following with essentially imperceptible time lags.

The TIFS model following system employs two techniques simultaneously -- model following by feedforwards and model following by error loops. The function of the error loops is familiar and conceptually easy to understand. Model following with feedforward signal paths only is less familiar and is illustrated in this example below.

It can be demonstrated that the expression for the TIFS control time history to simulate an aircraft by either response feedback or model following by feedforwards is the same except that y_m replaces y_p. Assume, as an example, that the equations of motion of the TIFS (the plant) and the model are the simple first order equations

$$\dot{y}_p = a y_p + b \delta_p \tag{2.25}$$

and

$$\dot{y}_m = c y_m + d \delta_m \ , \ y_p(0) = y_m(0) \tag{2.26}$$

Now define the plant control as

$$\delta_p = k_1 \delta_m - k_2 y_p \tag{2.27}$$

(The presence of y_p denotes a response feedback control law.)

Thus

$$\dot{y}_p = (a - b k_2) y_p + b k_1 \delta_m \tag{2.28}$$

Comparison of (2.28) with (2.26) indicates the necessary relationships that must be satisfied to perfectly match the model responses:

$$a - b k_2 = c \qquad \text{giving} \quad k_2 = b^{-1}(a-c) \tag{2.29}$$

and

$$b k_1 = d \qquad \text{giving} \quad k_1 = b^{-1} d \tag{2.30}$$

As the model is changed the values of the feedbacks must be determined to simulate the motion of the model. The control time history obtained is

$$\delta_p = k_1 \delta_m - k_2 y_p = b^{-1} d \delta_m - b^{-1}(a-c) y_p \tag{2.31}$$

Now, using the same example, let the plant control be produced from model feedforwards according to the equation

$$b\delta_p = \dot{y}_m - ay_m \tag{2.32}$$

(The motivation for this choice is obtained by solving (2.25) for $b\delta_p$ and asking what δ_p will make $y_p = y_m$.) One can define $\mathcal{E} = y_m - y_p$ and $\dot{\mathcal{E}} = \dot{y}_m - \dot{y}_p$ and by subtracting (2.25) from (2.32) obtain the result:

$$\dot{\mathcal{E}} = a\mathcal{E}; \text{ and since } \mathcal{E}(0) = 0 \text{ then } \mathcal{E}(t) = 0, \; t > 0.$$

Thus the control law is independent of the model parameters c and d and changes in c and d such as might be done in an experiment do not affect the control law if mechanized as indicated in (2.32).

By introducing the equation of motion of the model in the control law,

$$b\delta_p = cy_m + d\delta_m - ay_m = (c-a)y_m + d\delta_m \tag{2.33}$$

The control law expressed in this form is identical to (2.31) obtained from the response-feedback technique except that y_m replaced y_p.

Although, as previously described, the control motion sequence for the in-flight simulation is unique, the feedforward model-following technique is better suited to the examination of many changes in the stability and control derivatives of the model than is the response-feedback method. In both cases it is necessary to have an adequate knowledge of the TIFS parameters to do a satisfactory simulation. For feedforward model following, this information is required to make the proper gain adjustments. However, when feedback loops are introduced in the model-following concept to compare the states of the plant with those of the model, then the control law is less dependent upon the exact stability and control data of the plant. Another way of looking at the comparison is to say that the feedforward model-following concept is to introduce by use of the feedforwards a unity transfer function between the states of the model and the states of the plant, while the response-feedback

technique on the other hand attempts to augment the stability and control derivatives of the plant to the extent that they become equivalent to those of the model, and thus achieve equivalence between the responses to control inputs. (It should be noted that control derivative changes are obtained by interconnects between control surfaces and by changing gearing ratios.) For response-feedback systems, the feedback gain is varied as needed to provide the necessary augmentation required for matching. This type of system can be very sensitive to variations in the stability and control derivatives of the plant with flight conditions. On the other hand, when the model-following concept is used, the feedback gains introduced can be selected to minimize the sensitivity to changes in plant characteristics with flight conditions. Model following theory is set forth in more detail in Reference 10.

The extension of the simple example above to the complete airplane equations is straightforward using vector-matrix notation. The solution of the feedforward derivation problem reduces to the solution of algebraic simultaneous equations for the control quantities. When the equations of motion can be linearized and expressed as

$$\dot{x}_p = F_p x_p + G_p u_p \qquad x_p , x_m \quad \text{n x 1 vectors}$$

$$\dot{x}_m = F_m x_m + G_m u_m \qquad u_p , u_m \quad \text{m x 1 vectors}$$

and F_p , F_m , G_p and G_m are matrices,

the algebraic equations in u_p using motivation like that leading to (2.32) are thus

$$G_p u_p = \dot{x}_m - F_p x_m \tag{2.34}$$

analogous to Equation (2.32). The conditions under which (2.34) has solutions for u_p and under which they are unique are those discussed in Section 2.2, but it must be noted that the capabilities of TIFS (i.e., independent control of all six degrees-of-freedom) are sufficient, but not always necessary. Variable stability airplanes with less than six independent controls can match a restricted range of models.

The feedforward mechanization can also be derived in terms of transfer functions. The equations of motion of the plant (TIFS) can be written as

$$\left[x_p(s)\right] = \left[TF(s)\right]\left[u_p(s)\right] \tag{2.35}$$

where $\left[TF(s)\right]$ is the matrix of transfer functions, and to achieve perfect model following a control law $\left[u_p(s)\right] = \left[H(s)\right]\left[x_m(s)\right]$ must be obtained such that $\left[x_p(s)\right] = \left[x_m(s)\right]$. From the above statement, it becomes rather obvious that if $\left[H(s)\right] = \left[TF(s)\right]^{-1}$ then

$$\left[x_p(s)\right] = \left[TF(s)\right]\left[H(s)\right]\left[x_m(s)\right] = \left[I\right]\left[x_m(s)\right] \tag{2.36}$$

Thus

$$u_p(s) = \left[TF(s)\right]^{-1}\left[x_m(s)\right] \tag{2.37}$$

Let us look further into the details of producing the control time histories in real time. Neglecting Z_{δ_e} and Z_{δ_x} for the moment, Equation (2.45) in Section 2.4 can be used to solve for the direct lift flap command.

$$\begin{aligned}(Z_{\delta_z})_p \Delta\delta_{z_c} &= (\Delta\alpha_m - \Delta\theta_m)s - Z_{\alpha_p}\Delta\alpha_m \\ &= \frac{g}{V_{T_m}}\Delta n_{z_m} - Z_{\alpha_p}\Delta\alpha_m \quad \text{using (2.52)}\end{aligned} \tag{2.38}$$

These equations indicate several alternate methods to mechanize the control motions required for model following.

1)

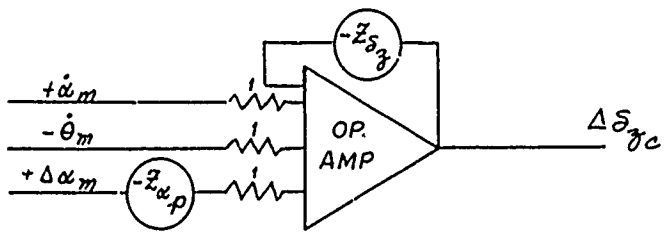

or Δn_{z_m} could be used to replace $\dot{\alpha}_m$ and $\dot{\theta}_m$ as

2)

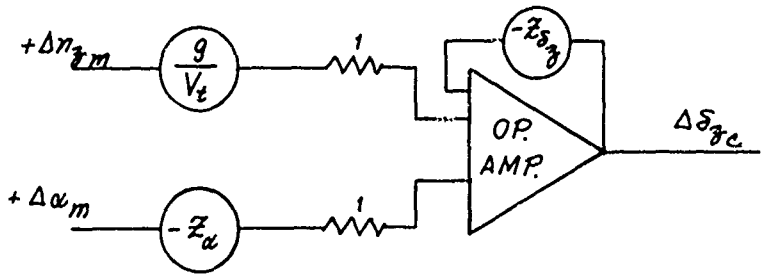

Another technique would be to write the feedforward expression

$$\Delta\delta_{z_c} = \left(\frac{\delta_{z_c}}{\dot{\alpha}}\right)\dot{\alpha}_m + \left(\frac{\delta_{z_c}}{\dot{\theta}}\right)\dot{\theta}_m + \left(\frac{\delta_{z_c}}{\alpha}\right)\Delta\alpha_m$$

$$= \left(\frac{\delta_{z_c}}{n_z}\right)\Delta n_{z_m} + \left(\frac{\delta_{z_c}}{\alpha}\right)\Delta\alpha_m \qquad (2.39)$$

where

$$\left(\frac{\delta_{z_c}}{\dot{\alpha}}\right) = \frac{1}{Z_{\delta_{z_p}}} \; ; \; \left(\frac{\delta_{z_c}}{\dot{\theta}}\right) = \frac{-1}{Z_{\delta_{z_p}}} \; ; \; \left(\frac{\delta_{z_c}}{\alpha}\right) = \frac{-Z_{\alpha_p}}{Z_{\delta_{z_p}}} .$$

$$\left(\frac{\delta_{z_c}}{n_z}\right) = \frac{g}{V_{t_p} Z_{\delta_{z_p}}}$$

This latter technique does not allow convenient individual control over each stability and control derivative of the plant as is possible when the former technique is utilized.

Although illustrated for a simplified equation, the application of these concepts to the full set of linearized equations is straightforward. Both ideas, however, are based on a linearization of the equations of motion about a trim condition. While this may be satisfactory for relatively small perturbations about the trim conditions, errors in control motion could result for large variations in altitude or velicity from the initial condition. If the velocity perturbation is relatively small with respect to the initial condition, but altitude variations are large such as in flying a relatively constant speed approach, then it would be desirable to add a feedforward based on the change in dynamic pressure with altitude. This is relatively easy to accomplish if

the linearization of the equations of motion also includes a perturbation in air density. If the velocity perturbations are also large compared to the initial condition, then alternate techniques are needed. One method would be to treat the terms sensitive to velocity and dynamic pressure changes, which are constants in a linearization, as functions of those variables directly, i.e., g/V or $\bar{q}S$. This technique would increase the equipment required to compute the control motions of the plant to achieve model following, but is relatively easy to accomplish.

As previously stated in this section and as discussed, for example, in References 1 and 4, the sensitivity to errors in the feedforwards can be reduced when feedbacks are introduced which compare the desired state of the model with the achieved state of the plant in the control law. In fact, as the feedback gain is increased, the control law becomes less dependent upon the feedforwards. However, there are practical limits on the values of the feedback gains based on closed-loop stability, sensor noise, etc. A sensitivity minimization approach to the determination of feedback gains is briefly described in Reference 4. In practice, the feedback gains can be selected based on the maximum gain available that will not significantly compromise closed-loop stability or result in undesirable control surface rates of motion which could place excessive demands on the hydraulic system used to actuate the control surfaces of the plant. Since the feedback gains were designed to be constants to simplify the control system complexity, it should be noted that the effect on the output of the control surface will be a function of dynamic pressure since the actual control effectiveness of the surface is a function of dynamic pressure. Thus the aerodynamic gain will vary with flight condition. This increases the actual feedback system gain as dynamic pressure increases and could result in closed-loop instabilities. This condition can be minimized if the feedback gain is selected at the highest dynamic pressure to be encountered in the simulation or by making the feedback gains functions of dynamic pressure to control their gain and closed-loop system stability.

The actual choice of feedback signals to the control surface is dependent upon the sensor signals available and the primary degrees of freedom

that the control surface will control. For example, the elevator is not an effective device for direct control of velocity, thus it would be of little value to feed back velocity to the elevator. The elevator controls primarily pitch attitude and rate, thus it would be of value to feed back errors in these responses to the elevator. Similar physical arguments for the choice of feedback error signals to the control surfaces are applicable. In addition, it was previously indicated that the direct lift flap feedforward could be mechanized in terms of $\dot{\alpha}$ and q or Δn_z. While feedback of Δn_z might be efficient, the acceleration signals sensed by the aircraft could have a poor signal-to-noise ratio. Thus, this type of feedback is not utilized in TIFS.

2.4 LIMITATIONS ON MOTION SIMULATED BASED ON COMPATIBILITY OF INITIAL CONDITIONS

The preceding section discussed the concept of feedforward model following. The desired control law was obtained by replacement of the plant state vector by the model state vector. Thus, if the plant and the model are initially at the same trim condition, perfect matching of the motion of the model to pilot commands could be achieved. The purpose of this subsection is to briefly examine the situation where the plant is unable to initially trim to the same condition as the model.

The control law for feedforward model following can be stated in terms of the changes in state and control from trim; thus the control law is not an explicit function of the initial condition. However initial conditions affect the stability and control derivatives used in the F and G matrices of (2.34), for example. Therefore, while it is possible to match the perturbed state vector of the model even if the initial conditions are not matched, it would not be possible to match added responses which are dependent upon the initial conditions. For example, consider the illustration of speed mismatch (discussed in Reference 2) concerned with matching Δn_z in maneuvers with trim speed mismatch. If the perturbed aircraft states $\Delta\theta$ and $\Delta\alpha$ are matched, then, since Δn_z is dependent on trim velocity (see Equation (2.47) below), it would not be possible to match the Δn_z time history. However, as discussed

in both References 2 and 11, it would be possible to define a pseudo state vector such that a trade-off is achieved, (i.e., achieve Δn_z following by relaxation of following on another state or states of the aircraft). Since the pilot normally has no way to sense $\Delta\alpha$, it is a reasonable variable to trade. Thus a pseudo angle of attack is derived which would allow matching of the load factor time history to control inputs. It will be obvious below that, for this example, the control time history achieved is the linear combination of two control time histories, one which is required to perfectly match the model states plus an additional part which is a function of the speed mismatch and the trade-off between angle of attack and normal acceleration following. In the limit, as the speed mismatch approaches zero, the control motion obtained is identical to that required for perfect matching of the responses of the aircraft.

Recall from the previous section that for linearized equations of motion the feedforward model-following control law is given by Equation (2.34). However, due to the mismatch of initial velocity, it is now necessary to define a pseudo state vector which is required to achieve model following of the desired responses. Thus define

$$\dot{x}^*_m = \dot{x}_m + [C]\,\dot{x}_m \tag{2.40}$$

$$x^*_m = x_m + [C]\,x_m \tag{2.41}$$

Substitution of the pseudo state vector for the model state vector will now yield the control law required for model following of the desired responses.

$$G_p u_p = \dot{x}_m + [C]\,\dot{x}_m - F_p\left\{x_m + [C]\,x_m\right\} \tag{2.42}$$

$$G_p u_p = \dot{x}_m - F_p x_m + [C]\,\dot{x}_m - F_p [C]\,x_m \tag{2.43}$$

Thus

$$G_p u_p = G_p\left[u_{p_1} + u_{p_2}\right] \tag{2.44}$$

where $G_p u_{p_1}$ can be defined as $\dot{x}_m - F_p x_m$ and $G_p u_{p_2}$ can be defined as $[C]\dot{y}_m - F_p[C]y_m$. Thus $G_p u_{p_2}$ is a function of the matrix $[C]$ which is dependent upon the velocity mismatch and the desired response matching.

Now let us examine the example of acceleration following with velocity mismatch. The Z -force equation of motion (in the linearized form presented in Reference 1) can be written as follows for an aircraft in trim level flight, neglecting the effects of ΔV, since we are primarily concerned with the initial response to abrupt control inputs:

$$Z_{\delta_{e_p}} \Delta\delta_{e_p} + Z_{\delta_{y_p}} \Delta\delta_{y_p} + Z_{\delta_{x_p}} \Delta\delta_{x_p} = \dot{\alpha}_p - \dot{\theta}_p - Z_{\alpha_p} \Delta\alpha_p \tag{2.45}$$

with $\Delta\alpha_p = \alpha_p - \alpha_{trim_p}$ and $\Delta n_z = V_{trim}/g\ (\dot{\alpha} - \dot{\theta})$. Since it is desired to match Δn_z and $\dot{\theta}$ with velocity mismatch, then a pseudo angle of attack can be defined by equating Δn_z at the two trim conditions for the model and plant

$$\dot{\alpha}_p^* = \dot{\alpha}_m + \left(1 - \frac{V_{t_m}}{V_{t_p}}\right)(\dot{\theta}_m - \dot{\alpha}_m) \tag{2.46}$$

and

$$\Delta\alpha_p^* = \Delta\alpha_m + \left(1 - \frac{V_{t_m}}{V_{t_p}}\right)(\Delta\theta_m - \Delta\alpha_m) \tag{2.47}$$

A pseudo state vector can now be defined as

$$\begin{bmatrix} q_m \\ \Delta\theta_m \\ \Delta V_m \\ \Delta\alpha_m^* \end{bmatrix} = \begin{bmatrix} q_m \\ \Delta\theta_m \\ \Delta V_m \\ \Delta\alpha_m \end{bmatrix} + \begin{bmatrix} 0 & 0 & 0 & 0 \\ 0 & 0 & 0 & 0 \\ 0 & 0 & 0 & 0 \\ 0 & \left(1 - \frac{V_{t_m}}{V_{t_p}}\right) & 0 & -\left(1 - \frac{V_{t_m}}{V_{t_p}}\right) \end{bmatrix} \begin{bmatrix} q_m \\ \Delta\theta_m \\ \Delta V_m \\ \Delta\alpha_m \end{bmatrix} \tag{2.48}$$

Thus

$$[C] = \begin{bmatrix} 0 & 0 & 0 & 0 \\ 0 & 0 & 0 & 0 \\ 0 & 0 & 0 & 0 \\ 0 & \left(1 - \frac{V_{t_m}}{V_{t_p}}\right) & 0 & -\left(1 - \frac{V_{t_m}}{V_{t_p}}\right) \end{bmatrix} \tag{2.49}$$

Substitution of (2.46) and (2.47) into (2.45) yields (neglecting $Z_{\delta_{e_p}}$ and $Z_{\delta_{x_p}}$)

$$Z_{\delta_{z_p}} \Delta\delta_{z_p} = \dot{\alpha}_m + \left(1 - \frac{V_{t_m}}{V_{t_p}}\right)(\dot{\theta}_m - \dot{\alpha}_m) - \dot{\theta}_m - Z_{\alpha_p}\left\{\Delta\alpha_m + \left(1 - \frac{V_{t_m}}{V_{t_p}}\right)(\Delta\theta_m - \Delta\alpha_m)\right\} \tag{2.50}$$

Thus

$$Z_{\delta_{z_p}} \Delta\delta_z = \left[\dot{\alpha}_m - \dot{\theta}_m - Z_{\alpha_p}\Delta\alpha_m\right] + \left(1 - \frac{V_{t_m}}{V_{t_p}}\right)\left[\dot{\theta}_m - \dot{\alpha}_m - Z_{\alpha_p}(\Delta\theta_m - \Delta\alpha_m)\right] \tag{2.51}$$

which is the form of the control previously described in (2.44).

If it is further assumed that $Z_{\delta_{e_m}}$ is also zero, then

$$\Delta n_{z_m} = \frac{V_{t_m}}{g}(\dot{\alpha}_m - \dot{\theta}_m) = \frac{V_{t_m}}{g} Z_{\alpha_m} \alpha_m \tag{2.52}$$

Substitution of this expression into the above equation and using the definitions

$$\frac{m}{\bar{q}S} = \frac{C_{L_{trim}}}{g} \quad \text{and} \quad \Delta\gamma_m = \Delta\theta_m - \Delta\alpha_m \tag{2.53}$$

the following expression results

$$\Delta\delta_z = \frac{C_{L_{trim}}}{C_{\gamma_{\delta_z}}}\left[\Delta n_z \left(1 - \frac{Z_{\alpha_p} V_{t_p}}{Z_{\alpha_m} V_{t_m}}\right) + \left(1 - \frac{V_{t_m}}{V_{t_p}}\right)\frac{Z_{\alpha_p} V_p}{g}\ \Delta\gamma_m\right] \tag{2.54}$$

which is equivalent to the result obtained in Reference 2. Substitution of the appropriate numbers for a particular simulation under consideration will determine the direct lift flap deflection limits on the longitudinal simulation envelope for the velocity mismatch condition (see Sections 3.4 and 4.5).

Reference 2 also describes the effect of velocity mismatch on lateral-directional maneuvers.

Another form of initial condition mismatch is the possibility of trim attitude mismatch. In this condition it is possible to achieve a velocity match, but either it is impossible or undesirable to trim the plant to the same attitude as the model. For this condition, it would be desirable to define an

axis system in the model which is parallel to the axis system of the plant in its trim condition and to then match the states of this rotated axis system of the model to determine the control motion required for simulation. A similar concept is described in Reference 1. While the motion of the model cockpit would be simulated, difficulties could be encountered based on the sensitivity of the pilot's orientation to the motion. For example, in this condition the total acceleration at the cockpit acting on the pilot would be matched; however, the acceleration components acting on the pilots would not be correct unless the seat could be tilted to compensate for the attitude mismatch. Thus while such a simulation could be performed in the manner described, the value of this simulation procedure would be limited by the sensitivity of the pilot to the acceleration components in the plane of symmetry of the aircraft. This limitation would not be encountered if the nose of the model aircraft were cranked to the attitude of the plant reference axis. Thus attitude mismatch simulations could be physically interpreted as the evaluation of the model aircraft with the nose of the model rotated through an angle equivalent to the attitude mismatch. For this condition it is possible to achieve perfect following at the cockpit.

A variation of this problem of attitude mismatch where the difference in trim attitude is relatively small is described in Reference 9. For that investigation, it was not possible for TIFS to achieve the angle of attack of the model at low speeds without compromising the simulation envelope. However, the particular interest for that program was to evaluate aerodynamic nonlinearities which occurred at high angle of attack and low speeds approaching the 1.2 V_S for the TIFS. In this investigation the model and plant initial trim conditions were the same; however, the aerodynamic data was shifted by a constant value. In this manner the high angle of attack effects could be investigated without placing the TIFS aircraft at these high angles. Physically, this simulation technique can be interpreted as a shift in the model zero lift line.

Thus to briefly summarize the ideas in this section, it has been indicated that in-flight simulation is not limited to identical initial conditions

of the plant (TIFS) and model. Simulations are possible with a reduced simulation envelope, etc. for mismatch conditions. It must be remembered, however, that in this case it is no longer possible to match all items of interest and trade-offs must be made as required to ensure an adequate investigation of the desired problem under evaluation.

2.5 TRANSFORMATIONS, SENSORS, AND GUST ENVIRONMENT

In order to assure that model following has been achieved during an in-flight simulation, it is necessary to be able to compare the responses of the model with those obtained by the plant. This comparison is also required in the feedback signals used to reduce the sensitivity of the following to inaccuracies in the feedforward gains. In order to make this comparison, the responses must be compared at a selected location and in the same axis system. The equations of motion of the model would normally be computed at the center of gravity of the model, while the sensors determine the responses of the plant at the center of gravity of the plant. In addition, angular velocities and Euler angles, etc. are determined in a specific body axis of the plant. Comparisons between the model and plant (TIFS) responses are performed by transformation of the model responses to the plant center of gravity for quantities that are position-sensitive (e.g., angle of attack, sideslip, velocity). The transformations are based on the kinematics of a rigid body and are discussed in Reference 12. The exact transformations are nonlinear and sometimes complex, but simplifications can often be used in producing required signals. Responses which are axis-sensitive (e.g., angular velocities and attitudes) must be compared in a selected axis system, normally that of the plant measurements. The transformations used when the axis system of the model and plant are parallel are presented in Reference 8. It must also be remembered that the initial conditions supplied to the model in flight are signals from the plant sensor output and must be appropriate to the axis system utilized to compute the equations of motion of the model aircraft. Through the use of simple rotations, the equations of motion of the model can always be written in an axis system parallel to the axis of the plant measurement. From the kinematics of rigid

bodies, once the motions of the model and the plant have been matched at any point, then the rigid body motion at all points (e.g., the pilot station) is also matched provided the relationship between the model and the plant orientation is fixed.

In order to implement any in-flight simulation, it is necessary to be able to determine the state of the aircraft by the use of sensors. The sensor signals used for model following on the TIFS aircraft are described in References 1 and 4. Based on the discussion previously presented in this section to develop the equations of motion of an aircraft, it is desirable that both inertial and total signals be available for the simulation. In addition, the signals used for model following should not introduce undesirable noise and should possess a unity transfer function in the frequency range of primary interest to the simulation. If these conditions are not reasonably satisfied then comparison of the states of the model and the plant would be contaminated by excessive noise or would be dependent upon the ability to compensate for the sensor dynamics.

For flight in smooth air, the principles of variable stability are readily grasped. Consideration of atmospheric turbulence, however, introduces some additional points. First, consider the behavior of a variable stability airplane when it encounters turbulence during a test flight. The action of a response-feedback system is essentially the same as altering the aerodynamic stability derivatives of the test airplane. If this is done in such a way as to reproduce the set of stability derivatives of another airplane that is to be simulated, then it will be the altered set of derivatives that determines the test airplane's response to the turbulence it encounters. The response accordingly is that of the airplane being simulated, and so we can say that a response-feedback variable stability airplane simply responds as it should to the turbulence it encounters. One word of caution is necessary, however, in connection with this statement. In case the air is turbulent, it is necessary to distinguish the two kinds of angle of attack -- inertial and aerodynamic. If the variable stability system alters C_{m_α} on the basis of a measurement of aerodynamic angle of attack, then the effect of a gust on the

airplane's pitching moment will be reproduced correctly as stated above. This would not be true, however, if the angle of attack used in the variable stability system were to be computed by subtracting flight path angle from pitch attitude.

With a model-following system, the situation is different. If the model responds only to the pilot's control inputs, there will be no outputs from the model due to the variable stability airplane encountering turbulence. The signals compared for model following should be inertial since the motion equations of the model are computing inertial motion, and by following the inertial signals the system would tend to act as a gust alleviation system. In addition, by measuring the gust components (α_g , β_g , q_g , p_g , and V_g) and knowing the gust-sensitive stability derivatives of the plant, a modified control law can be developed to input signals to the plant controls to alleviate the gust. The ability to alleviate the natural atmospheric environment then allows control over the simulation of atmospheric disturbances.

Once the natural atmospheric environment is sensed and alleviated, the experimenter can use the same measured gust signals as disturbances to the model producing the motion the model would experience flying in that actual gust environment. Or for a more controlled experiment he can feed a taped gust signal to the model. Lastly, he could omit feeding disturbances to the model to produce the smooth-air environment within the capability of the gust alleviation system.

In regard to producing correct responses to canned turbulence, the importance of having the direct lift flaps and side force surfaces that are available in TIFS should be emphasized. These surfaces can generate directly the forces required to produce the correct responses. Applying canned turbulence only to the aileron, elevator and rudder servos clearly is insufficient, in that it can produce correct moments on the airplane but not the correct forces simultaneously. Since pilot rating of the handling qualities of an aircraft can be quite sensitive to the effect of the turbulence environment, the ability to alleviate and simulate gusts can be quite important to controlling an in-flight simulation experiment.

SECTION III

ATTITUDE AND FLIGHT PATH IN UNACCELERATED FLIGHT

In this section and Section IV, the basic trim attitude, flight path and dynamic motion capabilities are discussed. From this basic data the limits of a specific simulation can be determined. A running example is used to illustrate how these limits can be estimated. The variables of concern in this section are the pitch and yaw Euler angles, θ and ψ; the flight path angles, γ and χ; the airspeed, V; and the aerodynamic angles, α and β. Section IV deals with the ranges of body angular rates p, q, and r; body angular accelerations, $\dot{p}$, $\dot{q}$, and $\dot{r}$; and linear accelerations n_x, n_y, and n_z.

The Euler angles θ and ψ are related kinematically to the angles γ, χ, α, and β and hence are similarly constrained. The relationships for small angles are

$$\theta = \gamma + \alpha \tag{3.1}$$

and

$$\psi = \chi - \beta \tag{3.2}$$

In what follows, the limits on γ, χ, α, and β are discussed and Equations (3.1) and (3.2) should be used to relate these to θ and ψ.*

3.1 GENERAL RELATIONSHIPS FROM THE FORCE EQUATIONS

The variables V, γ, χ, α and β are related through the balance of forces. Equations (2.1), (2.4) and (2.16) state this balance in a mixed axis system where (2.1) is along the wind x axis and (2.4) and (2.16) are along body y and z axes. It is convenient to use pure wind axes to express simulation relationships since then C_L and C_D can be used directly without reference to the body axes of the TIFS and the model. It is perhaps also helpful to modify these wind axis equations so that the flight path angle rates

---

* For velocity-matched simulation, there is no limit on χ and therefore no limit on ψ. The limitation on χ arises when matching ψ with velocity not matched.

with respect to the earth, $\dot{\gamma}$ and $\dot{\chi}$ appear separately since, for flight path matching, such as is required for one-to-one landing approach simulation, the angles γ and χ are matched. The modified wind axis system differs from conventional wind axes only by a rotation $-\mu$ about the x_w axis to bring the z_w axis into the vertical plane (see Figure 3.1). (The angles χ, γ, and μ are the Euler angles locating the conventional wind axis system after the notation of Miele in Reference 13.) Then the force equations become

$$m\dot{V} = T_{x_w} - \bar{q} S C_D - mg \sin\gamma \tag{3.3}$$

$$\cos\gamma \cdot mV\dot{\chi} = (T_{y_w} + \bar{q} S C_Y)\cos\mu - (T_{z_w} - \bar{q} S C_L)\sin\mu \tag{3.4}$$

$$-mV\dot{\gamma} = (T_{y_w} + \bar{q} S C_Y)\sin\mu + (T_{z_w} - \bar{q} S C_L)\cos\mu + mg\cos\gamma \tag{3.5}$$

To match $\dot{V}$, $\dot{\chi}$, and $\dot{\gamma}$ and thus V, χ, and γ for initial conditions matched and c.g.'s coincident,

$$\frac{1}{m}(T_{x_w} - \bar{q} S C_D) = \frac{1}{m_m}(T_{x_{w_m}} - \bar{q}_m S_m C_{D_m}) \tag{3.6}$$

$$\frac{1}{m}(T_{y_w} + \bar{q} S C_Y) = \frac{1}{m_m}(T_{y_{w_m}} + \bar{q}_m S_m C_{Y_m}) \tag{3.7}$$

$$\frac{1}{m}(T_{z_w} - \bar{q} S C_L) = \frac{1}{m_m}(T_{z_{w_m}} - \bar{q}_m S_m C_{L_m}) \tag{3.8}$$

With this one-to-one matching, the altitude is matched so that $\bar{q} = \bar{q}_m$, and therefore in unaccelerated flight, or for TIFS and model c.g.'s and cockpits coincident in accelerated flight,

$$-\frac{T_{x_w}}{\bar{q} S} + C_D = \frac{W/S}{(W/S)_m}\left(-\frac{T_{x_{w_m}}}{\bar{q}_m S_m} + C_{D_m}\right) \tag{3.9}$$

$$\frac{T_{y_w}}{\bar{q} S} + C_Y = \frac{W/S}{(W/S)_m}\left(\frac{T_{y_{w_m}}}{\bar{q}_m S_m} + C_{Y_m}\right) \tag{3.10}$$

$$-\frac{T_{z_w}}{\bar{q} S} + C_L = \frac{W/S}{(W/S)_m}\left(-\frac{T_{z_{w_m}}}{\bar{q}_m S_m} + C_{L_m}\right) \tag{3.11}$$

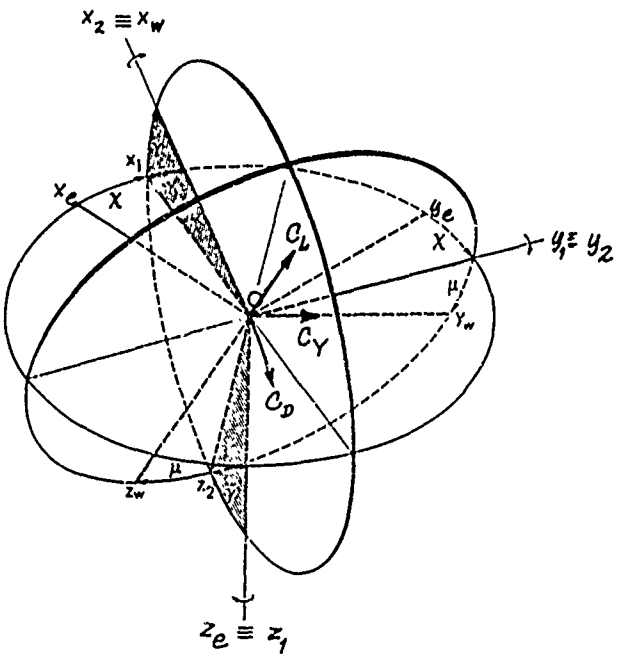

Figure 3.1 System of Rotations Leading From Earth Axes to Modified Wind Axes (χ and γ'), to μ Wind Axes

The C_L and C_D of TIFS are functions of direct lift flap deflection as well as angle of attack, Fowler flap deflection, and landing gear position. The term $T_{z_w}/\bar{q}S$ in Equation (3.11) is small compared with C_L and can be neglected for most simulation work. Also, $C_{L_{\delta_e}}$ can be neglected without much loss of accuracy. Therefore, a particular simulation requirement in terms of δ_z and δ_x can be determined by expanding Equations (3.9) and (3.11) in terms of δ_x and δ_z, solving Equation (3.11) for δ_z and, using that result, solving Equation (3.9) for δ_x. Equation (3.10) can be solved for δ_y but there is an important coupling through $C_{Y_{\delta_r}}$ which makes it necessary to solve the yawing moment equations as well (see Section 4, Equation 4.4).

3.2 TIFS AERODYNAMIC FORCES AND THRUST

The C_L and C_D functions have been determined in wind tunnel tests (Reference 14), and flight tests have been conducted to provide final substantiation (primarily Flights 27 and 28). The flight test data have generally agreed with the wind tunnel except near $C_{L_{max}}$. These data have been analyzed and reported in Reference 15. Analytical expressions which are suitable for simulation planning have been determined to fit the experimental data. They are

$$C_L = .15 + .105\alpha + .012\delta_e + .34\left(\frac{\delta_z + 3.5}{30.}\right)\left[\frac{.3 + \left(\frac{\delta_z + 3.5}{30.}\right)^2}{.1 + \left(\frac{\delta_z + 3.5}{30.}\right)^2}\right] + .25\left(\frac{\delta_F}{40.}\right) \quad (3.12)$$

and

$$C_D = C_{D_0} + kC_L^2 \quad (3.13)$$

where

$$C_{D_0} = .028 + .023\left(\frac{\delta_z}{30.}\right)^2 + .037\left(\frac{\delta_F}{30.}\right)^2 + .027G + .045\left(\frac{\delta_y}{30.}\right)^2$$

$$k = .037 + .034\left(\frac{\delta_z}{30.}\right)^2 - .011\left(\frac{\delta_y}{30.}\right)^3$$

G = 0 or 1 depending on whether the landing gear is up or down, and all angles are in degrees.

These expressions were obtained for $\beta = 0$ but can be used for a small range of β.

There are six limitations which bound the regions of permissible C_L and C_D in 1 g flight. They are:

1) Direct lift flap deflection limits of $\pm 35°$.
(These are operational limits. The physical stops in the flap drive mechanism are located at $\pm 40°$.)

2) δ_f vs. α for stall.

3) δ_f vs. α for high speed buffet.

4) δ_f vs. C_L for aft fuselage structural limit.

5) V_{max} (or equivalently $C_{L\,min}$ in 1 g flight).

6) δ_F vs. V_e structural limit.

Items 1), 2) and 5) are self-explanatory. The buffet and aft fuselage structural limits, items 3) and 4), are discussed more fully in Section IV. Item 6) is a standard C-131 structural limitation. These limits and the others above can be described analytically as follows

1) $$-35.^\circ \leq \delta_f \leq 35.^\circ \tag{3.14}$$

2) $$\alpha \leq 10.4 - 1.46\left(\frac{\delta_f + 3.5}{30}\right)\left(\frac{.3 + \left(\frac{\delta_f + 3.5}{30}\right)^2}{.1 + \left(\frac{\delta_f + 3.5}{30}\right)^2}\right) \tag{3.15}$$

3) $$\alpha \geq -1.52 - 7.39\left(\frac{\delta_f + 3.5}{30.}\right)\left(\frac{.3 + \left(\frac{\delta_f + 3.5}{30}\right)^2}{.1 + \left(\frac{\delta_f + 3.5}{30}\right)^2}\right) \tag{3.16}$$

4) $$C_L \geq .16 + .14\left(\frac{\delta_f + 3.5}{30}\right)\left(\frac{.3 + \left(\frac{\delta_f + 3.5}{30}\right)^2}{.1 + \left(\frac{\delta_f + 3.5}{30}\right)^2}\right) \tag{3.17}$$

5) $$V_e \leq 295 \text{ KEAS or } C_L \geq .19 \tag{3.18}$$

6) $$\delta_F \leq \frac{40}{66}(206 - V_{e_{KT}}) \leq 40 \tag{3.19}$$
(all angles in degrees).

The C_L function, together with the limits defined above, is plotted in Figure 3.2. This graph does not show the effect of Fowler flap deflection; however, that can be added analytically without difficulty using Equations (3.12) and (3.19).

The TIFS thrust force acts along the fuselage reference line so that $T_x = T$ and $T_z = T_y = 0$. Therefore,

$$\begin{aligned} T_{x_W} &= T \cos\alpha \cos\beta \approx T \\ T_{y_W} &= -T \cos\alpha \sin\beta \approx -T \frac{\beta}{57.3} \\ T_{z_W} &= -T \sin\alpha \approx -T \frac{\alpha}{57.3} \end{aligned} \tag{3.20}$$

An analytical representation of the thrust force was determined and documented in Reference 1 for preliminary design work. It gives thrust as the following function of true airspeed, altitude and throttle position

$$T = (\delta_x - 34.)\left[320. + \frac{V}{100}\left(8.88 \frac{h_p}{10^4} - 36.4\right) - 63.2 \frac{h_p}{10^4}\right] \tag{3.21}$$

where T is in pounds

δ_x is in degrees, $34.^\circ \leq \delta_x \leq 90^\circ$

V is in ft/sec

and h_p is in ft

The side force coefficient as a function of δ_y, β, and α has been defined by wind tunnel test and substantiated at $\delta_z = \delta_F = 0$ by flight tests reported in Reference 4. The wind tunnel data were fitted analytically in TIFS Memo 127 for the situation $\delta_z = \delta_F = 0$. The body axis C_Y was used. That analytical fit is quoted here with the appropriate transformation term added to give C_Y in wind axes, i.e.,

$$C_Y = \frac{C_y}{\cos\beta} + C_D \tan\beta \approx C_y + C_D \beta_{RAD} \approx C_y + \left(.029 + .068\alpha_{RAD} + .164\delta_y^2\right)\beta_{RAD}.$$

The resulting expression is

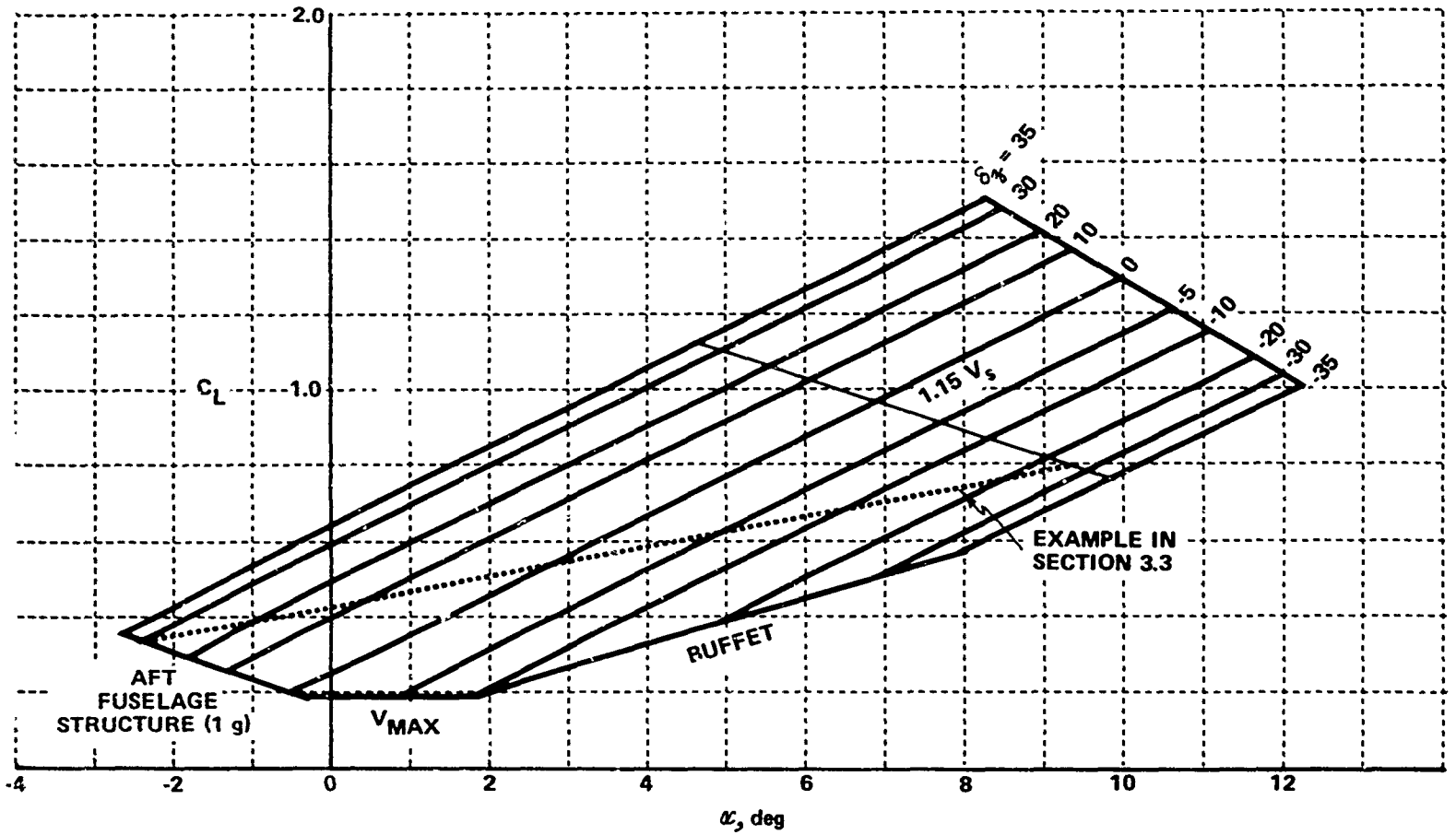

Figure 3.2 Lift Capability, $\delta_f = \delta_e = 0$

$$C_Y = -.017\beta + \left(1. - .23\frac{\alpha}{10}\right)\left[.075\left(\frac{\delta_y - .72\beta}{10}\right) - .0056\left(\frac{\delta_y - .72\beta}{10}\right)^3\right] + .005\delta_r + .367\frac{r}{V}$$

All angles in degrees, V in fps, and $-12.3° \leq \beta \leq 12.3°$.

This relation is derived for $\delta_g = \delta_F = G = 0$ but will be assumed applicable to conditions involving non-zero flap deflection and/or gear down until more flight tests can be made. The $C_{Y_{TRIM}}$ is plotted in Figure 3.3 for $\alpha = 5°$ using Equations (3.22), (4.16), and (4.17). (Including the trim position of the rudder makes a significant difference in the value of $C_{Y_{TRIM}}$.)

The value of $C_{Y_{\delta_r}}$ assumed here is taken from TIFS Memo 167 and the number for C_{Y_r} is from TIFS Memo 565. The numbers in TIFS Memo 565 are derived from flight tests but in some instances are not judged reliable. In these cases the data based on wind tunnel tests in TIFS Memos 127 and 167 are used.

3.3 DETERMINATION OF SIMULATION RANGE -- AN EXAMPLE

Consider the one-to-one simulation of a large bomber on an emergency landing approach. The bomber's gross weight is high and the approach speed is high. Table 3.1 summarizes the pertinent parameters describing the model. Table 3.2 summarizes the analytical description of TIFS as presented above and in Section IV.

Several variables will be examined to determine the range of simulation around the nominal trim speed, which for this example is assumed to be 190 knots.

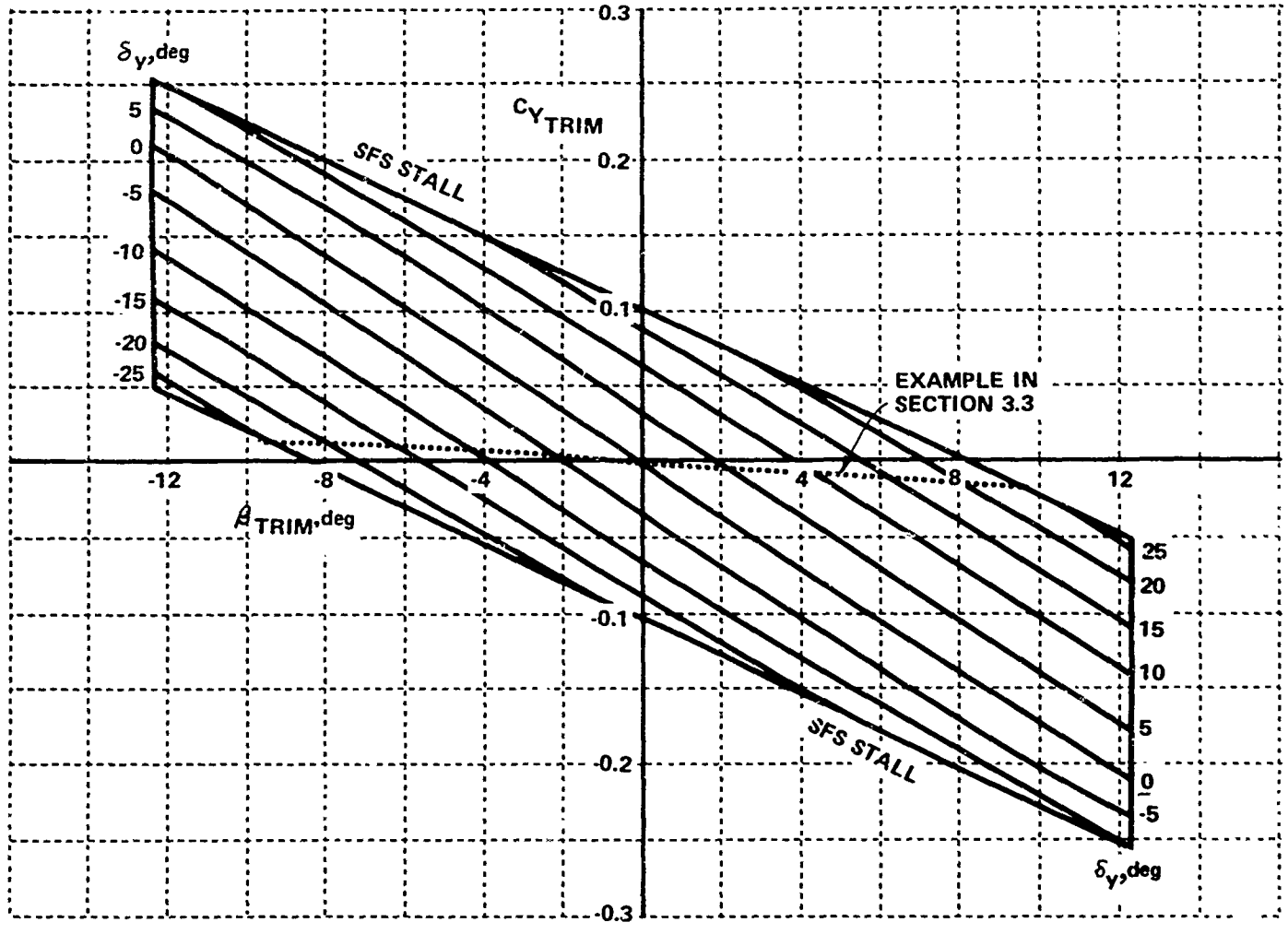

Figure 3.3 Trim Side Force Capability, α = 5 Degrees

TABLE 3.1

ASSUMED MODEL PARAMETERS

$$C_L = 1.47 + .13\alpha + .015\delta_e + 2.39\frac{q}{V} + .17\frac{\dot{\alpha}}{V}$$

$$C_D = .120 + .0384\, C_L^{\,2}$$

$$C_Y = -.012\beta + .0026\delta_r + .00046\delta_a + .037\frac{r}{V}$$

$$T = (\delta_T - 30) \cdot 1000 \text{ lb, in the } x, z \text{ plane along } x \text{ axis}$$

$$C_\ell = -.0003\beta + .0002\delta_r - .0013\delta_a - .74\frac{p}{V} + .25\frac{r}{V}$$

$$C_m = -.31 - .013\alpha - .05\delta_e - 3.90\frac{q}{V} - 1.44\frac{\dot{\alpha}}{V}$$

$$C_n = .0025\beta - .0010\delta_r - .0002\delta_a - .13\frac{p}{V} - .18\frac{r}{V}$$

W = 350,000 lb	I_{xx} = 2,350,000 slug-ft^2
S = 1950. sq ft	I_{yy} = 6,750,000 slug-ft^2
$\bar{c}$ = 15.3 ft	I_{zz} = 8,890,000 slug-ft^2
b = 136.7 ft	I_{xz} = -90,000 slug-ft^2

TABLE 3.2

TIFS PARAMETERS

C_L = Equation (3.12)	W = 52,000 lb
C_D = Equation (3.13)	S = 920 sq ft
C_Y = Equation (3.22)	$\bar{c}$ = 9.52 ft
T = Equation (3.21)	b = 105.3 ft
C_ℓ = Equation (4.16)	I_{xx} = 239,000 slug-ft^2
C_m = Equation (4.18)	I_{yy} = 532,000 slug-ft^2
C_n = Equation (4.17)	I_{zz} = 764,000 slug-ft^2
	I_{xz} = negligible

3.3.1 Range in V and α

If a digital computer were used to calculate the TIFS control positions as V_m and α_m are varied, it would probably be programmed to solve (3.9), (3.11), and (4.18) for δ_y and δ_z increasing and decreasing the ΔV_M from trim until limits are encountered. For present purposes it is desirable to make some approximations so that hand computations and graphical solution can be made to gain some physical understanding of the limitations.

If, as suggested on page 40 the T_{z_W} terms are neglected in Equation (3.11), then $C_{L_{TRIM}} = \frac{W/S}{(W/S)_m} C_{L_{m_{TRIM}}}$. For trim, Table 3.1 gives $C_{m_m} = 0 = -.31 - .013\,\alpha_{m_{TRIM}} - .05\,\delta_{e_{m_{TRIM}}}$ or $\delta_{e_{m_{TRIM}}} = -6.2 - .26\,\alpha_{m_{TRIM}}$. Substituting for δ_{e_m} in the equation for C_{L_m} listed in Table 3.1 gives $C_{L_{m_{TRIM}}} = 1.38 + .126\,\alpha_{m_{TRIM}}$. Therefore with $W/S = 56.5$ and $(W/S)_m = 179.0$, $C_{L_{TRIM}} = (56.5/179.0)\, C_{L_{m_{TRIM}}}$ or $C_{L_{TRIM}} = .435 + .0398\,\alpha_{TRIM}$. A graphical solution for the δ_z vs. α variation to match α's is shown by the dashed line on Figure 3.1. The limits for this particular simulation turn out to be the aft fuselage structure at the high-speed end and the operational limit of 1.15 V at the low-speed end. The α limits can be read from Figure 3.2 and the velocity limits from the relation $V_{e_{KNOTS}} = \left(\frac{295.\, W/S}{C_L}\right)^{1/2}$. These are $-2.4 \leq \alpha_{DEG} \leq 9.4$ and $145. \leq V_{e_{KNOTS}} \leq 222.$

3.3.2 Range in γ

The basic relationships needed here are the approximation of (3.5) which gives $C_{L_{TRIM}} \approx \frac{W}{\bar{q} S}$ and (3.3) and (3.5) taken together which give

$$\tan \gamma \approx \frac{\frac{T}{\bar{q} S} - C_D}{C_L} \tag{3.23}$$

At each trim speed, $\tan \gamma$ and $\tan \gamma_m$ can be calculated for the δ_z specified by the dashed line in Figure 3.2. Then decisions can be made

regarding the use of the TIFS gear and Fowler flaps* to give an acceptable range of γ matching. For this example, an acceptable simulation range is obtained by operating with the gear down and $\delta_F = 0$. With $\delta_x = 34°$ giving $T = 0$ and $\delta_x = 90°$ giving T_{MAX} the range of γ available is shown in Figure 3.4. This is to be compared in the same figure with the model capability, $\delta_{T_m} = 30$ giving $T_m = 0$ and $\delta_{T_m} = 90$ giving $T_{m\,MAX} = 60{,}000$ lb. For a nominal approach point at 190 kt and a three-degree glide slope, the TIFS throttle will be trimmed at mid-range. There is ample range in γ to simulate typical deviations from the nominal conditions and up to a speed of 204 kt even a full throttle go-around can be matched. Above 204 kt, the TIFS gear must be up to simulate a full throttle go-around.

3.3.3 Range in β_{TRIM}

The range in trim sideslips is determined by solving (3.10), (4.2) and (4.4).

First, Equation (3.10) gives

$$C_Y = \frac{T}{\bar{q}S}\frac{\beta}{57.3} + \frac{W/S}{(W/S)_m}\left(C_{Y_m} - \frac{T_m}{\bar{q}_m S_m}\frac{\beta_m}{57.3}\right) \tag{3.24}$$

For a three-degree glide slope at $V = 190$ kt, $T/\bar{q}S = C_L \tan\gamma + C_D = (.458)(-.0523) + .0654 = .0414$ and $T_m/\bar{q}_m S_m = (1.45)(-.0523) + .201 = .125$. Therefore (3.24) becomes

$$\begin{aligned} C_Y &= (.0414)\frac{\beta}{57.3} - (.316)(.125)\frac{\beta_m}{57.3} + .316\,C_{Y_m} \\ &= 33.2 \times 10^{-6}\beta + .316\,C_{Y_m} \quad \text{since } \beta_m = \beta \\ &\approx .316\,C_{Y_m} \end{aligned} \tag{3.25}$$

* The landing gear effect is primarily drag with a small indirect effect on lift through the pitching moment change requiring an elevator angle change. However, the Fowler flap used to create drag must be balanced by a significant negative increment in δ_z to counter the lift change.

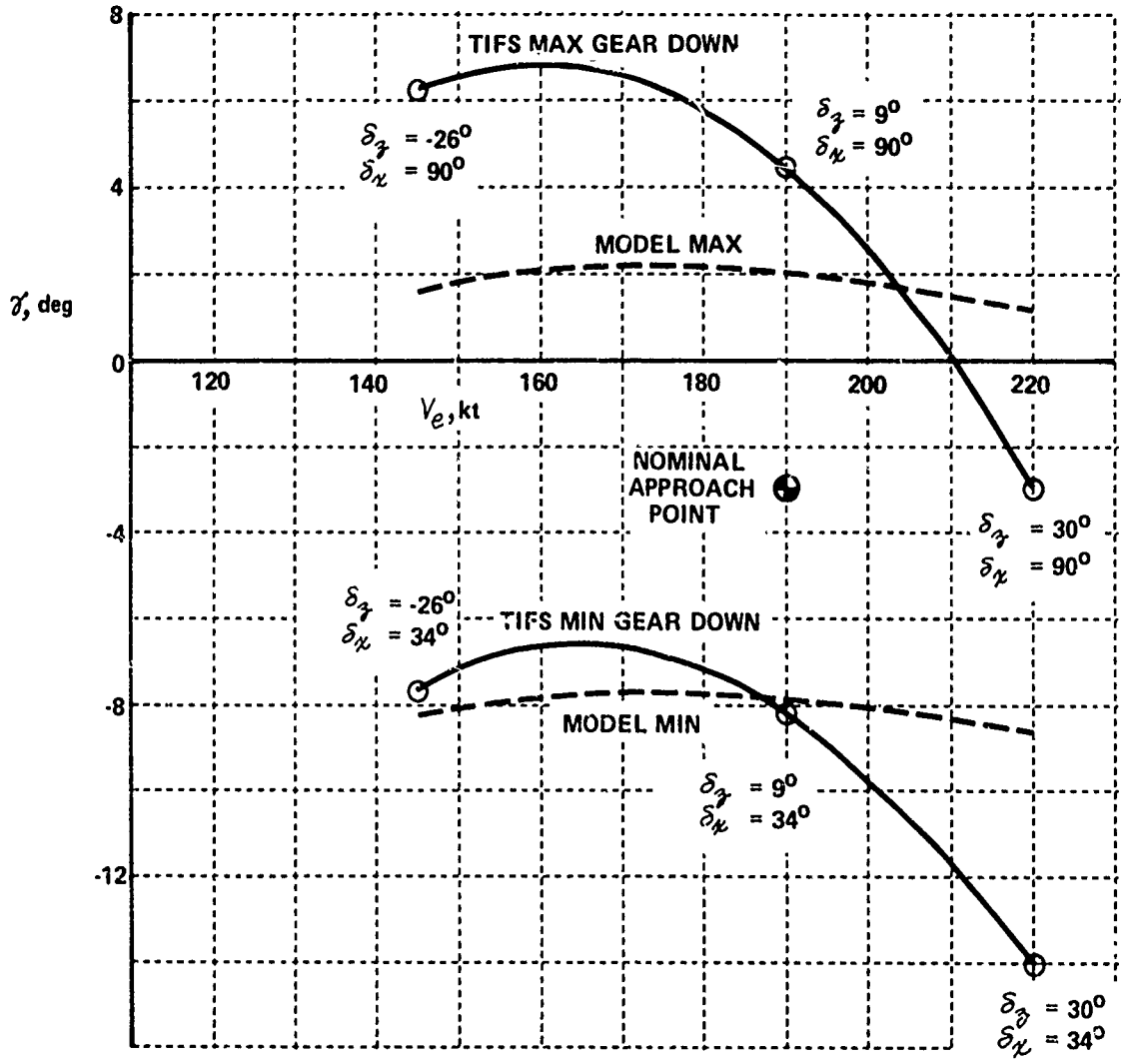

Figure 3.4 Vertical Flight Path Matching
Section 3.3 Example, $h_p = 0$, $\delta_f = 0$

Trimming the model using the data of Table 3.1 gives

$$C_{\ell_m} = 0 = -.0003\beta_m + .0002\delta_{r_m} - .0013\delta_{a_m}$$

$$C_{n_m} = 0 = .0025\beta_m - .0010\delta_{r_m} - .0002\delta_{a_m}$$

from which results $\delta_{r_{m_{TRIM}}} = 2.6\beta_{m_{TRIM}}$ and $\delta_{a_{m_{TRIM}}} = -.149\beta_{m_{TRIM}}$

Therefore

$$C_{Y_{m_{TRIM}}} = -.012\beta_{m_{TRIM}} + .0026(2.6\beta_{m_{TRIM}}) + .00046(-.149\beta_{m_{TRIM}})$$

or $$C_{Y_{m_{TRIM}}} = -.0053\beta_{m_{TRIM}} \qquad (3.26)$$

Using this equation in (3.25) gives

$$C_Y = -.0017\beta_{m_{TRIM}} = -.0017\beta_{TRIM} \text{ since } \beta\text{'s are matched} \qquad (3.27)$$

Plotting this line on Figure 3.3 gives a simulation range of $|\beta_m|_{TRIM} \leq 9.4°$ with the limit produced by side force surface stall.

The simulation is also limited by vertical tail structural loads. The structural limitations are discussed in Section IV. For trim sideslips under the conditions of this example, the structural limit is ± 7.40°. Therefore the structural limit governs.

3.3.3 Ranges in Crosswind Velocity and ϕ for Crosswind Simulation

When TIFS is flying in still air simulating an airplane flying with a crosswind, the crab angle is produced by sideslipping using the side force surfaces. Near the runway threshold, the evaluation pilot will perhaps make a transition to a wing-down sideslipping maneuver with the model to align his heading with the runway. The TIFS in this condition will be flying with practically no sideslip but with the wing down. The $W \sin \phi$ component is balanced by side force surface deflection. The maximum ϕ that can be achieved is thus limited by the maximum side force capability.

First, the maximum crosswind velocity is computed from $\Delta\psi_{m_{CRAB}} = \sin^{-1}\left(\frac{-\dot{y}_{m_{WIND}}}{V_m}\right) = -\beta_{TRIM}$ or $\dot{y}_{m_{WIND}} = V_m \sin\beta_{TRIM}$ where $\dot{y}$ is the crosswind component and V_m is the true airspeed of the model (Figure 3.5).

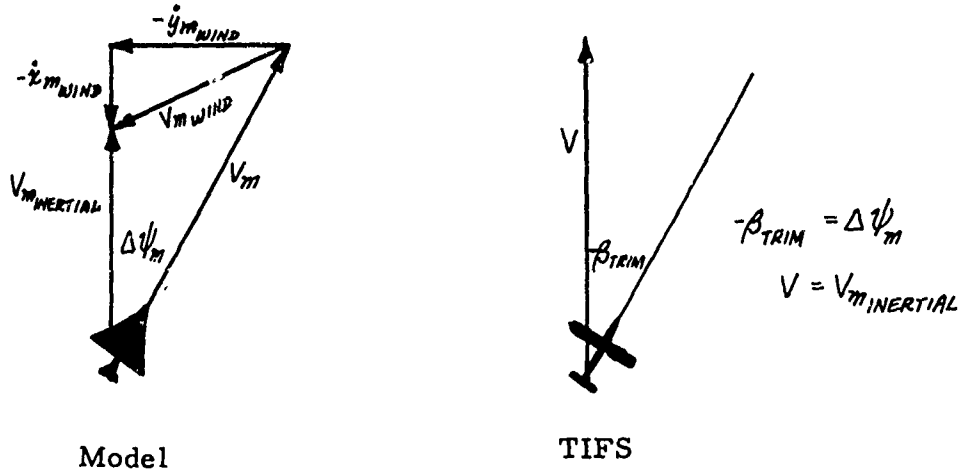

Model TIFS

Figure 3.5 Crosswind Simulation

Using Equation (3.4) multiplied by $\cos\mu$ plus Equation (3.5) times $\sin\mu$ the general side force condition with $\dot{\chi} = \dot{\gamma} = 0$ is

$$T_{y_W} + \bar{q}\,SC_Y + mg\cos\gamma\sin\mu = 0 \qquad (3.28)$$

With wings level, $\sin\mu = 0$ and therefore $T_{y_W} + \bar{q}SC_Y = 0$.
Also $C_\ell = C_n = 0$. These are just the conditions under which Figure 3.3 was derived. At V_e = 190 kt, α = 1.4° and therefore Figure 3.3 which is the capability at α = 5° is not exactly correct. However, as is evident from Equation (3.22), the angle of attack effect is not strong. Using Figure 3.3, the maximum trim sideslip with $T_{y_W} + \bar{q}SC_Y = 0$ or $C_Y = -\frac{T_{y_W}}{\bar{q}S} = \frac{T\beta}{\bar{q}S(57.3)} = \frac{.0414}{57.3}\beta$ (for a three-degree glide slope) = $.000723\beta$ is about 8.8°. This gives $(\dot{y}_{m_{WIND}})_{MAX}$ = 190(8.8/57.3) = 29.2 kt. This limit does not provide any margin for perturbations about the trim condition so a more reasonable maximum might be $(\dot{y}_{m_{WIND}})_{MAX}$ = 190(5.0/57.3) = 16.6 kt which would allow $\beta_M = \pm 4°$ about the trim condition while matching $\dot{\chi}_m$.

Second, the maximum bank angle after decrab is computed from (3.28) by writing

$$\frac{T_{y_W}}{\bar{q}S} + C_Y = -\frac{mg}{\bar{q}S}\cos\gamma\sin\mu \tag{3.29}$$

In this condition it is approximately true that $\sin\mu = \sin\mu_m$ and $\beta = 0$.

Therefore

$$C_{Y_{\beta=0}} \approx -\frac{mg}{\bar{q}S}\cos\gamma\sin\mu_m \tag{3.30}$$

or

$$(\sin\mu_m)_{MAX} = \frac{\bar{q}S}{mg\cos\gamma} C_{Y_{MAX_{\beta=0}}} \approx .219$$

from Figure 3.3, giving $\mu_{m_{MAX}} = 12.7°$ at 190 knot. Using (3.29) and the conditions $C_\ell = C_n = 0$ to trim the model in a steady sideslip with one wing down, the bank angle necessary to trim is given by $\mu_m = .304\,\beta_m$. Therefore, the model, for a decrab maneuver of 8.8°, needs to bank only about 2.7° - well within the TIFS capability of 12.7°.

3.4 ATTITUDE MATCHING WITH VELOCITY NOT MATCHED

Section IV discusses the problem of matching pitch attitude when there is a difference in the TIFS and model trim airspeeds. In this section, the basic relationships will be derived from the modified wind axis equations, (3.3), (3.4), and (3.5), and an example worked out.

First, the relationships between the wind axis Euler angles and the body axis Euler angles are needed. These can be obtained by equating like terms in the transformation from earth to wind axes which is

$$[T] = [\mu][\gamma][\chi] \tag{3.31}$$

in terms of wind axis Euler angles and

$$[T] = [\beta][\alpha]'[\phi][\theta][\psi] \tag{3.32}$$

The exact expressions for $\sin\gamma$ and $\sin\chi$ are

$$\sin\gamma = \cos\alpha\cos\beta\sin\theta - \sin\beta\sin\phi\cos\theta - \sin\alpha\cos\beta\cos\phi\cos\theta \tag{3.33}$$

and

$$\sin\chi = \frac{1}{\cos\gamma}\left(\cos\alpha\cos\beta\cos\theta\sin\psi + \sin\beta\sin\psi\sin\theta\sin\phi\right.$$
$$+\sin\beta\cos\psi\cos\phi + \sin\alpha\cos\beta\sin\psi\cos\phi\sin\theta \tag{3.34}$$
$$\left.-\sin\alpha\cos\beta\cos\psi\sin\phi\right)$$

For $\phi = 0$,

$$\sin\gamma = \sin(\theta-\alpha)\cos\beta \tag{3.35}$$

and

$$\sin\chi = \frac{1}{\cos\gamma}\left[\cos\beta\sin\psi\cos(\theta-\alpha) + \sin\beta\cos\psi\right] \tag{3.36}$$

Small angle assumptions on β and γ give $\gamma = \theta - \alpha$ and $\chi = \psi + \beta$ as in (3.1) and (3.2).

Next, consider a change in flight path at constant speed with accelerations matched. From (3.4) and (3.5)

$$V\dot{\chi}\cos\gamma = V_m\dot{\chi}_m\cos\gamma_m \tag{3.37}$$

and

$$V\dot{\gamma} = V_m\dot{\gamma}_m \tag{3.38}$$

Integrating these equations with the small angle assumption $\cos\gamma \doteq 1$ gives

$$V\Delta\chi = V_m\Delta\chi_m \tag{3.39}$$

and

$$V\Delta\gamma = V_m\Delta\gamma_m \tag{3.40}$$

Using (3.1) and (3.2), the increments from trim of the angles of sideslip and attack of TIFS when the attitude match is imposed – $\Delta\theta = \Delta\theta_m$ and $\Delta\psi = \Delta\psi_m$ are given by

$$\Delta\beta = \Delta\beta_m + \left(\frac{V_m}{V} - 1\right)\Delta\gamma_m \tag{3.41}$$

and

$$\Delta\alpha = \Delta\alpha_m - \left(\frac{V_m}{V} - 1\right)\Delta\gamma_m \tag{3.42}$$

Finally consider the steady conditions following maneuver and power adjustment when a new rate of climb or a new heading or a combination of the two has been established at the trim airspeed. Because the trim airspeed is not changed, $\Delta\alpha_m \doteq 0$, and because trim wings-level flight is assumed, $\Delta\beta_m = 0$. Then

$$\Delta\gamma_{m_{MAX}} = \left(\frac{V_m}{V} - 1\right)^{-1}\Delta\beta_{MAX} \tag{3.43}$$

and

$$\Delta\gamma_{m_{MAX}} = -\left(\frac{V_m}{V} - 1\right)^{-1}\Delta\alpha_{MAX} \tag{3.44}$$

where $\Delta\beta_{MAX}$ and $\Delta\alpha_{MAX}$ are the limits TIFS can achieve at the particular trim airspeed while maintaining straight wings-level flight. From Equations (3.4) and (3.5) these are the ranges of β and α for

$$C_{Y_{TRIM}} = \frac{T}{\bar{q}S}\,\frac{\beta_{TRIM}}{57.3} \tag{3.45}$$

and

$$C_{L_{TRIM}} \doteq \frac{W}{\bar{q}S} - \frac{T}{\bar{q}S}\,\frac{\alpha_{TRIM}}{57.3} \tag{3.46}$$

Consider as an example the model at 380 knots and TIFS at 190 knots, both initially in level flight. In Section 3.3.1 the model trim is given by $C_{L_{m_{TRIM}}} = 1.38 + .126\,\alpha_{m_{TRIM}}$. At $V_{e_m} = 380$ kt. $C_{L_{m_{TRIM}}} \approx (W/S)_m/\bar{q}_m = 179/490 = .366$. If $\alpha_{m_{TRIM}}$ is computed using these relationships it will be highly negative. The reason is that the model as described in Table 3.1 is in a landing approach configuration with considerable flap deflection. For the purposes of this example assume that when the model's flaps are at zero the trim lift coefficient is given by $C_{L_{m_{TRIM}}} = .190 + .126\,\alpha_{m_{TRIM}}$. Then

$\alpha_{m_{TRIM}} = 1.4° = \theta_{m_{TRIM}}$. To produce $\theta_{TRIM} = 1.4°$ at $V_e = 190$ kt, the TIFS uses $\delta_{\gamma_{TRIM}} = -4°$. At this speed the TIFS thrust coefficient $T/\bar{q}S$ is small and can be neglected so that (3.45) and (3.46) reduce to $C_{Y_{TRIM}} = 0$ and $C_{L_{TRIM}} = W/\bar{q}S$. This gives, from Figure 3.2, $\alpha_{MIN} = -1.8°$ determined by $\delta_\gamma = 35°$, $\alpha_{MAX} = 6.0°$ determined by the buffet boundary, and, from Figure 3.3, $|\beta|_{MAX} = 8.2°$. Therefore from (3.43) and (3.44), $|\Delta\gamma_m|_{MAX} = 8.2°$, $\Delta\gamma_{MIN} = -6.0°$ and $\Delta\gamma_{MAX} = 1.8°$. This capability is probably sufficient to examine handling qualities along a given heading up to moderate rates of descent and would certainly be adequate to simulate small disturbance tasks such as in-flight refueling.

SECTION IV

DYNAMIC MOTION

The body angular rates p, q, and r, angular accelerations $\dot{p}$, $\dot{q}$, and $\dot{r}$, and linear accelerations n_x, n_y, and n_z are related through the six rigid body equations of motion. Equations (3.9), (3.10), and (3.11) express the force relationships and Equations (4.2), (4.3) and (4.4) express the moment relationships for one-to-one motion reproduction. One can, for any given input to the model, determine how far that input can be scaled up before one or more of the TIFS controls or structural loads reaches a limit. This type of analysis is perhaps best accomplished through computer integration of the equations. It does not lend itself readily to the derivation of analytical limits. However, there are two special cases which are of interest and can be rather easily handled without solving the equations of motion - steady accelerated flight and acceleration immediately following abrupt control inputs. These two cases will be examined in this section.

4.1 GENERAL RELATIONSHIPS

The moment equations are most conveniently written in body axes. They are as follows

$$
\begin{aligned}
&I_{xx}\dot{p} - I_{xz}\dot{r} + q\left[(I_{zz} - I_{yy})r - I_{xz}p\right] = \bar{q}\,SbC_\ell \\
&I_{yy}\dot{q} + r\left[(I_{xx} - I_{zz})p - I_{xz}r + I_{xz}p^2\right] = \bar{q}\,S\bar{c}C_m + z_T T_x - x_T T_z \\
&I_{zz}\dot{r} - I_{xz}\dot{p} + q\left[(I_{yy} - I_{xx})p + I_{xz}r\right] = \bar{q}\,SbC_n
\end{aligned}
\tag{4.1}
$$

It is evident that if the inertia coupling terms are important the equations for exact model following are more complicated than those derived from the force equations. It is not possible, in general, to obtain relationships involving only the right hand side applied moments. (If the model and TIFS moments of inertia all have the same ratio, i.e., $\frac{I_{xx}}{I_{xx_m}} = \frac{I_{yy}}{I_{yy_m}} = \frac{I_{zz}}{I_{zz_m}} = \frac{I_{xz}}{I_{xz_m}}$, this is one instance when the inertia coupling terms are the same for $p = p_m$, $q = q_m$, and $r = r_m$.) However, for the class of airplane

TIFS is designed to simulate, and the tasks of primary concern such as landing approach, the inertia coupling terms are negligible and matching $\dot{p}$, $\dot{q}$ and $\dot{r}$ in parallel TIFS and model axis systems is achieved when, for $\bar{q} = \bar{q}_m$

$$\left[C_m + \frac{z_T T_x}{\bar{q} S\bar{c}} - \frac{x_T T_z}{\bar{q} S\bar{c}}\right] = \frac{I_{yy}/S\bar{c}}{(I_{yy}/S\bar{c})_m}\left[C_{m_m} + \left(\frac{z_T T_x}{\bar{q} S\bar{c}}\right)_m - \left(\frac{x_T T_z}{\bar{q} S\bar{c}}\right)_m\right] \tag{4.2}$$

$$C_\ell = \frac{I_{xx}/Sb}{(I_{xx}/Sb)_m} C_{\ell_m} \tag{4.3}$$

$$C_n = \frac{I_{zz}/Sb}{(I_{zz}/Sb)_m} C_{n_m} \tag{4.4}$$

For dynamic motions, it is usually desired to match the linear and angular accelerations of the pilot's seat. Moving the TIFS moment controls according to Equations (4.2), (4.3), and (4.4) will match the angular accelerations of the seat. The linear accelerations are matched if the TIFS force controls are moved according to Equations (3.4) suitably modified to account for non-coincident c.g. positions. To obtain the required expressions, it is convenient if the original force equations are written in body axes.

The general situation considered here is depicted in Figure 4.1.

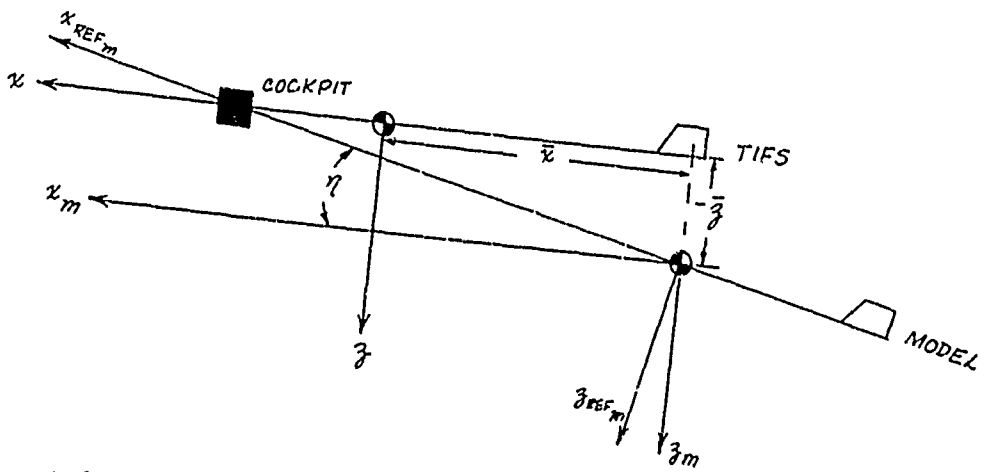

Figure 4.1 General TIFS and Model Body Axis Alignment

The pilot's seat in the TIFS cockpit is brought into alignment with the seat in the model. In general there will be an angle η between the TIFS x body axis and the model x_{REF_m} body axis required to align the pilot's seats and displacements $\bar{x}$ and $\bar{z}$ between the TIFS and model c.g.'s. Writing the model force equations in a body-axis system, x_m, y_m, z_m, which is parallel to the TIFS axis system, x, y, z, the required model following with the TIFS c.g. linear accelerometers is obtained when

$$\begin{bmatrix} n_x \\ n_y \\ n_z \end{bmatrix}_{\substack{TIFS \\ CG}} = \begin{bmatrix} n_{x_m} \\ n_{y_m} \\ n_{z_m} \end{bmatrix}_{\substack{MODEL \\ CG}} + \begin{bmatrix} \dot{p}_m \\ \dot{q}_m \\ \dot{r}_m \end{bmatrix} \times \begin{bmatrix} \bar{x} \\ 0 \\ \bar{z} \end{bmatrix} + \begin{bmatrix} p_m \\ q_m \\ r_m \end{bmatrix} \times \begin{bmatrix} p_m \\ q_m \\ r_m \end{bmatrix} \times \begin{bmatrix} \bar{x} \\ 0 \\ \bar{z} \end{bmatrix} \tag{4.5}$$

where " x " denotes the vector cross product.*

The linear accelerometer signals are related to applied loads by

$$\begin{bmatrix} n_x \\ n_y \\ n_z \end{bmatrix}_{CG} = \frac{\bar{q}S}{m} \begin{bmatrix} C_x \\ C_y \\ C_z \end{bmatrix} + \frac{1}{m} \begin{bmatrix} T_x \\ 0 \\ T_z \end{bmatrix} \tag{4.6}$$

Therefore Equation (4.5) becomes

$$\frac{\bar{q}S}{m} \begin{bmatrix} C_x \\ C_y \\ C_z \end{bmatrix} + \frac{1}{m} \begin{bmatrix} T_x \\ 0 \\ T_z \end{bmatrix} = \frac{\bar{q}_m S_m}{m} \begin{bmatrix} C_x \\ C_y \\ C_z \end{bmatrix}_m + \frac{1}{m_m} \begin{bmatrix} T_x \\ 0 \\ T_z \end{bmatrix}_m + \begin{bmatrix} \dot{q}_m \bar{z} \\ \dot{r}_m \bar{x} - \dot{p}_m \bar{z} \\ -\dot{q}_m \bar{x} \end{bmatrix} \tag{4.7}$$

+ centrifugal acceleration terms

To obtain the relationship in terms of model and TIFS wind axes coefficients, the transformation from wind to body axes is introduced

$$\left[L_{W \to B}\right] = \left[\alpha\right]\left[\beta\right]' \tag{4.8}$$

---

* By the definition of cross product,

$$\left[a_1\ a_2\ a_3\right]' \times \left[b_1\ b_2\ b_3\right]' = \left[a_2 b_3 - a_3 b_2 \mid a_3 b_1 - a_1 b_3 \mid a_1 b_2 - a_2 b_1\right]'$$

This is an orthogonal transformation so that the inverse is equal to the transpose. Then Equation (4.7) becomes

$$\frac{\bar{q}S}{m}\begin{bmatrix}-C_D\\ C_y\\ -C_L\end{bmatrix}+\frac{1}{m}\begin{bmatrix}T_{x_W}\\ T_{y_W}\\ T_{z_W}\end{bmatrix}=\left[L_{W\to B}\right]'\left[L_{W\to B}\right]_m\left\{\frac{\bar{q}_m S_m}{m_m}\begin{bmatrix}-C_{D_m}\\ C_{y_m}\\ -C_{L_m}\end{bmatrix}+\frac{1}{m_m}\begin{bmatrix}T_{x_{W_m}}\\ T_{y_{W_m}}\\ T_{z_{W_m}}\end{bmatrix}\right\}$$
$$+\left[L_{W\to B}\right]'\begin{bmatrix}\dot{q}_m\bar{z}\\ \dot{r}_m\bar{x}-\dot{p}_m\bar{z}\\ -\dot{q}_m\bar{x}\end{bmatrix}+\left[L_{W\to B}\right]'\begin{bmatrix}\text{centrifugal}\\ \text{accelerations}\end{bmatrix} \tag{4.9}$$

This equation expresses the TIFS forces in wind axes in terms of the model forces in the model wind axes, the displacement of the c.g.'s, the model angles of attack and sideslip, and the TIFS angles of attack and sideslip. The TIFS and model angles of attack and sideslip are related through the equations for $\sin\alpha$, $\sin\beta$, etc. in terms of u, v, and w and the relation

$$\begin{bmatrix}u\\ v\\ w\end{bmatrix}=\begin{bmatrix}u_m\\ v_m\\ w_m\end{bmatrix}+\begin{bmatrix}p_m\\ q_m\\ r_m\end{bmatrix}\times\begin{bmatrix}\bar{x}\\ 0\\ \bar{z}\end{bmatrix} \tag{4.10}$$

again using the vector cross product.
Therefore the transformation $\left[L_{W\to B}\right]'$ which is a function of the TIFS α and β can be computed entirely from model variables and the entire right hand side of (4.9) can be computed from model variables.

If the c.g.'s are coincident then $\alpha=\alpha_m$, $\beta=\beta_m$ and $\left[L_{W\to B}\right]'=\left[L_{W\to B}\right]=1$. The terms due to c.g. displacement are zero and Equation (4.9) reduces to Equations (3.6), (3.7), and (3.8). (Note that $\bar{q}=\bar{q}_m$ in general, only if the c.g.'s are coincident or flight is unaccelerated.)

If the small-angle assumption is made on α, α_m, β, and β_m so that $\sin\alpha$ is replaced by α, $\cos\alpha$ by 1.0, etc. and products $\alpha\beta$, etc. are dropped, then

$$\left[L_{W\to B}\right]'\left[L_{W\to B}\right]_m \approx \begin{bmatrix} 1 & \beta-\beta_m & \alpha-\alpha_m \\ -(\beta-\beta_m) & 1 & 0 \\ -(\alpha-\alpha_m) & 0 & 1 \end{bmatrix} \tag{4.11}$$

and

$$\left[L_{W\to B}\right]' \approx \begin{bmatrix} 1 & \beta & \alpha \\ -\beta & 1 & 0 \\ -\alpha & 0 & 1 \end{bmatrix} \tag{4.12}$$

and

$$\begin{bmatrix} u \\ v \\ w \end{bmatrix} \approx V \begin{bmatrix} 1 \\ \beta \\ \alpha \end{bmatrix} \tag{4.13}$$

From (4.10) and (4.13),

$$\beta = \frac{V_m \beta_m + r_m \bar{x} - p_m \bar{z}}{V_m + q_m \bar{z}}$$

and

$$\alpha = \frac{V_m \alpha_m - q_m \bar{x}}{V_m + q_m \bar{z}}$$

so the transformation matrices are

$$\left[L_{W\to B}\right]'\left[L_{W\to B}\right]_m \approx \begin{bmatrix} 1 & \dfrac{-\beta_m q_m \bar{z} + r_m \bar{x} - p_m \bar{z}}{V_m + q_m \bar{z}} & \dfrac{-\alpha_m q_m \bar{z} - q_m \bar{x}}{V_m + q_m \bar{z}} \\ & 1 & 0 \\ \text{with skew symmetry as in 4.11} & & 1 \end{bmatrix} \tag{4.14}$$

and

$$\left[L_{W\to B}\right]' \approx \begin{bmatrix} 1 & \dfrac{V_m \beta_m + r_m \bar{x} - p_m \bar{z}}{V_m + q_m \bar{z}} & \dfrac{V_m \alpha_m - q_m \bar{x}}{V_m + q_m \bar{z}} \\ & 1 & 0 \\ \text{with skew symmetry as in 4.12} & & 1 \end{bmatrix} \tag{4.15}$$

Equations (4.9) with (4.14) and (4.15) express in manageable form the general relationships producing cockpit motion model following. They can be further simplified in specific examples and used to determine the maximum TIFS control inputs to match particular extreme model motions.

4.2 TIFS AERODYNAMIC AND THRUST MOMENTS

The Convair aerodynamics report on the CV-340 turboprop version, Reference 16, serves as a primary source for much of the rolling and yawing moment information presently used for TIFS analysis work. This data has been augmented by analysis and flight test as reported in TIFS Memos 127 and 565. The relations used in this report are the following

(all angles in degrees, V in fps)

$$C_\ell = (-.0018 + .00005\alpha)\beta + .0005\delta_r + (-.0017 + .00001|\delta_a|)\delta_a$$
$$-.00005\delta_y + .14\frac{r}{V} - .48\frac{p}{V} \qquad (4.16)$$

$$C_n = (.0019 - .00007\alpha)\beta - .0019\delta_r - .00017\delta_a + .00017\delta_y$$
$$-.127\frac{r}{V} + (-.015 - .0045\alpha)\frac{p}{V} - .027\frac{T\times 10^{-3}}{\bar{q}} \qquad (4.17)$$

The pitching moment data derived from the TIFS wind tunnel tests (Reference 15) must be corrected substantially because the general-purpose nose is being used instead of the SST nose which was tunnel tested. Flight test data in the form of δ_e to trim versus V_e has been obtained but it contains power effects which were not present in the wind tunnel. A discussion of the pitching moment variation with α is presented in Reference 4. The final equation used in this report is based on the flight tests with power corrections taken from Reference 1, dynamic and control derivatives from Reference 1, and direct lift flap and Fowler flap corrections from Reference 15.

$$C_{m_{CG}} = \left(\frac{x_{CG}}{9.52} - .266\right)C_L + .103 - .092C_{L_{\substack{\delta_f=0\\ \delta_e=0}}} + .081C^2_{L_{\substack{\delta_f=0\\ \delta_e=0}}} - .104C^3_{L_{\substack{\delta_f=0\\ \delta_e=0}}} - .015G$$
$$+\left(.086 - .070C_{L_{\substack{\delta_f=0\\ \delta_e=0}}}\right)\left(\frac{\delta_\gamma}{30}\right) + \left(.018 + .006G_{\substack{\delta_f=0\\ \delta_e=0}}\right)\left(\frac{\delta_\gamma}{30}\right)^2$$
$$+\left(-.023 + .016C_{L_{\substack{\delta_f=0\\ \delta_e=0}}}\right)\left(\frac{\delta_\gamma}{30}\right)^3 + \left\{.15 + .005\alpha + (-.68 + .030\alpha)\frac{T\times 10^{-3}}{q}\right\}\left(\frac{\delta_\gamma}{40}\right)$$
$$+ .74\frac{T\times 10^{-3}}{q} - .035\delta_e - 1.41\frac{\dot{\alpha}}{V} - 3.74\frac{q}{V} \qquad (4.18)$$

4.3 STRUCTURAL DESIGN CONSTRAINTS AND CONTROL SERVO CHARACTERISTICS

The dynamic motions of TIFS are governed by how fast and how far the controls can be moved and the accelerations and aerodynamic loads the structure can stand. This section documents the limitations as of October, 1971.

4.3.1 Structural Design Constraints

The C-131H was originally designed to + 2.5, - 1.0 g's maneuver load factor at speeds up to 283 KEAS and + 2.5, -0.0 g's at the 353 KEAS dive speed. Due to the TIFS forward fuselage nose-down pitching moment and the use of direct lift flap both trailing edge up and down at high speeds, these design numbers are reduced. Figures 4.2 through 4.7 have been prepared to indicate the present load factor limits as a function of flap deflection due to the loads in several different areas and due to aerodynamic buffet.

The load factor is limited to the 75% allowable load point rather than 100% to give some consideration to the point that TIFS as a handling qualities simulator will be maneuvered more frequently than the standard C-131H. Also this extra margin allows for possible inadvertent overshoot.

As the reader progresses from Figure 4.2 to Figure 4.7, the airspeed is increased in 25 mph increments. The limits change from purely aerodynamic limits at 152 knots (175 mph) to almost purely structural limits at 260 knots (300 mph). The curves are taken directly from the maneuver loads and structural capabilities calculated in the addendum to TIFS Memo No. 423, the fuselage loads report for the 49,000 zero fuel weight condition and the addendum to the wing loads report, TIFS Memo No. 491. The buffet boundary for negative δ_z was determined from flight tests during the envelope expansion in May of 1971 and the stall boundary from early flight tests.

The curves are obtained analytically by trimming the airplane at 1 g with the flap at the specified position and then with the flap fixed at that position maneuvering to the g limit specified. For example, for W = 49,000 lb, fixing the flap at δ_f = - 5° at 240 kt (Figure 4.6) and maneuvering to 2.08 g's puts 75% of the load for zero margin in the area of the cargo door.

Also on Figures 4.4 to 4.7, specific points along the 1 g line have been plotted to indicate where the gust limits fall. These are obtained by positioning the flap at 1 g and then superimposing a vertical or side gust (40 K* fps at 210 kt, 30 K fps at 240 kt, 15 K fps at 285 kt, and linear interpolation between). These extreme gust inputs are not superimposed on maneuvering conditions. Furthermore, they are plotted at the 100% limit load points rather than the 75% points because of their low probability of occurrence.

As is indicated in Figures 4.4 to 4.7, all the gust points fall outside the 75% limit load maneuver curves or the buffet boundary except the side gust condition at V_e = 240 kt and the vertical gust at V_e = 218 kt which are only slightly inside. Therefore gust conditions are not of concern as long as the operation is within the 75% limit load maneuver boundaries as specified in Figures 4.4 to 4.7.

Safety trip signals are included in the system to provide for automatic implementation of these boundaries since they are too complicated for the safety pilot to provide.

The C-131H vertical tail structure was designed to accommodate engine failure cases, extreme side gusts equal to the vertical gusts quoted above, and full rudder trim sideslip up to 170 knots. The resulting structural capability is defined by a closed area on a plot of β vs. δ_r which is roughly

---

* $K = 1.33 - 2.67\,(W/S)^{-3/4}$

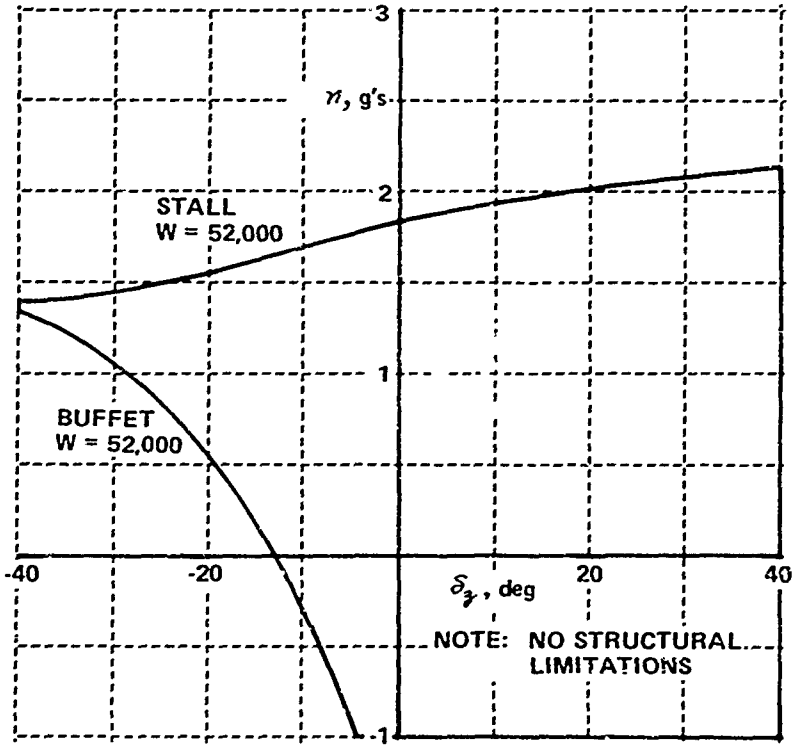

Figure 4.2 Load Factor Limitations
V_e = 152 Knots (175 mph)

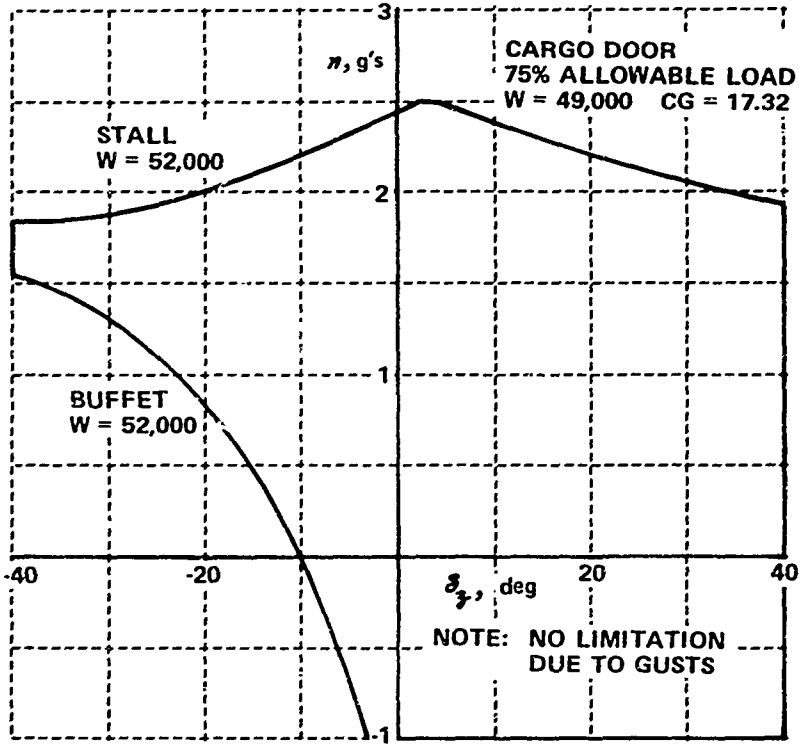

Figure 4.3 Load Factor Limitations
V_e = 174 Knots (200 mph)

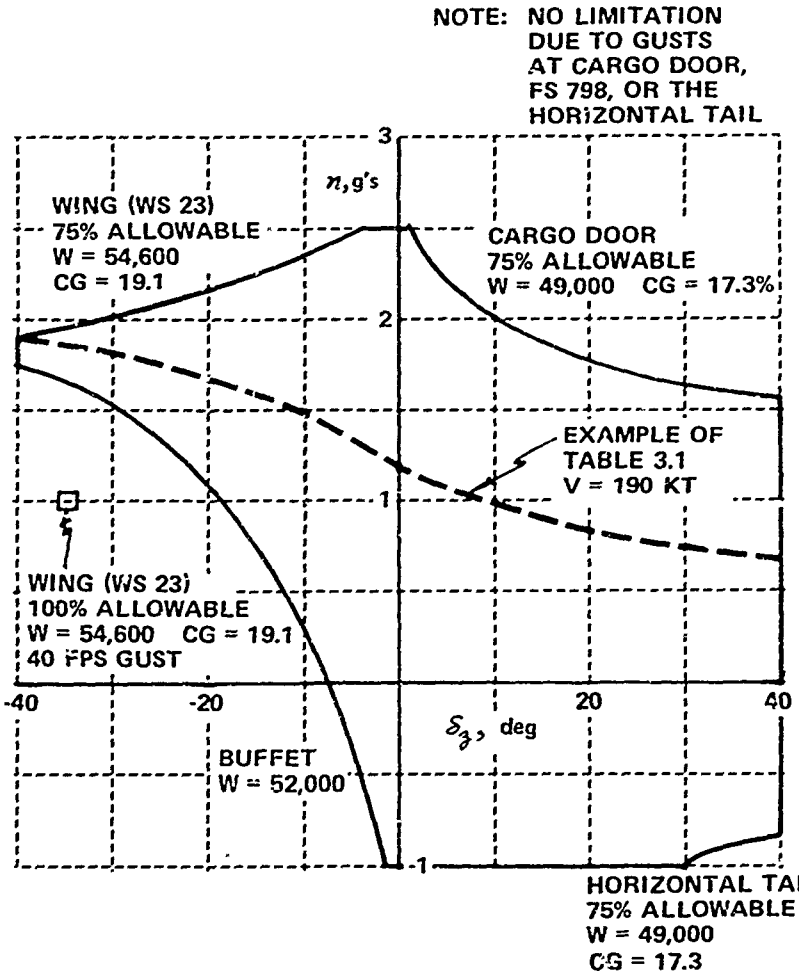

Figure 4.4 Load Factor Limitations
V_e = 196 Knots (225 mph)

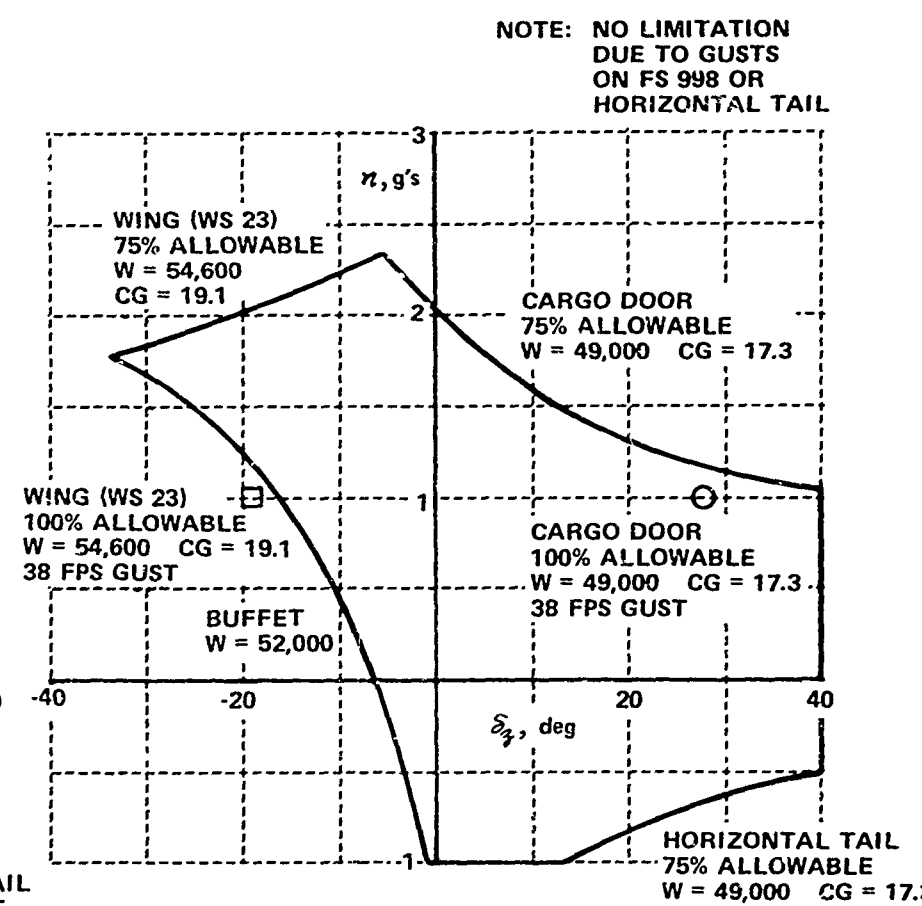

Figure 4.5 Load Factor Limitations
V_e = 218 Knots (250 mph)

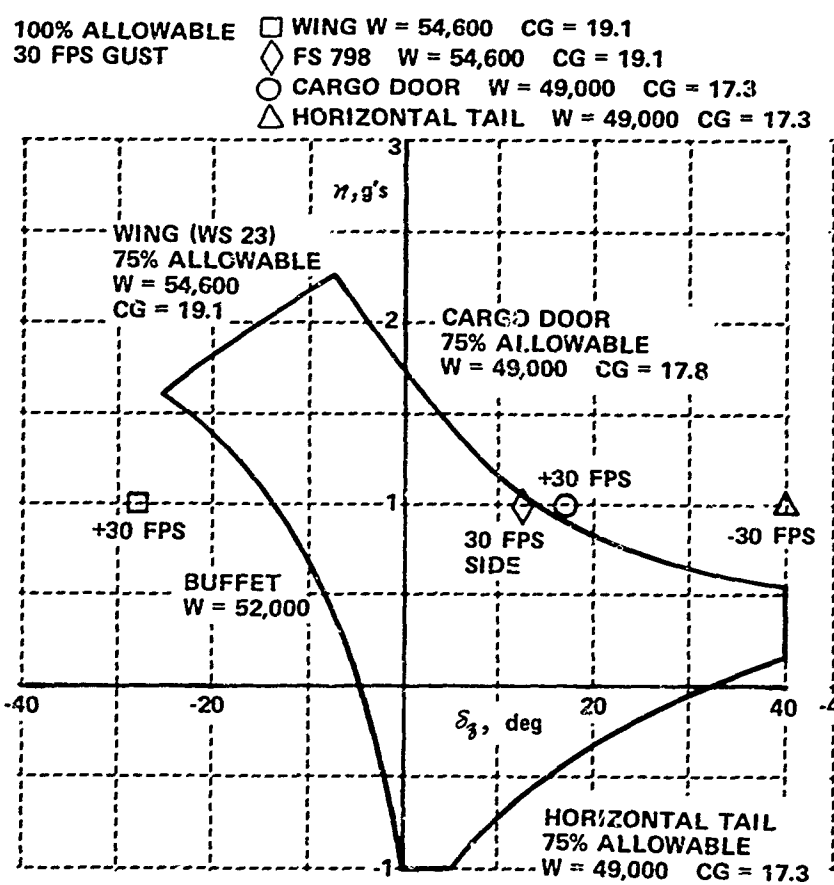

Figure 4.6 Load Factor Limitations
V_e = 240 Knots (275 mph)

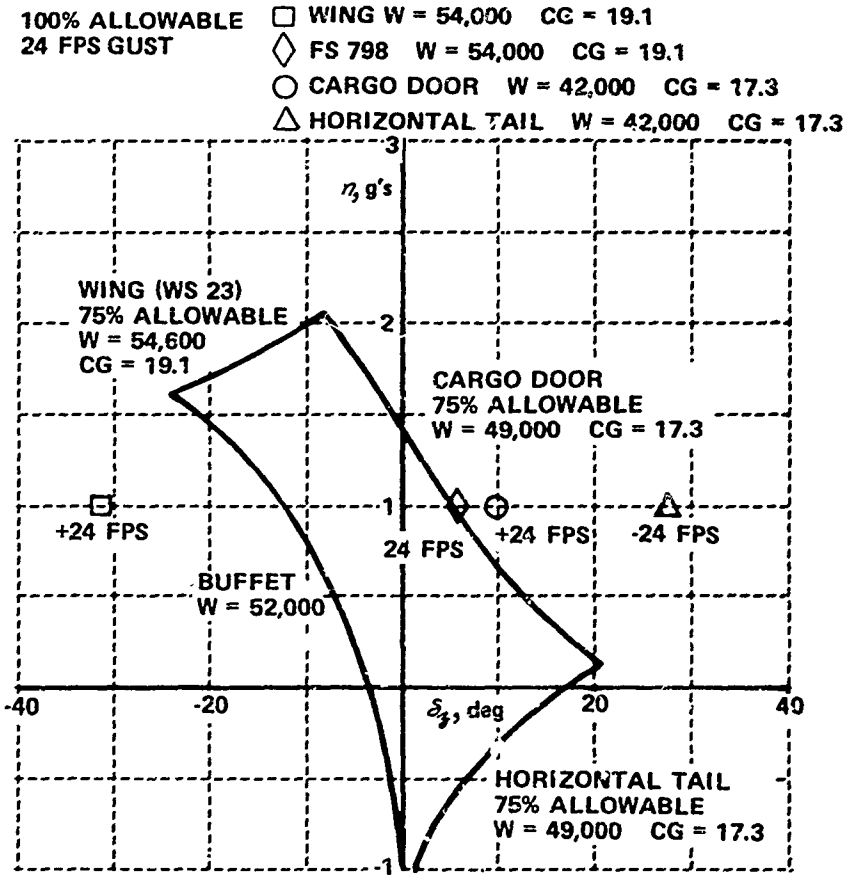

Figure 4.7 Load Factor Limitations
V_e = 260 Knots (300 mph)

elliptical. An exact ellipse which fits inside this closed area is given by

$$\left(\beta_{VT}^2 - .521\beta_{VT}\delta_r + .586\delta_r^2\right)\left(\frac{\bar{q}}{1010}\right)^2 = 1 \qquad (4.19)$$

where $\beta_{VT} = \beta - 36.6\frac{r}{V} + 11.4\frac{p}{V}$

all angles in degrees, V in fps, and $\bar{q}$ in psf.

The closed area and the ellipse are shown in Figure 4.8. This ellipse roughly defines the boundary for 75% allowable load on the vertical tail. For trim sideslips at $\delta_y = 0$ (i.e., $C_\ell = C_n = 0$) Equations (4.16) and (4.17) solved simultaneously give $\delta_{r_{trim}} = .87\,\beta_{trim}$ for $\alpha_{trim} = 5°$. Therefore (4.19) reduces to

$$\beta_{TRIM\ MAX.}^2\left(\frac{\bar{q}}{1010}\right)^2 = 1 \qquad (4.20)$$

$$\text{or} \quad \beta_{\substack{TRIM \\ MAX \\ \delta_y=0}} = \frac{1010}{\bar{q}}$$

4.3.2 Control Servo Characteristics

Table 4.1 presents the aspects of control servo performance of importance in determining dynamic motion capability. The hinge moment capability designed into the structure and the actuator determines the control deflections that could be achieved with the maximum pressure relief valve settings. Note that for all controls the actuator design strength approximately matches the C-131H flight control system and surface structural design. However, the current hinge moment capability for the C-131H controls is limited by the relief valves to values which the pilot can overpower (the throttle is limited by slipping of the mechanical clutch).

These limits can be translated to surface deflection limits as a function of dynamic pressure. The expressions needed for these calculations are tabulated in Table 4.1. For the elevator, aileron, and rudder, the aerodynamic hinge moment data is taken from Reference 16 with a tab deflection gear ratio of .5 for the elevator and .81 for the aileron. The rudder servo acts directly

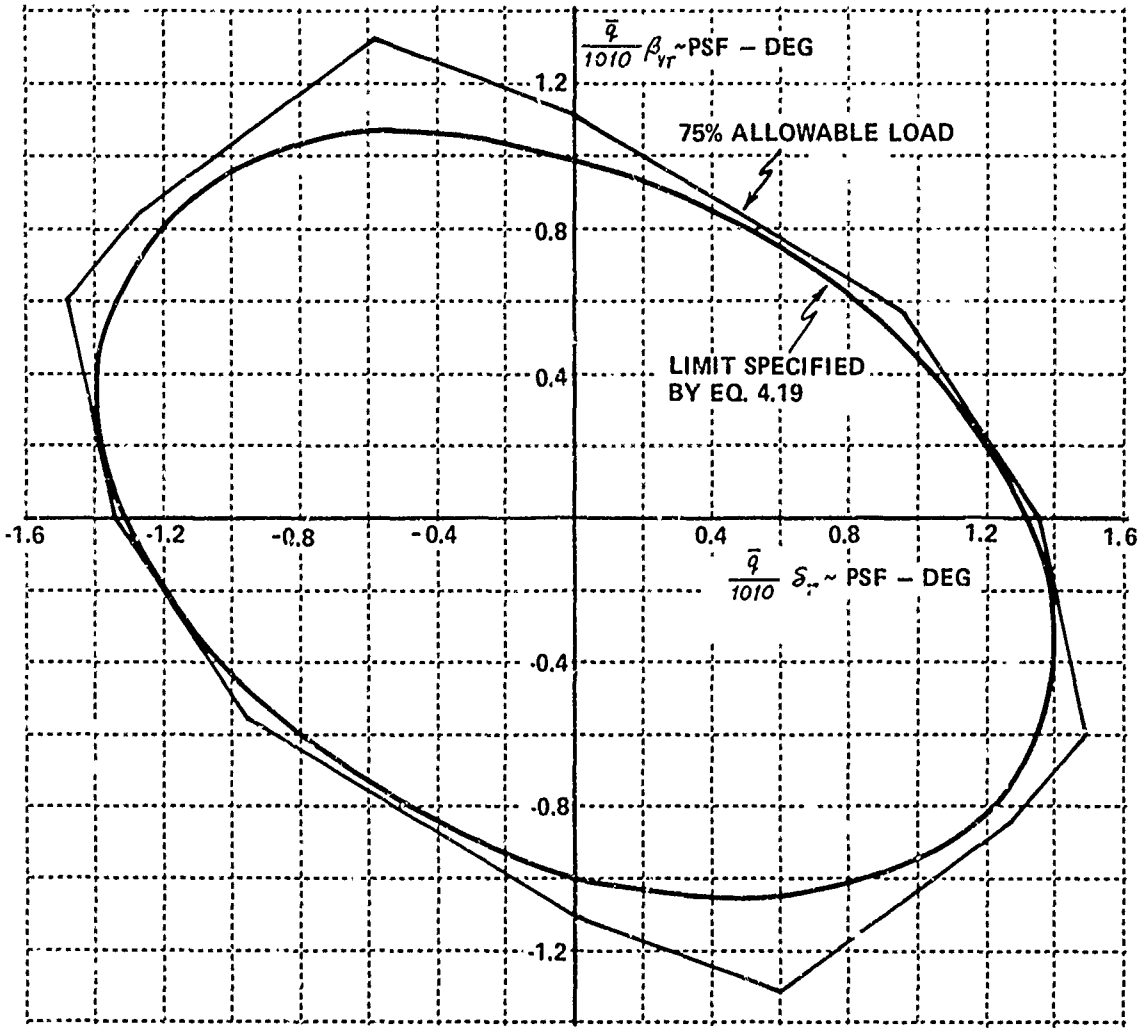

Figure 4.8 Vertical Tail Load Restriction on Sideslip

TABLE 4.1

CONTROL SERVO CHARACTERISTICS

	Travel deg	Surface Design Hinge Moment (Ref. 16) ft-lbs	Design Servo Hinge Moment (Ref. TM486) ft-lb	Current Hinge Moment Limit (Ref. 16) ft-lb	Current Relief Valve Setting (Ref. 16) psi	Deflection Limits Due to Hinge Moment Limits (Ref. 4 & 16) deg
Elevator	-26., + 12	1124.	1027.	207.	424	$\pm 632.\ \bar{q}^{-1}$
Total Aileron	± 48	410.	410.	148.	265	$\pm 2230.\bar{q}^{-1}\left(1+\frac{2\alpha}{30}\right)^{-1}$
Rudder	± 18	1205.	1205.	1205.	975	$\pm 1980.\bar{q}^{-1}$
SFS	± 30	3750. (TM471)	3750.	1310.	500	$\pm 3200.\ \bar{q}^{-1}$
DLF	± 40	8000. (TM197)	8000.	8000.	1325 TEU 1430 TED	$\pm 10,700.\ \bar{q}^{-1} - 4.7(1+.29\alpha)$
Throttle	34. to 90.	17.3 (TM486)	17.3	17.3	17.3	34. to 90.

Control	Surface Rate Limit (no load) (Ref. 4) deg/sec	Surface Rate Limit Under Design Servo Hinge Moment (Ref. 3) deg/sec	Frequency for 90° Phase Lag (Ref. 4) Hertz
Elevator	88.	60.	2.0
Total Aileron	77.	60.	3.7
Rudder	76.	60.	3.0
SFS	89.	60.	7.0
DLF	58.	40.	4.1
Throttle	NA	NA	.3

on the surface bypassing the spring tab so no tab deflection is included. The throttle travel is limited electronically and these limits can be changed, so the limits listed are the mechanical stops. The hinge moment data for the SFS and DLF were taken from flight test reported in Reference 16.

The SFS moment is overly limited because early flight tests were run at conservative settings, which are currently satisfactory, and there has been no simulation requirement to purchase relief valves and pressure transducers with a range extended to the 3750 ft-lb design level. The DLF moment will probably be reduced later to be more compatible with the DLF deflection limits at V_e = 240 kt due to the general structural considerations mentioned in Section 4.3.1.

4.4 DETERMINATION OF SIMULATION DYNAMIC RANGE -- AN EXAMPLE

4.4.1 Abrupt Accelerations

If the TIFS control is deflected at maximum rate to its limit at a particular airspeed, the resulting abrupt acceleration of the rigid body can be calculated from the following expressions

$$\Delta n_{x_W} = \frac{\Delta T_{x_W}}{W} \qquad \Delta \dot{p} = \frac{\Delta C_\ell \bar{q} S b}{I_{xx}}$$

$$\Delta n_{y_W} = \frac{\Delta C_y \bar{q} S}{W} \qquad \Delta \dot{q} = \frac{\Delta C_m \bar{q} S \bar{c}}{I_{yy}} \qquad (4.21)$$

$$\Delta n_{z_W} = \frac{-\Delta C_L \bar{q} S}{W} \qquad \Delta \dot{r} = \frac{\Delta C_n \bar{q} S b}{I_{zz}}$$

Using the data of Table 3.2 and the deflection limits of Table 4.1, the following information is obtained at V_e = 190 kt simulating the model of Table 3.1 at sea level. (The control coupling effects have been neglected here although they can be easily included in a more elaborate analysis, i.e., the DLF's produce moments as well as force, etc.).

Δn_{x_W} The trim throttle setting is $\delta_{x_{TRIM}}$ = 66.3° for level flight. The limits are $\delta_{x_{MAX}}$ = 90° and $\delta_{x_{MIN}}$ = 34°. Therefore using Equation (3.21), ΔT_{MAX} = 4800 lb and ΔT_{MIN} = - 6600 lb giving $-.13 \leq \Delta n_x \leq .09$ g's.

Δn_{y_W} The trim side force surface deflection is $\delta_{y_{TRIM}} = 0$. The hinge moment limit allows $\delta_{y_{MAX}} = \frac{3200}{127.3} = 26.2°$ which is past the stall angle of the surface. Therefore using the δ_y for SFS stall, at α_{TRIM} = .68° $\Delta C_{y_{MAX}}$ = .103 from Equation (3.22) and $-.22 \leq \Delta n_{y_W} \leq .22$ g's.

Δn_{z_W} The trim direct lift flap deflection is $\delta_{y_{TRIM}}$ = 9°. Table 4.1 indicates that full surface deflection is available. Therefore using Equation (3.12) and considering δ_z abruptly moved to 35.° or -35.° gives $-.526 \leq \Delta n_{z_W} \leq 1.44$ g's.

$\dot{p}$ The trim aileron deflection is $\delta_{a_{TRIM}} = 0$. Table 4.1 indicates that the hinge moment limit occurs at $\delta_a = \pm 17.4°$. Using Equation (4.16) gives $-75. \leq \dot{p} \leq 75.$ deg/sec^2.

$\dot{q}$ The trim elevator deflection can be computed from (4.18) if a TIFS c.g. is specified. However, Table 4.1 indicates $\Delta\delta_e = \pm 5.2$ is available from trim and to avoid a lengthy computation, the reasonable assumption is made that ± 5.2° can be obtained without exceeding the elevator travel limits. Then using $C_{m_{\delta_e}} = -.035$ from Equation (4.18), the result $-20.8 \leq \dot{q} \leq 20.8$ deg/sec^2 is obtained.

$\dot{r}$ The trim rudder deflection is approximately zero. Therefore Table 4.1, together with $C_{n_{\delta_r}} = -.0019$, gives $-27.4 \leq \dot{r} \leq 27.4$ deg/sec^2.

The capability above could be evaluated for the model of Table 3.1 if maximum model control travel were specified and the sizes of abrupt model maneuvers to perform the mission simulated were specified. This will not be done here since the procedure is straightforward using the model-following equations (3.6), (3.7), (3.8), (4.2), (4.3), and (4.4).

If the model and the TIFS c.g.'s are not coincident, then the equations for model following are (4.2), (4.3), (4.4), and (4.9). Consider, for example, that the model and the TIFS c.g.'s are misaligned by $\bar{x}$ = 50 feet and $\bar{z}$ = -10 feet. For an abrupt model elevator motion, $\Delta C_{L_m} = C_{L_{\delta e_m}} \Delta\delta_{e_m}$ and $\Delta C_{m_m} = C_{m_{\delta e_m}} \Delta\delta_{e_m}$. Equation (4.9) with (4.14) and (4.15) give, in the instant following the model input

$$\frac{\bar{q}S}{m}\begin{bmatrix} -C_D \\ C_y \\ -C_L \end{bmatrix} + \frac{1}{m}\begin{bmatrix} T_{x_W} \\ T_{y_W} \\ T_{z_W} \end{bmatrix} \approx \frac{\bar{q}_m S_m}{m_m}\begin{bmatrix} -C_{D_m} \\ C_{y_m} \\ -C_{L_m} \end{bmatrix} + \frac{1}{m_m}\begin{bmatrix} T_{x_{W_m}} \\ T_{y_{W_m}} \\ T_{z_{W_m}} \end{bmatrix} + \begin{bmatrix} 1 & 0 & \alpha_m \\ 0 & 1 & 0 \\ \alpha_m & 0 & 1 \end{bmatrix}\begin{bmatrix} \dot{q}_m \bar{z} \\ 0 \\ -\dot{q}_m \bar{x} \end{bmatrix} \qquad (4.22)$$

where $\left[L_{W\to B}\right]'\left[L_{W\to B}\right]_m = I$, since all body rates are zero initially. The only alteration to the situation with the centers of gravity coincident is the addition of $\dot{q}_m(\bar{z} - \alpha_m \bar{x})$ to the drag equation and $\dot{q}_m(\alpha_m \bar{z} - \bar{x})$ to the lift equation.

4.4.2 Steady Rolling Performance

A rapid aileron input with associated rudder and side force surface inputs as necessary to produce a pure roll rate motion can be analyzed to predict maximum roll capability. Equations (3.22), (4.16), and (4.17) can be solved simultaneously for δ_a maximum as given by Table 4.1 and steady roll rate achieved, i.e., $C_\ell = 0$ and $C_y = C_n = 0$. For TIFS the needed rudder,

aileron and side force surface deflections will be small so that a good approximation of the final answer will be obtained by writing

$$.48\,\frac{p_{EXT}}{V} = \left(-.0017 + .00001\left|\delta_a\right|_{EXT}\right)\delta_{a_{EXT}} \qquad (4.23)$$

where $\delta_{a_{EXT}} = \dfrac{2230.}{\bar{q}\left(1+\frac{2\alpha}{30}\right)}$

At sea level, $V_{FPS} = V_{e_{FPS}} = 29.\,\bar{q}^{1/2}$ giving

$$p_{EXT} = \frac{29.\,\bar{q}^{1/2}}{.48}\left\{.0017 - \frac{0.023}{\bar{q}\left(1+\frac{2\alpha}{30}\right)}\right\}\frac{2230}{\bar{q}\left(1+\frac{2\alpha}{30}\right)} \qquad (4.24)$$

For the model of Table 3.1 flying at 190 kt, Equation (4.23) gives 17.9 deg/sec.

4.4.3 Steady Normal Acceleration

Figures 4.2 to 4.7 can be used together with the calculated DLF motion to determine the structural limits on steady maneuvering. The other limit which should be considered is the elevator hinge moment limit of Table 4.1.

Examine the lift relationship of Equation (4.9). In simplified form for symmetrical maneuvers

$$-\frac{\bar{q}S}{m}C_L + \frac{T_{z_W}}{m} \approx -\frac{\bar{q}_m S_m}{m_m}C_{L_m} + \frac{T_{z_{W_m}}}{m_m} + \frac{q_m\left(\alpha_m \bar{z} + \bar{x}\right)}{V_m + q_m \bar{z}}\left(-\frac{\bar{q}_m S_m}{m_m}C_D + \frac{T_{x_{W_m}}}{m_m}\right) \qquad (4.25)$$

The correction term for c.g. mismatch is negligible for the example and the T_{z_W}/m terms can be dropped as in Section III to give $C_L = \dfrac{W/S}{(W/S)_m}C_{L_m}$ as before. (The c.g. mismatch term is not negligible in the drag equation, however.) Using the C_{L_m} and C_{m_m} equations of Table 3.1 to eliminate δ_{e_m} gives $C_{L_m} = 1.38 + .126\,\alpha_m + 1.22\,q_m/V_m$. The relationship $\Delta n_{z_m} = -\frac{V_m}{g}\frac{q_m}{57.3} = -\dfrac{\Delta C_{L_m}}{C_{L_{m_{TRIM}}}}$ can now be used to obtain at 190 kt the equation

$C_{L_m} = 1.38 + .128\,\alpha_m$. This gives $C_L = C_{L_m}\,\frac{56.5}{179.} = .435 + .0404\,\alpha_m$ which is practically the same line on Figure 3.2 as obtained before for unaccelerated flight.

The direct lift flap deflection as a function of normal acceleration can now be plotted using $n_z = -C_L/C_{L_{TRIM}}$. The resulting curve is shown on Figure 4.4. That graph shows the position of the limiting curves for V_e = 196 knots, but for present purposes, the result will be approximately correct for 190 knots. That result is $.7 \leq -n_z \leq 1.85$ g's.

4.4.4 Gust and Structural Mode Simulation

Usually the reproduction of the rigid body response to pilot inputs does not directly involve the actuator high-frequency response limits because the inputs and motions are moderately slow. However, the primary consideration in gust and structural mode simulation is actuator bandwidth and rate limit. The structural modes of the TIFS itself are also very important because the prediction and control of cockpit motion beyond TIFS structural resonances is quite complex and continuous excitation at TIFS structural frequencies might cause fatigue problems.

Table 9.2 lists the three lowest-frequency symmetric and antisymmetric TIFS structural mode frequencies and estimated damping ratios. Comparing these frequencies with the approximate actuator bandwidth limits listed in Table 4.1, it is evident that above 3 to 4 hertz both the capacity to produce control motion and the ability to analyze the cockpit motion on a rigid-body basis deteriorate.

However, the most power in the gust spectrum is concentrated below $f = \frac{L}{2\pi V}$ hertz, which for altitudes below 10,000 feet where $L < 1000$ feet, is 0.1 to 1.1 hertz depending on airspeed and altitude. Also, for the very large airplanes TIFS is designed to simulate, the structural frequencies of the prominent modes are often in the 1. to 3. hertz range. Certainly if the interaction of structural flexibility with pilot control action is in question, the

interest in motion reproduction in a deterministic sense is limited to the low-frequency range where the pilot has the ability to exercise closed-loop control.

The limits on structural motion reproduction are easily determined if one assumes sinusoidal oscillations producing a specified peak of cockpit acceleration. Then the amplitude of flap and side force surface motion required is given indirectly by

$$\Delta n_{z_W} \approx \frac{\Delta C_y(\delta_y)}{C_{L_{TRIM}}} \tag{4.26}$$

$$\Delta n_{y_W} \approx \frac{-\Delta C_L(\delta_z)}{C_{L_{TRIM}}} \tag{4.27}$$

For example, at V_e = 190 kt, $C_{L_{TRIM}}$ = .458 so that $\Delta C_y = \Delta C_L$ = .0458 will produce .1 g peak acceleration. From Equations (3.12) and (3.22) with $\delta_{z_{TRIM}}$ = 0 deg and $\delta_{y_{TRIM}}$ = 0, peak deflections of $-7° \leq \delta_y \leq 7°$ and $6° \leq \delta_z \leq 14.°$ are required. If the oscillation is at 1. hertz, then the peak rates will be $\dot{\delta}_y$ = 44 deg/sec and $\dot{\delta}_z \cong$ 31. deg/sec. (This number is approximate since δ_z will not be sinusoidal.) These numbers are below the surface rate limits in Table 4.1. One can easily derive the levels of acceleration in a given flight condition where the rate limits will occur.

The limits for gust simulation can be determined on a deterministic basis by an analysis similar to that above. A discrete rapid gust time history will produce model accelerations which in turn will require direct lift flap and side force surface deflection to produce TIFS accelerations accordint to Equations (4.26) and (4.27).

On a probabilistic basis, the likelihood of the DLF's or SFS's exceeding their rate or position limits can be predicted using an analysis like the one used in TIFS Memo No. 130. This analysis is formulated in terms of gust-alleviating the TIFS airplane, but it can be easily interpreted to cover the gust simulation problem as well.

Following this analysis, the expected number of times per second

that $\dot{\delta}$ exceeds a given level with positive slope (i.e., $\ddot{\delta} > 0$) for a single Gaussian process is given by Rice's equation

$$N(\dot{\delta}) = N_{0,\dot{\delta}}\, e^{\left(-\frac{\dot{\delta}^2}{2\sigma_{\dot{\delta}}^2}\right)} \tag{4.28}$$

where

$$N_{0,\dot{\delta}} = \frac{1}{2\pi\sigma_{\dot{\delta}}}\left[\int_{-\infty}^{\infty} \omega^2\, \Phi_{\dot{\delta}}(\omega)\, d\omega\right]^{1/2} \tag{4.29}$$

and

$$\sigma_{\dot{\delta}} = \left[\int_{-\infty}^{\infty} \Phi_{\dot{\delta}}(\omega)\, d\omega\right]^{1/2} \tag{4.30}$$

The power spectrum of the control rate is given by

$$\Phi_{\dot{\delta}}(\omega) = \left|\frac{\dot{\delta}(s)}{w_g(s)}\right|^2_{s=i\omega} \Phi_{w_g}(\omega) \tag{4.31}$$

where Φ_{w_g} is the gust spectrum and $\frac{\dot{\delta}(s)}{w_g(s)}$ is the transfer function relating gust input to control motion. The previous analysis used a simple linear gust alleviation relation

$$C_{L_\alpha}\left(\frac{57.3(-w_g)}{V}\right) + C_{L_{\delta_z}}\delta_{z_c} = 0 \tag{4.32}$$

and the DLF actuator dynamics

$$\frac{\delta_z(s)}{\delta_{z_c}(s)} = \frac{\omega_n^2}{s^2 + 2\zeta\omega_n s + \omega_n^2} \tag{4.33}$$

leading to

$$\frac{\dot{\delta}_z(s)}{w_g(s)} = \frac{\omega_n^2\, \frac{57.3\, C_{L_\alpha}}{V C_{L_{\delta_z}}}\, s}{s^2 + 2\zeta\omega_n s + \omega_n^2} \tag{4.34}$$

The gust spectrum assumed was

$$\Phi_{w_g}(\omega) = \frac{L}{2\pi V}\, \frac{1 + \frac{3L^2}{V^2}\omega^2}{\left[1 + \frac{L^2}{V^2}\omega^2\right]^2}\, \sigma_{w_g}^2 \tag{4.35}$$

If gust simulation limits are desired, then an equally simple linear relation treating the velocity-matched situation is

$$C_{L_{\alpha_m}} \left(- \frac{57.3 \omega_{g_m}}{V} \right) + \frac{(W/S)_m}{(W/S)} C_{L_{\delta_\gamma}} \delta_{\gamma_c} = 0 \qquad (4.36)$$

leading to

$$\frac{\dot{\delta}_\gamma(s)}{\omega_{g_m}(s)} = \frac{\omega_n^2 - \dfrac{57.3 \dfrac{(W/S)}{(W/S)_m} C_{L_{\alpha_m}}}{V C_{L_{\delta_\gamma}}} s}{s^2 + 2\zeta\omega_n s + \omega_n^2} \qquad (4.37)$$

The integrals indicated in (4.29) and (4.30) can be evaluated for factorable forms such as those above using Appendix E of Reference 17.

The results for gust alleviation using (4.34) have been worked out in TIFS Memo No. 130 for V_e = 200 kt at 10,000 feet where L = 1000 feet. Using $C_{L_\alpha}/C_{L_{\delta_\gamma}}$ = 5.22, ω_n = 10 rad/sec, ζ = .7, the integrals (4.29) and (4.30) were evaluated as $N_{0,\dot{\delta}_\gamma}$ = 1.65 and $\sigma_{\dot{\delta}}$ = 1.50 σ_{ω_g}. For a gust environment with σ_{ω_g} = 8 ft/sec the number of times per second the DLF's would exceed $|\dot{\delta}_\gamma|$ = 60 deg/sec is given by

$$2N(60) = 2(1.65) e^{-\left(\frac{60}{\sqrt{2}\,12.0}\right)^2}$$
$$= .0125 \times 10^{-3} \text{ sec}^{-1}$$

or a system limit encountered every 22.2 hours. The 40 deg/sec limit (occurring only at rated load) would be encountered every 76. seconds on the average.

4.5 ACCELERATION AND ATTITUDE MATCHING WITH VELOCITY NOT MATCHED

In Section 3.4 the steady flight special case of general velocity mismatched simulation was examined. That discussion is now extended to include general maneuvering with velocity held constant. The situation treated previously was to start at one trim condition and move to another rate of climb or heading keeping speed constant. Now the procedure is to start at a trim condition and enter a maneuver which is maintained until the DLF's

and SFS's, which are producing the acceleration while attitude is being matched, encounter limits. As is illustrated in Figure 4.9 for the case of

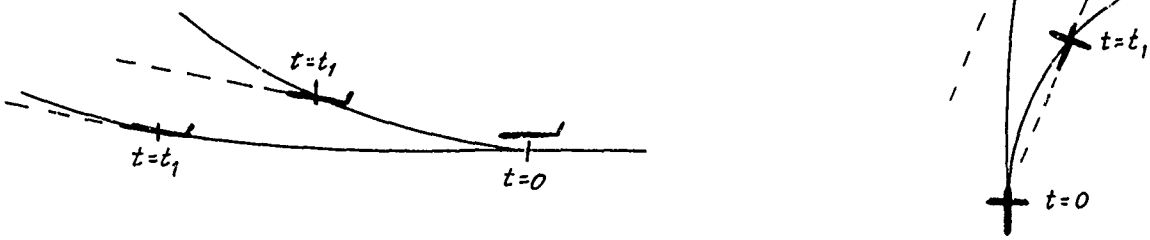

Pullup Level Turn

Figure 4.9 Speed Mismatched Manuevers

a slower flying simulator, for a pullup the simulator angle of attack becomes negative and for a right turn the simulator sideslips to the right to maintain an attitude match. If the maneuver is continued, the flaps or side force surfaces or both will move to their stops. The flap and side force surface capabilities are reflected in γ' and χ limits. These limits are derived in what follows.

4.5.1 General Analysis

Equations (3.39) and (3.40), the starting point for this analysis, can be rewritten in terms of total γ' and χ by assuming a level flight condition initially and a flight path heading which is along the heading reference axis. Then

$$V\chi = V_m \chi_m \tag{4.38}$$

and

$$V\gamma' = V_m \gamma_m \tag{4.39}$$

These equations can be expanded using (3.33) and (3.34) to express χ_m and γ_m in terms of $(\alpha_m - \alpha)$ and $(\beta_m - \beta)$ using small angle assumptions. The TIFS capability can then be estimated since α and β ranges are related to control effectiveness.

Start by assuming α and β are small. Then

$$\sin\gamma = \sin\theta - \beta\sin\phi\cos\theta - \alpha\cos\phi\cos\theta$$

and

$$\sin\chi = \frac{1}{\cos\gamma}(\cos\theta\sin\psi + \beta\sin\psi\sin\theta\sin\phi + \beta\cos\psi\cos\phi + \alpha\sin\psi\cos\phi\sin\theta - \alpha\cos\psi\sin\phi)$$

Without further small angle assumptions on θ and γ, the expression for $\sin\gamma$ can be simplified as follows:

$$\sin\gamma = \sin\theta - (\beta\sin\phi + \alpha\cos\phi)\cos\theta$$

$$= \sin(\theta - \beta\sin\phi - \alpha\cos\phi) \quad \text{for } (\beta\sin\phi + \alpha\cos\phi) \text{ small}^*$$

and thus $$\gamma = \theta - \beta\sin\phi - \alpha\cos\phi \tag{4.40}$$

With the further assumptions that θ and γ are small (the assumption that γ is small is needed anyhow for (4.38) to be valid), the expression for $\sin\chi$ can be simplified as follows:

$$\sin\chi = \sin\psi + \beta\cos\psi\cos\phi - \alpha\cos\psi\sin\phi$$

$$= \sin\psi + (\beta\cos\phi - \alpha\sin\phi)\cos\psi$$

$$= \sin(\psi + \beta\cos\phi - \alpha\sin\phi) \quad \text{for } (\beta\cos\phi - \alpha\sin\phi) \text{ small}$$

and thus $$\chi = \psi + \beta\cos\phi - \alpha\sin\phi \tag{4.41}$$

Note that it has not been necessary to assume ϕ or ψ to be small in deriving (4.40) and (4.41) so that these expressions are useful in computing results for reasonably level turns at large bank angles through large heading changes.

---

* If $|\alpha| < a$ and $|\beta| < a$, then $|\beta\sin\phi + \alpha\cos\phi| < \sqrt{2}\,a$

Using (4.40) and (4.41) in (4.38) and (4.39) and imposing the requirement that $\phi = \phi_m$ and $\psi = \psi_m$ results in

$$\gamma_m = \left(\frac{V_m}{V} - 1\right)^{-1}\left[(\alpha_m - \alpha)\cos\phi_m + (\beta_m - \beta)\sin\phi_m\right] \tag{4.42}$$

and

$$\chi_m = \left(\frac{V_m}{V} - 1\right)^{-1}\left[(\alpha_m - \alpha)\sin\phi_m - (\beta_m - \beta)\cos\phi_m\right] \tag{4.43}$$

(Note that these are extensions of (3.41) and (3.42)

To translate (4.42) and (4.43) into δ_z and δ_y requirements, the right hand sides of (3.4) and (3.5) are needed. It is also necessary to note that $\mu = \mu_m$ is implied by $\phi = \phi_m$ in this simulation within the small angle assumptions on α, β, θ, and γ. This is demonstrated by equating (3.31) and (3.32) to obtain

$$\sin\mu\cos\gamma = \cos\alpha\sin\beta\sin\theta + \cos\beta\sin\phi\cos\theta - \sin\alpha\sin\beta\cos\phi\cos\theta$$

or $$\sin\mu \approx \sin\phi$$

and thus $$\mu \approx \phi \tag{4.44}$$

Therefore (3.4) and (3.5) can be combined to give

$$\frac{T_{y_w} + \bar{q} S C_y}{W} = \frac{T_{y_{w_m}} + \bar{q}_m S_m C_{y_m}}{W_m} \tag{4.45}$$

and

$$\frac{T_{z_w} - \bar{q} S C_L}{W} = \frac{T_{z_{w_m}} - \bar{q}_m S_m C_{L_m}}{W_m} \tag{4.46}$$

4.5.2 Plane of Symmetry Maneuvers

For pullups and pushovers, $\chi_m = \chi = 0$ and $\phi_m = \phi = 0$. Therefore (4.43) is not applicable and (4.42) reduces to

$$\gamma_m = \left(\frac{V_m}{V} - 1\right)^{-1}(\alpha_m - \alpha) \tag{4.47}$$

and neglecting thrust effects, Equation (4.46) gives

$$\frac{C_L}{C_{L_{TRIM}}} = \frac{C_{L_m}}{C_{L_{TRIM_m}}} \tag{4.48}$$

Consider the example of Section 3.4 and Section 4.4.3. The model is described by $C_{L_m} = .190 + .126\,\alpha_m + 1.22\,q_m/V_m$. For $V_{e_{TRIM_m}} = 380$ kt at sea level, the relation

$$\frac{C_{L_m} - C_{L_{TRIM_m}}}{C_{L_{TRIM_m}}} = -\Delta n_{z_{W_m}} = \frac{V_m}{g}\,\frac{q_m}{57.3} \tag{4.49}$$

can be used to obtain

$$C_{L_m} = .187 + .128\,\alpha_m \tag{4.50}$$

Using (4.48) results in $C_L = 1.26\,C_{L_m} = .236 + .161\,\alpha_m$.

As in Section 3.4, the trim attitudes are matched when $\delta_z = 4$ deg and $\alpha = \alpha_m = 1.4$ deg. Suppose a 1.1 g pullup is executed. Then $C_{L_m} = 1.1\,(.366) = .402$ and $\alpha_m = 1.7$ deg. The TIFS angle of attack will start to move up to 1.7 degrees but as γ starts to become positive, it will decrease to maintain $\theta = \theta_m$. The TIFS C_L will move to .507 and as α decreases, δ_z will move more trailing edge down to maintain $C_L = .507$. Figure 4.4 indicates that the structural limit will not be encountered and therefore $\delta_{z_{LIMIT}} = 35$ deg. Figure 3.2 indicates that at $C_L = .507$ and $\delta_z = 35.$ deg, $\alpha = -1.2$ deg. (The TIFS $C_{L_{\delta_c}}$ is neglected here.) Therefore,

$$\gamma_{m_{MAX}} = \left(\frac{644}{322} - 1\right)^{-1}\left[1.7 - (-1.2)\right] = 2.9\ deg$$

$$n_{z_{W_m}} = -1.1$$

This provides about 10 seconds of sustained maneuver.

4.5.3 Level Turns

For level turns, $\gamma_m = 0$ and therefore (4.42) gives

$$(\alpha_m - \alpha)\cos\phi_m + (\beta_m - \beta)\sin\phi_m = 0 \tag{4.51}$$

Combining this with (4.43) gives

$$\gamma_m = -\left(\frac{V_m}{V} - 1\right)^{-1}\left(\frac{\beta_m - \beta}{\cos\phi_m}\right) \tag{4.52}$$

For a coordinated level turn (i.e., $n_{y_{W_m}} = 0$), $n_{z_{W_m}} = -\frac{1}{\cos\mu_m} = -\frac{1}{\cos\phi_m}$

Therefore,

$$\gamma_m = \left(\frac{V_m}{V} - 1\right)^{-1}(\beta_m - \beta)\, n_{z_{W_m}} \tag{4.53}$$

Applying Equation (4.45) for the coordinated turn gives

$$\frac{T_{y_W} + \bar{q} S C_y}{W} = 0 \text{ or } C_y \approx \frac{T}{\bar{q} S}\,\frac{\beta}{57.3} \approx 0$$

From Figure 3.3, $\beta = \pm 8.2°$ neglecting the small yaw rate effect on rudder position to trim. Therefore Equation (4.53) gives

$$\gamma_{m_{MAX}} = \left(\frac{644}{322} - 1\right)^{-1}(0.82)\, n_{z_{W_m}} = -8.2\, n_{z_{W_m}}$$

$$= 9° \text{ for a } 1.1 \text{ g turn}$$

This is the limit which is dictated by side force surface stall. However, the direct lift flap limit must be checked also. The analysis in 4.5.2 applies providing the minor effect of the different pitch rate in a turn is ignored. The result is that $(\alpha_m - \alpha)_{MAX} = 2.9$ deg.
From Equation (4.51)

$$(\beta - \beta_m)_{MAX} = (\alpha_m - \alpha)_{MAX} \cot\phi_m$$

$$= 2.9 \quad (2.2)$$

$$= 6.4 \text{ degrees.}$$

Therefore $\gamma_{m_{MAX}} = 6.4\ (1.1) = 7.0$ deg due to direct lift flap deflection limit. This provides about 5 seconds in the turn.

SECTION V

MODEL-FOLLOWING CAPABILITY

This section documents the numerical values of the model-following system gains that were used for the Phase I and Phase II in-flight research programs recently performed using the TIFS aircraft (References 8 and 9) The control laws actually used for these research programs will be presented and compared with those presented in the final technical report (Reference 4) for the design and development phase. In addition, examples of model following will be presented which indicate the model following achieved by the TIFS aircraft as of September 1971.

5.1 LATERAL-DIRECTIONAL CONTROL LAW

The feedforward lateral-directional control law is achieved by solution of the three-degree-of-freedom linearized lateral-directional equations of motion. Once the equations of motion are solved simultaneously (see Section II, Equation (2.34)) coefficients which multiply a particular state variable of the aircraft are "lumped" together to form the terms δ_i /model state variable. Either the model state variables (e.g., β), their derivatives (e.g., $\dot{\beta}$) or combinations of these terms (e.g., Δn_y) may be used. The total control law actually consists of three components:

a) feedforwards of model states, etc.,

b) feedbacks of error signals based on comparison of the model and plant states, and

c) gust alleviation signals.

$$
\begin{bmatrix} \delta_{a_c} \\ \delta_{r_c} \\ \delta_{y_c} \end{bmatrix} = \begin{bmatrix} \left(\frac{\delta_a}{\dot{p}_m}\right)\left(\frac{\delta_a}{p_m}\right) & 0 & 0 & 0 & 0 & 0 \\ 0 & \left(\frac{\delta_r}{p_m}\right)\left(\frac{\delta_r}{\phi_m}\right)\left(\frac{\delta_r}{\dot{r}_m}\right)\left(\frac{\delta_r}{r_m}\right)\left(\frac{\delta_r}{\dot{\beta}_{m_{TCG}}}\right) & 0 \\ 0 & 0 & 0 \left(\frac{\delta_y}{\dot{r}_m}\right) 0 & 0 \left(\frac{\delta_y}{n_{y_{m_{TCG}}}}\right) \end{bmatrix} \begin{bmatrix} \dot{p}_m \\ p_m \\ \phi_m \\ \dot{r}_m \\ r_m \\ \dot{\beta}_{m_{TCG}} \\ \beta_{m_{TCG}} \\ n_{y_{m_{TCG}}} \end{bmatrix}
$$

$$
+ \begin{bmatrix} \left(\frac{\delta_a}{e_p}\right)\left(\frac{\delta_a}{e_\phi}\right) & 0 & 0 & 0 \\ 0 & 0 \left(\frac{\delta_r}{e_r}\right)\left(\frac{\delta_r}{e_{\beta_{m_{TCG}}}}\right)\left(\frac{\delta_r}{\int e_{\beta_{m_{TCG}}}}\right) \\ 0 & 0 & 0 \left(\frac{\delta_y}{e_{\beta_{m_{TCG}}}}\right)\left(\frac{\delta_y}{\int e_{\beta_{m_{TCG}}}}\right) \end{bmatrix} \begin{bmatrix} e_p \\ e_\phi \\ e_r \\ e_{\beta_{TCG}} \\ \int e_{\beta_{TCG}} \end{bmatrix} + \begin{bmatrix} \left(\frac{\delta_a}{\beta_g}\right) \\ \left(\frac{\delta_r}{\beta_g}\right) \\ \left(\frac{\delta_y}{\beta_g}\right) \end{bmatrix} \beta_g \qquad (5.1)
$$

where the notation is that used in Reference 4, e.g., $e_p = p_m - p$. The lateral-directional feedforward and gust compensator gains used in References 8 and 9 are identical with those published in Reference 4 for the landing approach island and are presented in Table 5.1.

As more is learned about the performance of the system under different conditions the feedbacks and feedforwards are changed. The feedback gains presently used in lateral-directional model following are presented in Table 5.2 and compared to the lateral-directional feedback gains presented in Reference 4. The primary changes are an increase in the feedback gains to the aileron and the elimination of the heading error feedback to the rudder. These changes were made to obtain quicker and smoother roll following performance and improve both ψ and β following by removing the possible ambiguity of requiring the rudder to control both quantities. Examples of lateral-directional model following achieved during the research programs discussed in References 8 and 9 are presented in Section 5.3.

TABLE 5.1

LATERAL-DIRECTIONAL FEEDFORWARD AND GUST COMPENSATOR GAINS

Gain	Landing Approach Island	Up-and-Away Island
$(\delta_a/\dot{p}_m)$	-.535	-.298
(δ_a/p_m)	-1.227	-.8128
$(\delta_a/\beta_{m_{TCG}})$	-.6478	-.9676
(δ_r/p_m)	-.1473	-.0175
(δ_r/ϕ_m)	-.2487	-.2367
$(\delta_r/\dot{r}_m)$	-.896	-.476
(δ_r/r_m)	1.835	1.465
$(\delta_r/\dot{\beta}_{m_{TCG}})$	2.110	1.646
$(\delta_r/\beta_{m_{TCG}})$	1.438	1.438
$(\delta_y/\dot{r}_m)$	.6528	.3264
$(\delta_y/\beta_{m_{TCG}})$	2.218	2.085
$(\delta_y/n_{y_{m_{TCG}}})$	104.	51.7
(δ_a/β_g)	-.6478	-.9677
(δ_r/β_g)	1.439	1.438
(δ_y/β_g)	2.218	2.086

TABLE 5.2

MODEL-FOLLOWING GAINS (LATERAL-DIRECTIONAL)

Gain	Present Gains (Ref. 8 and 9)	Previous Gains (Ref. 4)
(δ_a/e_p)	-3.52	-1.6
(δ_a/e_ϕ)	-3.52	-3.0
(δ_r/e_r)	-2.0	-2.0
$(\delta_r/\sin e_\psi)$	0.0	-286.5
$(\delta_r/e_{\beta_{TCG}})$	1.69	1.695
$(\delta_r/\int e_{\beta_{TCG}})$	2.21	2.224
$(\delta_y/e_{\beta_{TCG}})$	10.0	10.0
$(\delta_y/\int e_{\beta_{TCG}})$	10.0	10.0

5.2 LONGITUDINAL CONTROL LAW

The feedforward portion of the longitudinal control law presently mechanized on the TIFS aircraft has been modified from the lumped parameter technique presented in Reference 4 and previously discussed for the lateral-directional control law. In place of the "lumped" parameter mechanization, the three-degree-of-freedom linearized longitudinal equations of motion were mechanized. This technique allows direct control of individual stability and control derivatives as discussed in Section 2.5. It was found to be advantageous during the preliminary flight evaluations of model following for the recently completed research programs to be able to quickly evaluate the effects of individual TIFS stability and control derivatives in an attempt to improve longitudinal model following. The equations for the computation of longitudinal feedforward command signals were programmed as foilows

$$-D_{\delta_x}\Delta\delta_{x_c} = \dot{V}_{m_{rcg}} + g(\sin\gamma_m - \sin\mathring{\gamma}_m) + D_V\Delta V_{m_{rcg}} + \left(D_\alpha^* + \frac{T_0\alpha_t}{m}\right)\Delta\alpha_{m_{rcg}} + D_{\delta_z}\Delta\delta_{z_c} \tag{5.2}$$

$$Z_{\delta_z}\Delta\delta_{z_c} = \frac{g}{V_t}\Delta n_{z_{m_{rcg}}} - Z_V\Delta V_{m_{rcg}} - Z_\alpha\Delta\alpha_{m_{rcg}} \tag{5.3}$$

$$M_{\delta_e}\Delta\delta_{e_c} = \dot{q} - M_q q - M_V\Delta V_{m_{rcg}} - M_{\dot{\alpha}}\dot{\alpha}_{m_{rcg}} - M_\alpha\Delta\alpha_{m_{rcg}} - M_{\delta_z}\Delta\delta_{z_c} \tag{5.4}$$

where D_α^* represents aerodynamic drag. Definitions of the linearized stability and control derivatives are presented in Reference 1. Although the longitudinal feedforward gains were mechanized in an equations-of-motion format, simultaneous solution of these equations will also yield "lumped" parameter feedforward gains. Thus the longitudinal control law can still be represented by this format and it is presented below.

$$
\begin{bmatrix} \delta_{a_c} \\ \delta_{\chi_c} \\ \delta_{\gamma_c} \end{bmatrix} = \begin{bmatrix} \left(\frac{\delta_e}{\dot{q}_m}\right)\left(\frac{\delta_e}{q_m}\right) & 0 & \left(\frac{\delta_e}{\Delta V_{m_{TCG}}}\right)\left(\frac{\delta_e}{\dot{\alpha}_{m_{TCG}}}\right)\left(\frac{\delta_e}{\Delta\alpha_{m_{TCG}}}\right) & 0 & \left(\frac{\delta_e}{\Delta n_{\gamma m_{TCG}}}\right) \\ 0 & \left(\frac{\delta_\chi}{\dot{V}_{m_{TCG}}}\right)\left(\frac{\delta_\chi}{\Delta V_{m_{TCG}}}\right) & 0 & \left(\frac{\delta_\chi}{\Delta\alpha_{m_{TCG}}}\right)\left(\frac{\delta_\chi}{\Delta\sin\gamma}\right)\left(\frac{\delta_\chi}{\Delta n_{\gamma m_{TCG}}}\right) & \\ 0 & 0 & \left(\frac{\delta_\gamma}{\Delta V_{m_{TCG}}}\right) & 0 & \left(\frac{\delta_\gamma}{\Delta\alpha_{m_{TCG}}}\right) \quad 0 \quad \left(\frac{\delta_\gamma}{\Delta n_{\gamma m_{TCG}}}\right) \end{bmatrix} \begin{bmatrix} \dot{q}_m \\ q_m \\ \dot{V}_{m_{TCG}} \\ \Delta V_{m_{TCG}} \\ \dot{\alpha}_{m_{TCG}} \\ \Delta\alpha_{m_{TCG}} \\ \Delta\sin\gamma \\ \Delta n_{\gamma m_{TCG}} \end{bmatrix}
$$

$$
+ \begin{bmatrix} \left(\frac{\delta_e}{e_q}\right)\left(\frac{\delta_e}{e_\theta}\right)\left(\frac{\delta_e}{\int e_\theta}\right) & 0 & 0 & 0 & 0 \\ 0 & 0 & 0 & \left(\frac{\delta_\chi}{e_{\dot{V}_{TCG}}}\right)\left(\frac{\delta_\chi}{e_{V_{TCG}}}\right) & 0 \quad 0 \\ 0 & 0 & 0 & 0 & 0 \quad \left(\frac{\delta_\gamma}{e_{\dot{\alpha}_{TCG}}}\right)\left(\frac{\delta_\gamma}{e_{\alpha_{TCG}}}\right) \end{bmatrix} \begin{bmatrix} e_q \\ e_\theta \\ \int e_\theta \\ e_{\dot{V}_{TCG}} \\ e_{V_{TCG}} \\ e_{\dot{\alpha}_{TCG}} \\ e_{\alpha_{TCG}} \end{bmatrix} + \begin{bmatrix} 0 \\ 0 \\ \left(\frac{\delta_\gamma}{\alpha_g}\right) \end{bmatrix} \alpha_g \qquad (5.5)
$$

Table 5.3 presents the feedforward gains that were used for the Phase I and Phase II research programs and compares them with the values presented for the landing approach island. The differences for the Phase I and Phase II values are related to the initial TIFS trim conditions and the fact that the Phase I gains were selected for a simulation velocity envelope from 160 to 120 knots, while the Phase II values were selected for a simulation velocity envelope from 200 to 160 knots. In addition, during the preliminary evaluations of model following for the Phase II program, it was determined that increasing the δ_{χ_c} signal would compensate for the influence of the throttle servo characteristics on signal gain.

TABLE 5.3

LONGITUDINAL FEEDFORWARD AND GUST COMPENSATOR GAINS

Gain	Phase I (Ref. 8)	Phase II (Ref. 9)	Landing Approach Island (Ref. 4)
$(\delta_e/\dot{q}_m)$	-.44	-.313	-.346
(δ_e/q_m)	-.203	-.172	0.0
$(\delta_e/\Delta V_{m_{TCG}})$	+.02	+.02	0.0
$(\delta_e/\dot{\alpha}_{m_{TCG}})$	-.130	-.110	0.0
$(\delta_e/\Delta\alpha_{m_{TCG}})$	-.010	+.206	0.0
$(\delta_e/\Delta n_{z_{m_{TCG}}})$	+2.061	+4.027	0.0
$(\delta_a/\dot{V}_{m_{TCG}})$	0	0	.296
$(\delta_x/\dot{V}_{m_{TCG}})$	6.283	12.566	8.311
$(\delta_x/\Delta V_{m_{TCG}})$	-.019	-.039	0.0
$(\delta_x/\Delta\alpha_{m_{TCG}})$	-2.364	-4.257	0.0
$(\delta_x/\Delta\sin\gamma)$	202.309	404.618	0.0
$(\delta_x/\Delta n_{z_{m_{TCG}}})$	-32.583	-67.0	0.0
$(\delta_z/\Delta V_{m_{TCG}})$	-.804	-.317	0.0
$(\delta_z/\dot{\alpha}_{m_{TCG}})$	0.0	0.0	-8.753
$(\delta_z/\Delta\alpha_{m_{TCG}})$	-10.604	-6.992	-7.844
$(\delta_z/\Delta n_{z_{m_{TCG}}})$	-91.584	-61.7216	0.0
(δ_z/q_m)	0.0	0.0	9.175
(δ_x/α_g)	0.0	0.0	2.037
(δ_z/α_g)	-7.26	-7.26	-7.979

Table 5.4 compares the feedback gains used in the longitudinal model system for the recent research programs with those presented in Reference 4.

TABLE 5.4

MODEL-FOLLOWING GAINS (LONGITUDINAL)

Gain	Present Gains (Ref. 8 and 9)	Previous Gains (Ref. 4)
(δ_e/e_q)	-1.0	-1.0
(δ_e/e_θ)	-5.538	13.75
$(\delta_e/\int e_\theta)$	-4.875	0.0
$(\delta_x/e_{\dot{V}})$	2.45	5.0
$(\delta_x/e_{\Delta V})$	4.992	9.0
$(\delta_x/\int e_{\Delta V})$	0.0	4.0
(δ_z/e_q)	0.0	-1.0
$(\delta_z/e_{\dot{\alpha}})$	-1.0	0.0
$(\delta_z/e_{\Delta\alpha})$	-5.0	-5.0
$(\delta_z/\int e_{\Delta\alpha})$	0.0	-5.0

A comparison of the longitudinal feedforward gains between those that would result from the equations-of-motion mechanization and the previous gains reported in Reference 4 indicates that the significant changes to the direct lift flap command signal were the replacement of the $\dot{w}$ and q feedforwards by a normal acceleration command and the inclusion of a velocity feedforward. It was determined during pre-evaluation flights that without the velocity feedforward, improper flap motion would occur as the aircraft was stabilized at different flight speeds at the same altitude. Thus the relationship between trim velocity and trim angle of attack for the model could not be satisfied unless a velocity feedforward were introduced. In addition, it was noted that incorrect flap position could occur with change in altitude. This was analyzed and it was determined that the introduction of a $\Delta\rho$ or Δh feedforward would correct this situation. In essence, when the equations of motion were linearized, dynamic pressure was expanded only in terms of ΔV, thus

$$q_0 = \tfrac{1}{2}\rho_c V_0^2$$

$$(q_0 + \Delta q) = \tfrac{1}{2}\rho_0 (V_0 + \Delta V)^2 \approx q_0 + \rho_0 V_0 \Delta V + \tfrac{1}{2}\rho_0 \Delta V^2 \qquad (5.6)$$

However, as the height changes, density changes occur, thus a more complete expansion would have the form

$$q_0 + \Delta q = \frac{1}{2}(\rho_0 + \Delta\rho)(V_0 + \Delta V)^2$$
$$= q_0 + \rho_0 V_0 \Delta V + \frac{V_0^2}{2}\Delta\rho \qquad \text{+ higher order terms} \tag{5.7}$$

where $\Delta\rho$ can be related to Δh by the definition of the appropriate atmospheric relationship (e.g., $\rho = K_0 + K_1 h + K_2 h^2$). This effect was not included in the feedforwards since it was determined that the model following would not be significantly affected for the relatively small altitude variations to be used in the planned evaluation program. The system was re-engaged prior to the landing approach evaluations if the configuration familiarization and airwork portions of the in-flight program were performed at altitudes significantly different from the ILS approach intercept altitude used in the program. Similarly, velocity feedforwards were also introduced into the command signals to the elevator and throttle servos. Essentially the modifications to the feedforward signals result from use of a more complete form of the linearized equations of motion with less simplifying assumptions than those previously reported in Reference 4.

5.3 IN-FLIGHT MODEL FOLLOWING

The following figures are representative of the model following achieved by the TIFS airplane during the research programs reported in References 8 and 9. Both longitudinal and lateral-directional responses are given. The model used is described in detail in the previously cited references; it basically consisted of a nonlinear kinematic representation of the equations of motion with small angle assumptions introduced on angle of attack and sideslip. Lateral-directional aerodynamics were based upon linearized derivatives, while the longitudinal derivatives included nonlinearities.

The responses shown on Figures 5-1 through 5-7 were obtained at the following flight condition:

$$V_{ind} = 135 \text{ knots}$$

$$h_p = 10,000 \text{ feet}$$

$$\delta_{F_{TIFS}} = 30° \qquad \delta_{\gamma_{TIFS}} = 17°$$

$$\gamma_{TRIM} = 0$$

The following inputs are illustrated on the figures:

Figure No.	Input	Source
5-1	Elevator step	Automatic
5-2	Elevator doublet	Evaluation pilot
5-3	Throttle step	Automatic
5-4	Aileron step	Automatic
5-5	Rudder doublet	Evaluation pilot
5-6	Rudder doublet	Evaluation pilot
5-7	Maneuvering flight	Evaluation pilot

In general, the model following illustrated on these figures is quite good. Similar examples of model following achieved on actual evaluation landing approaches in varying levels of turbulence are presented in References 8 and 9. Some errors in model following appear upon close examination of the time histories presented. Examination of the $\dot{V}$ time history on Figures 5-2, 5-3, and 5-5 indicates some distortion in the model following for these specific inputs. Examination of the static pressure signal for these records indicates that it is affected by sudden changes in thrust from the TIFS propellers and by yaw rate changes. Thus, it appears possible that model following in $\dot{V}$ could be improved for these specific inputs if the location of the static sources were improved. This effect is also shown on the $\sin\gamma$ following achieved on Figures 5-3 and 5-5. In addition, the angle of attack following for a rudder doublet indicates that the α_{VANE} signal is possibly distorted by local flow field changes resulting from yawing motion of the aircraft. However, it should be noted that the following achieved to gross maneuvering of the aircraft (i.e., Figure 5-6) does not indicate that

these effects are significant when all degrees of freedom of the aircraft are significantly excited, and thus the distortions indicated do not appear to limit the TIFS capability in model following. However, improvement in these signals is desirable. In addition, the $\dot{V}$ time history indicates a time lag on the order of one second to a throttle step command. This is related to the overall TIFS thrust response to throttle commands and indicates that compensation may be necessary for $\dot{V}$ following to high-frequency throttle commands. At present, any suggested system modifications are tentative based on limited in-flight evidence. It is anticipated that these effects will be examined in more detail during the pre-evaluation and checkout flying prior to the next TIFS research programs.

In terms of the cockpit environment, all records indicate a satisfactory level of model following on Δn_{z_p} and Δn_{y_p}.

Figures 5-5 and 5-6 are evaluation pilot rudder doublets for the same aircraft model on subsequent flights. Figure 5-5 indicates an amplification in the roll rate of the plant with respect to the model which is not as apparent upon examination of the roll rate following shown on Figure 5-6. The aileron step input command, Figure 5-4, indicates satisfactory roll rate following. Since the roll rate following has, in general, been satisfactory, the results in Figure 5-5 are unexplained at this point.

Figure 5-7 shows the model-following during general maneuvering.

In summary, the model-following performance presently available on the TIFS airplane is quite good. However, it appears that this performance might be enhanced by improvement in the location of the static pressure source signal required in the air data computations, compensation for the TIFS thrust dynamics and additional flow field corrections to the angle of attack vane sensor signal. These conclusions are tentative based on rather limited flight test data.

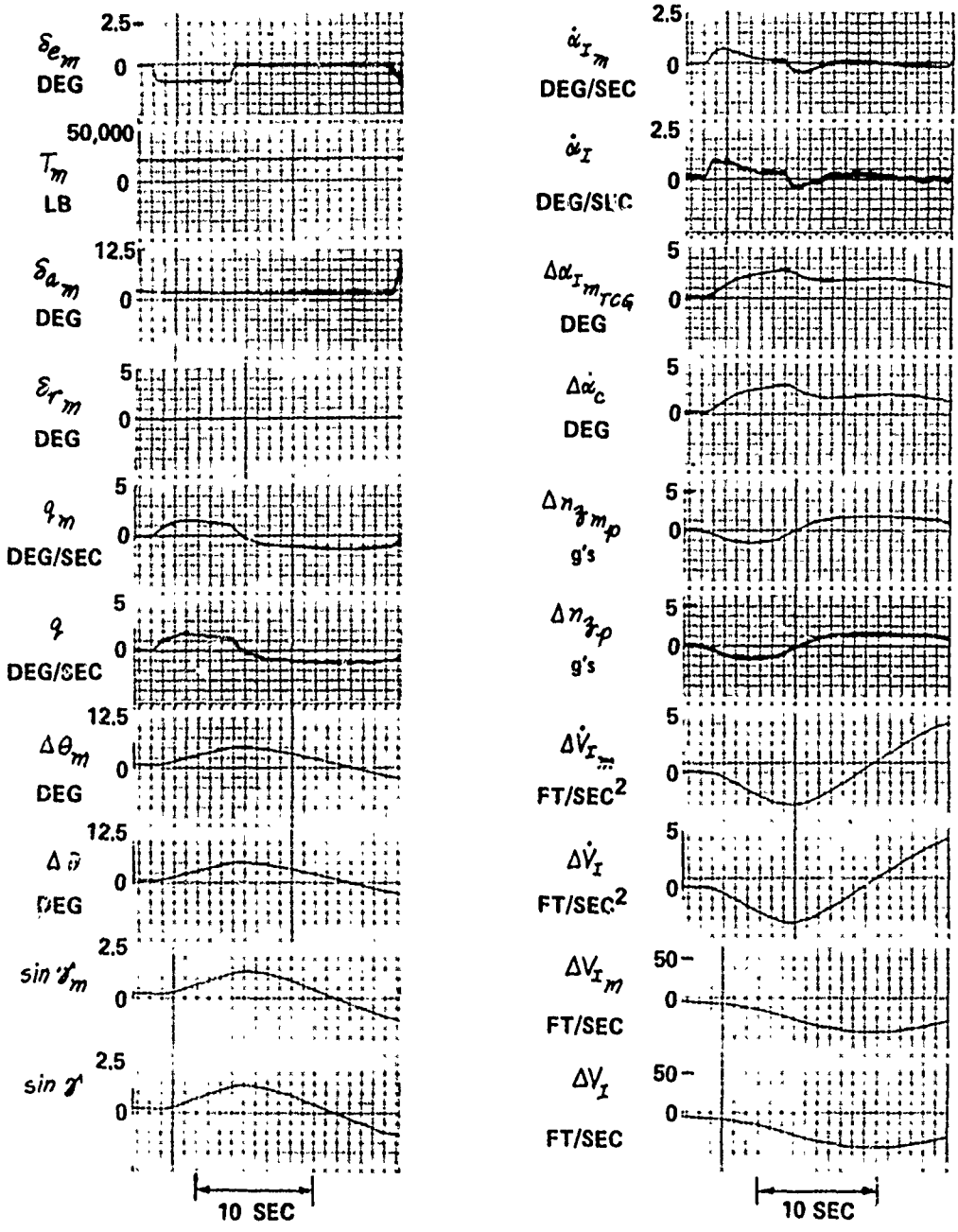

Figure 5.1 In-Flight Responses to Automatic Elevator Step Input

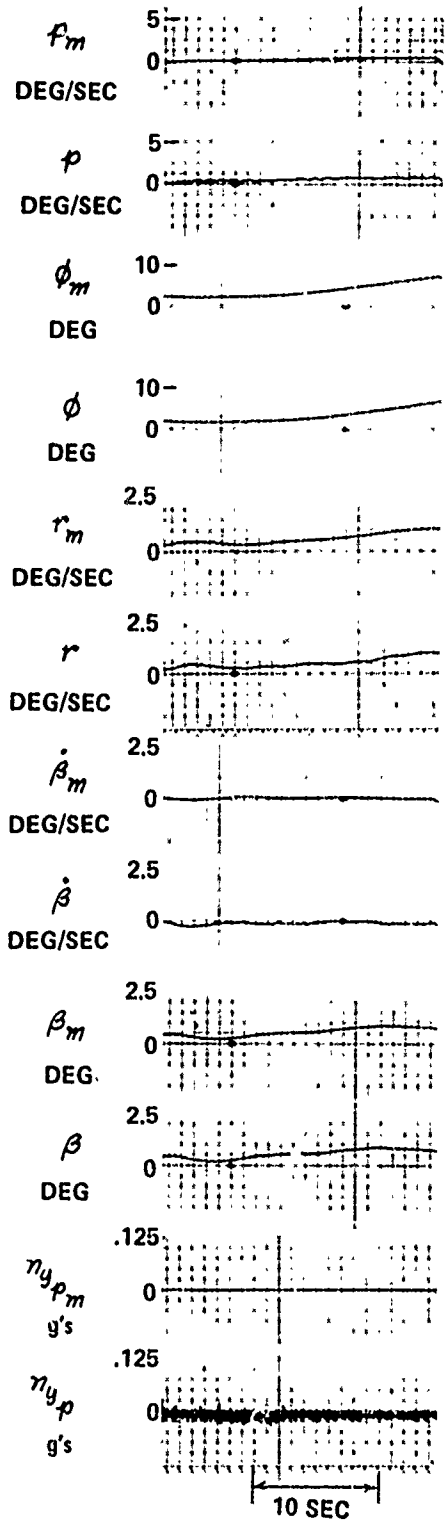

Figure 5.1 (con't) In-Flight Responses to Automatic Elevator Step Input

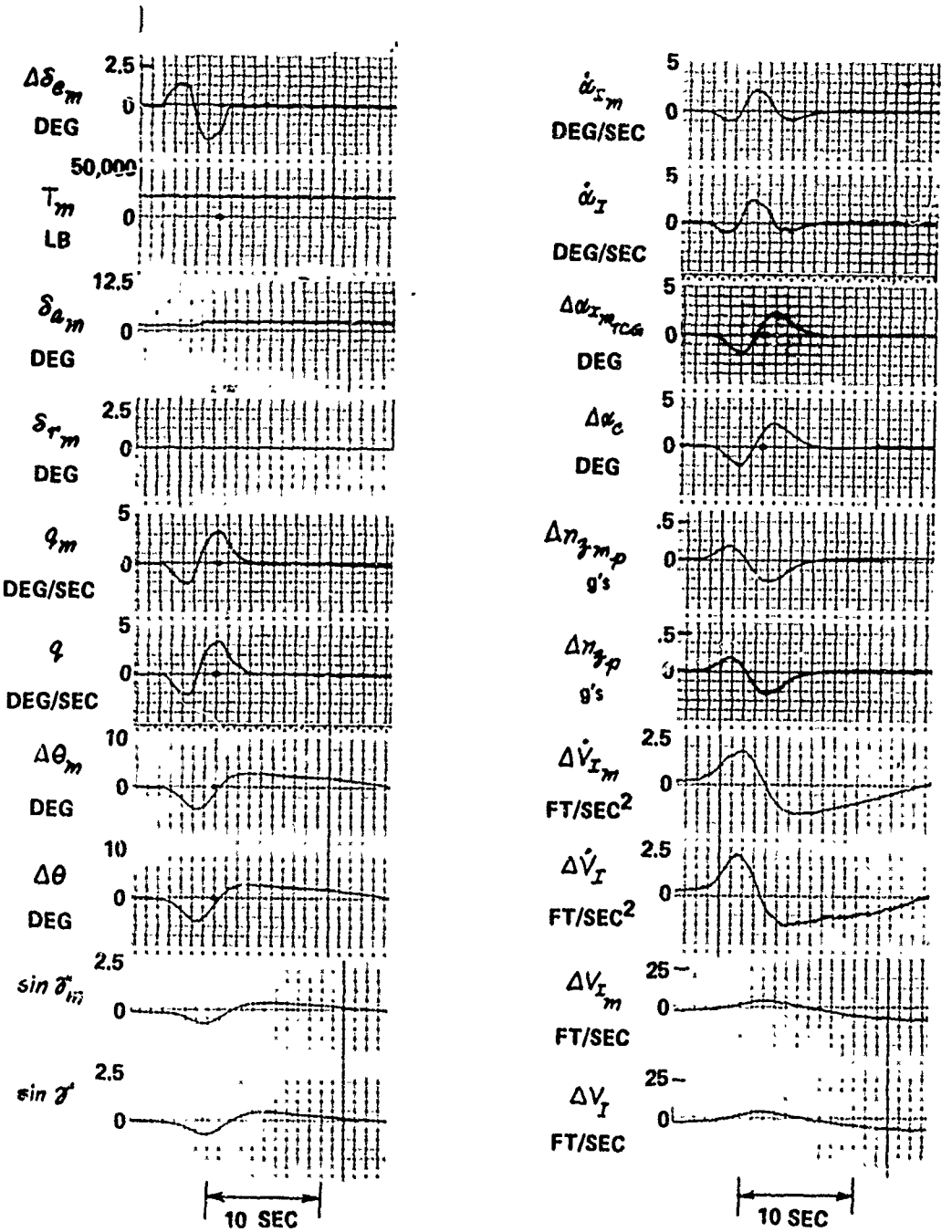

Figure 5.2 In-Flight Responses to Manual Elevator Doublet

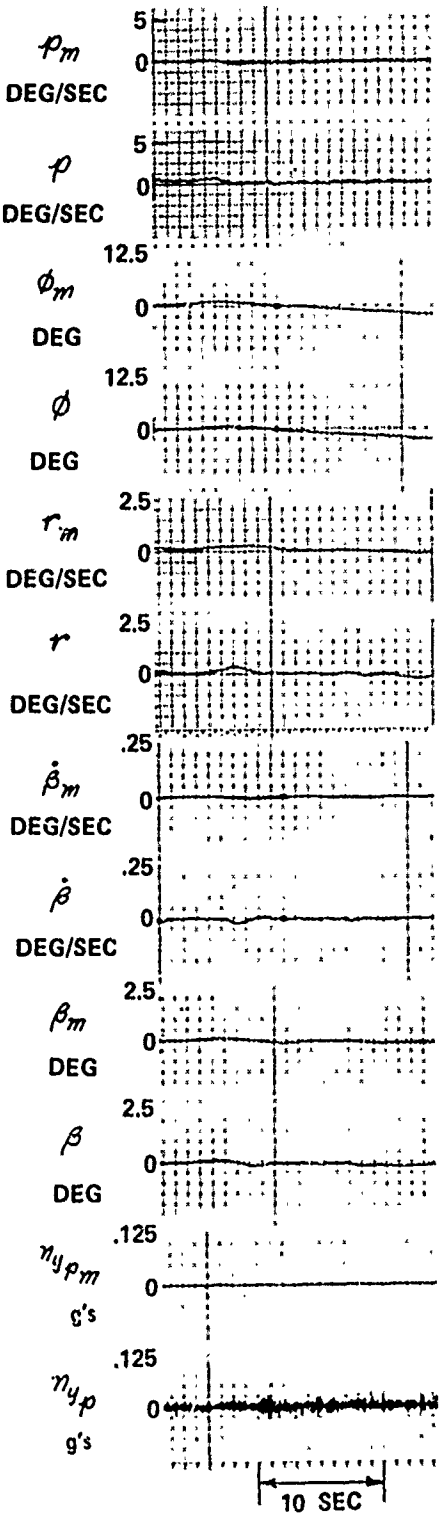

Figure 5.2 (con't) In-Flight Responses to Manual Elevator Doublet

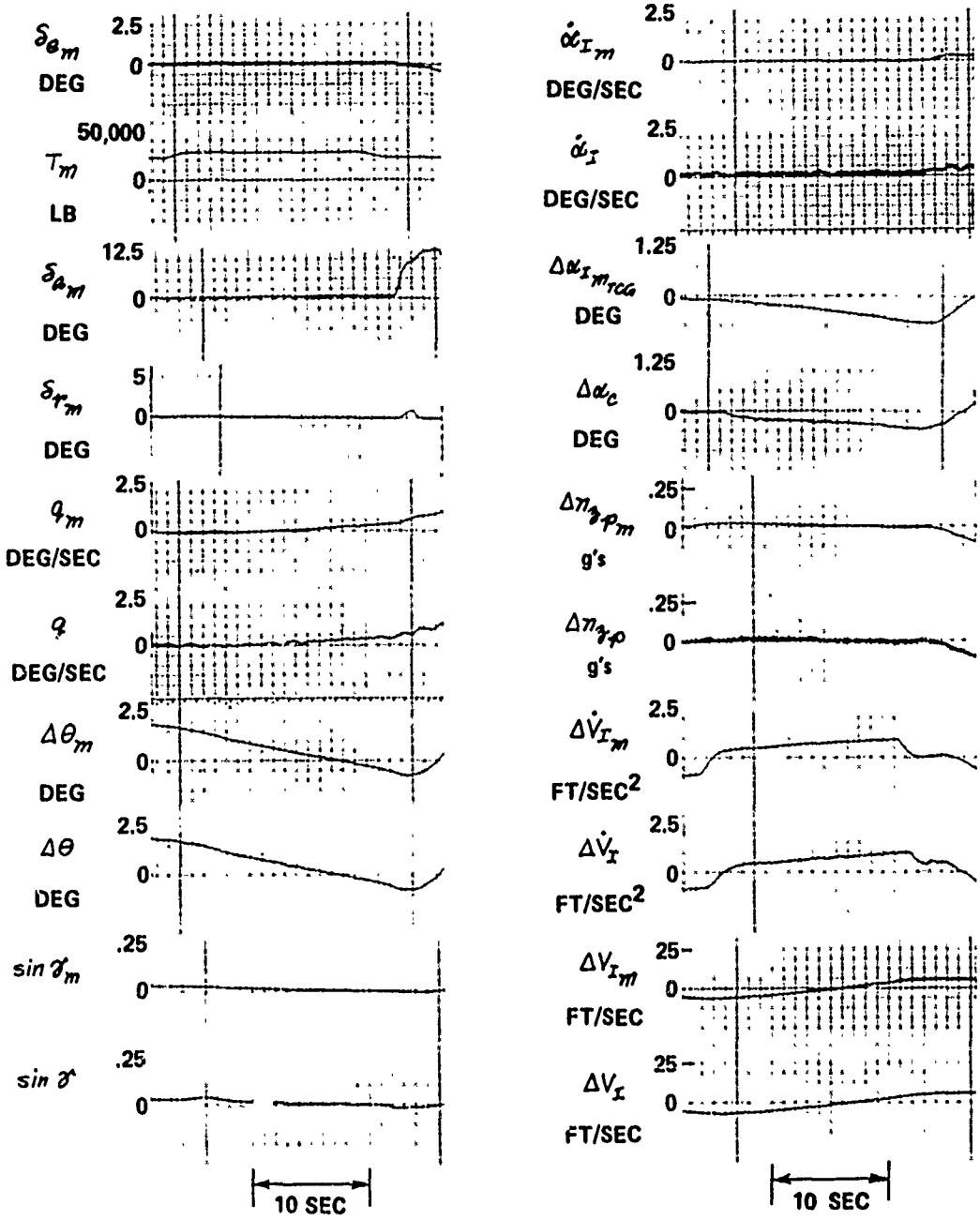

Figure 5.3 In-Flight Responses to Automatic Throttle Step

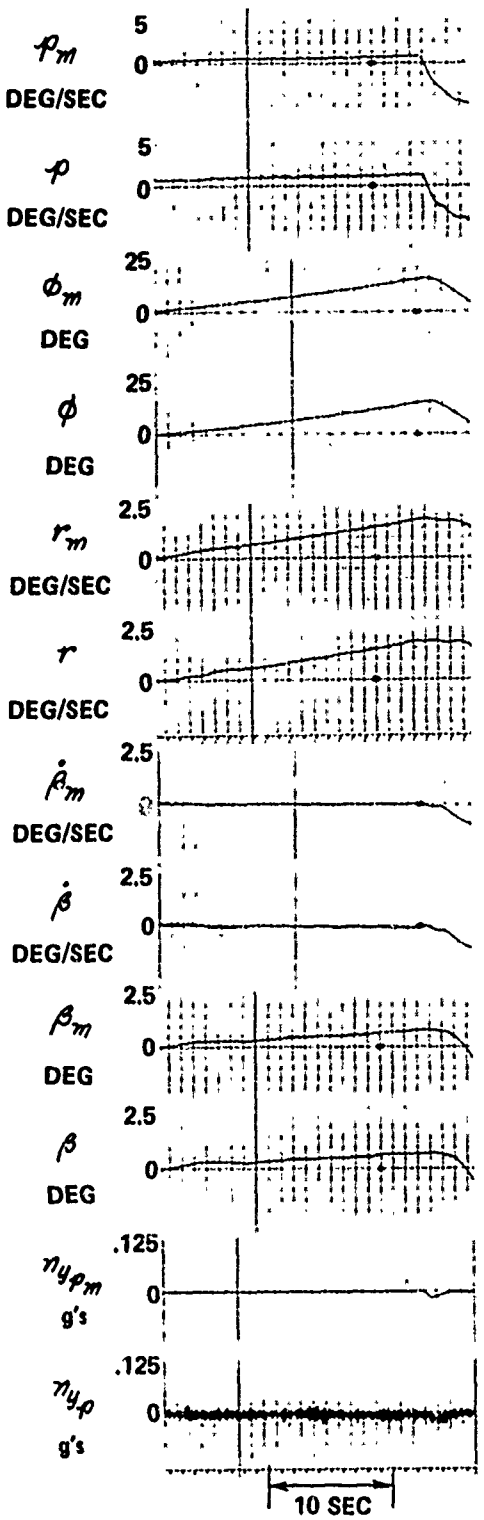

Figure 5.3 (con't) In-Flight Responses to Automatic Throttle Step

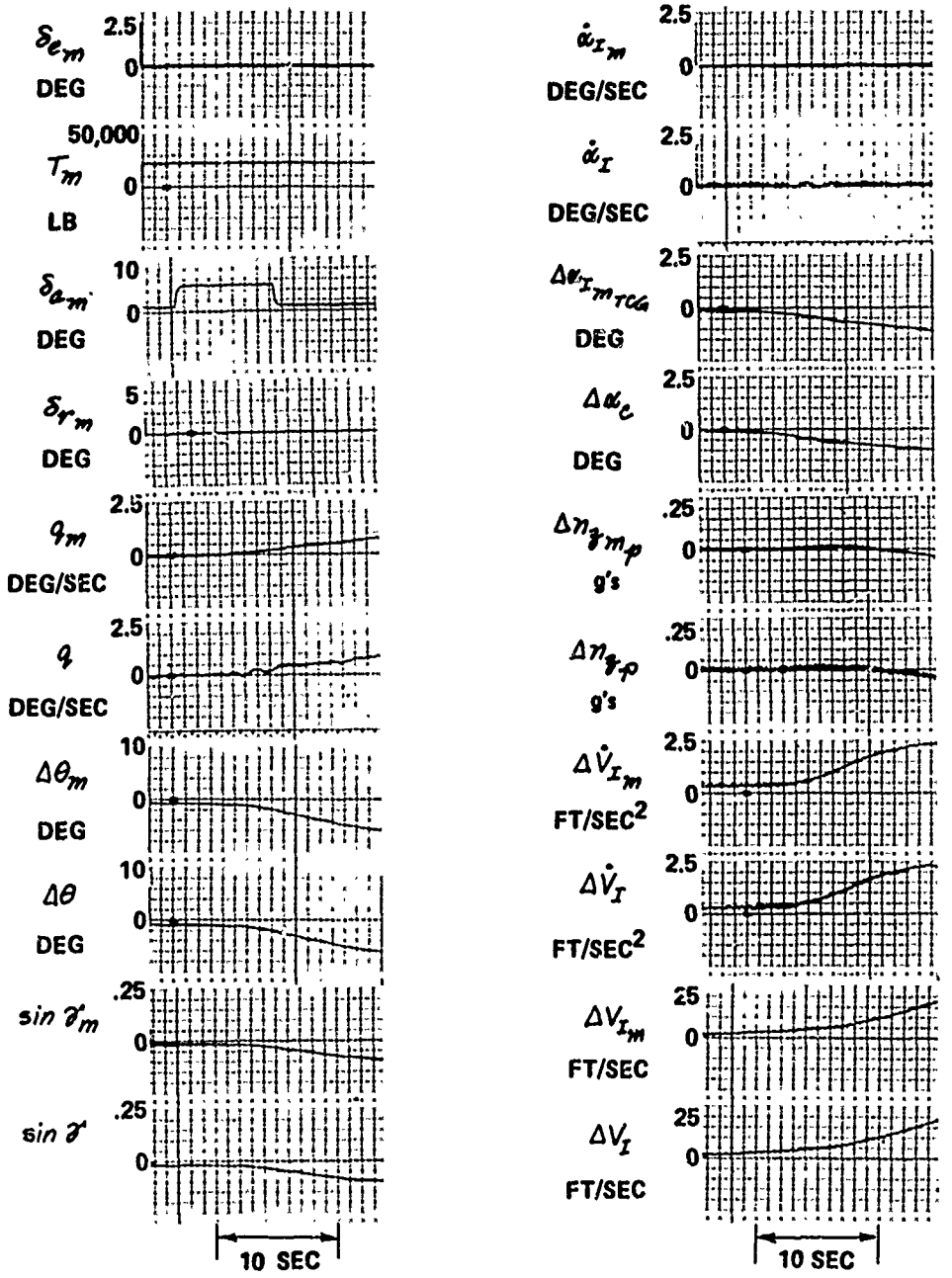

Figure 5.4 In-Flight Responses to Automatic Aileron Step

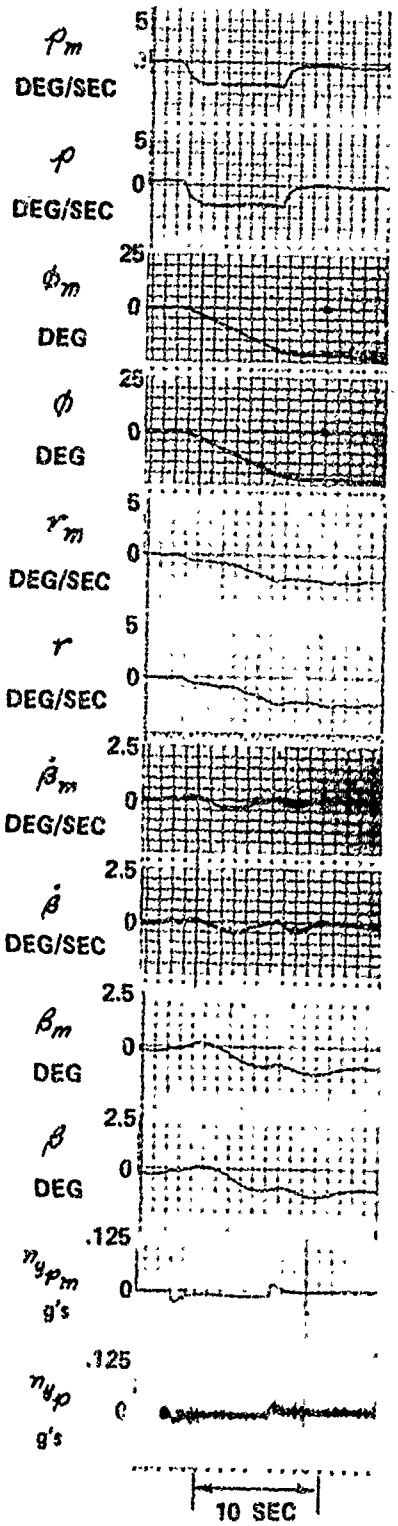

Figure 5.4 (con't) In-Flight Responses to Automatic Aileron Step

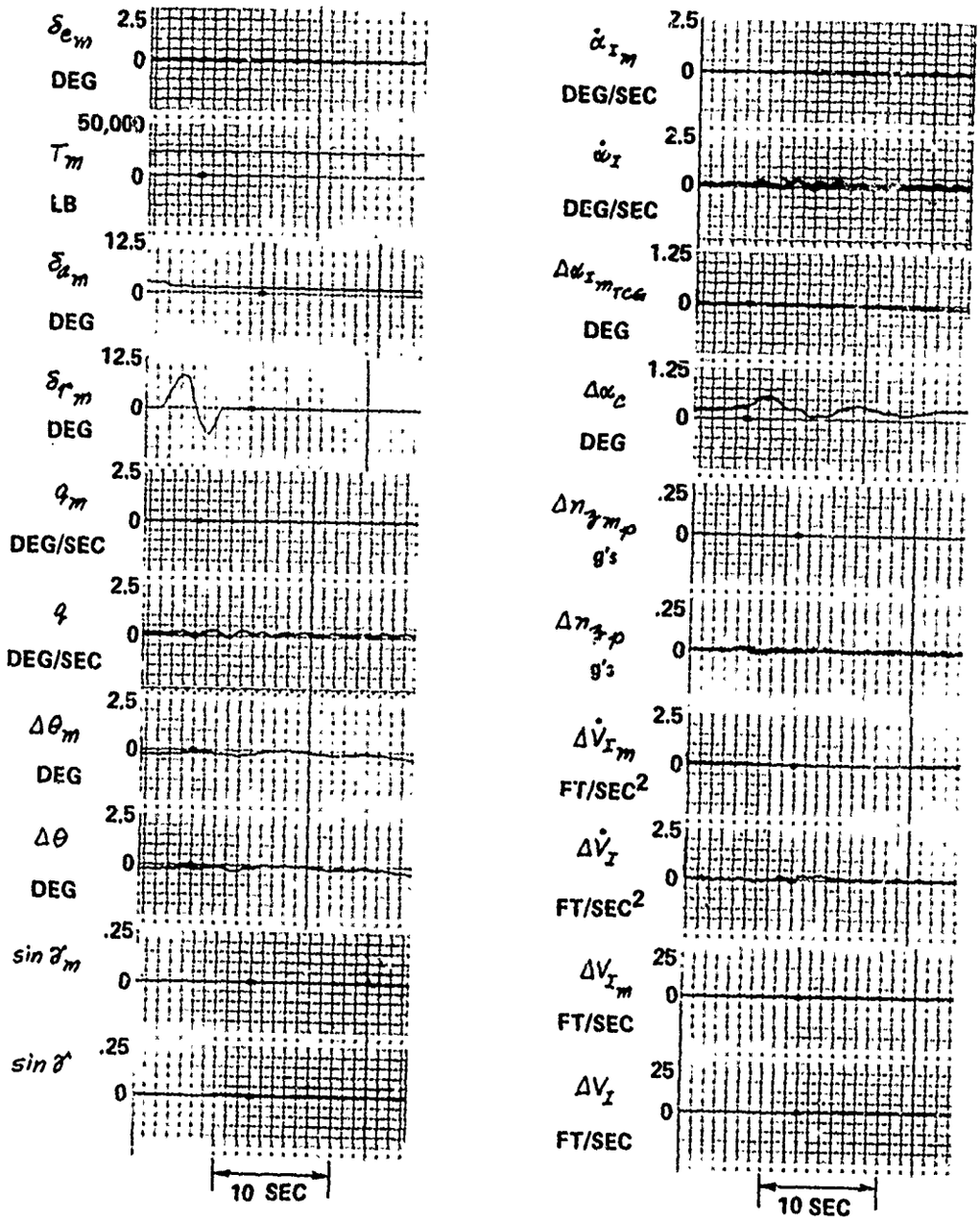

Figure 5.5 In-Flight Responses to Manual Rudder Doublet (First Flight)

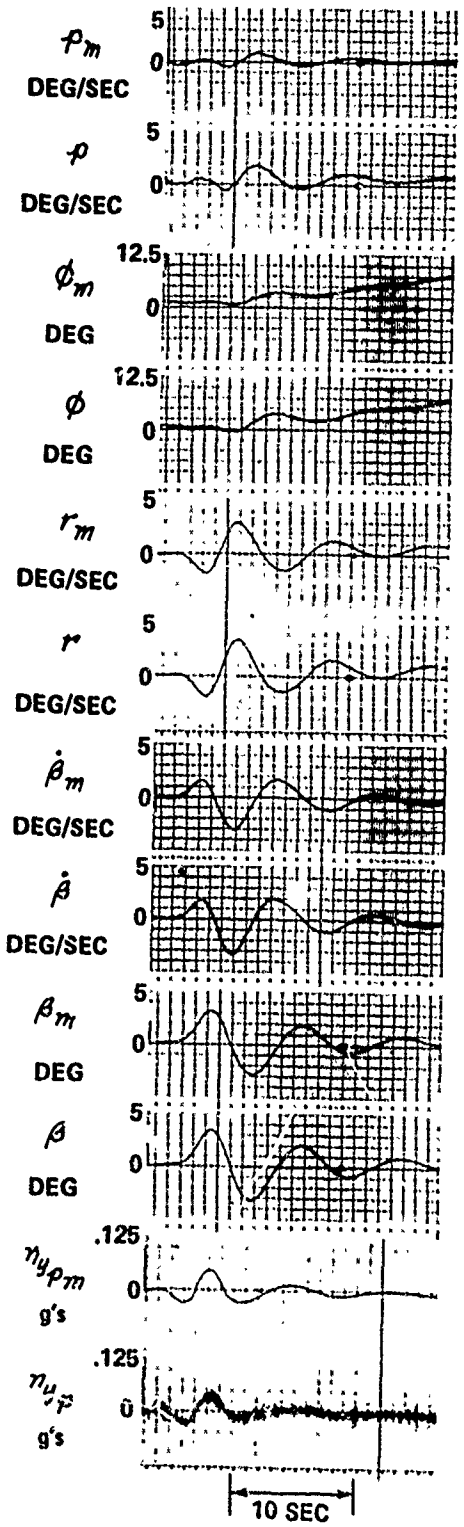

Figure 5.5 (con't) In-Flight Responses to Manual Rudder Doublet (First Flight)

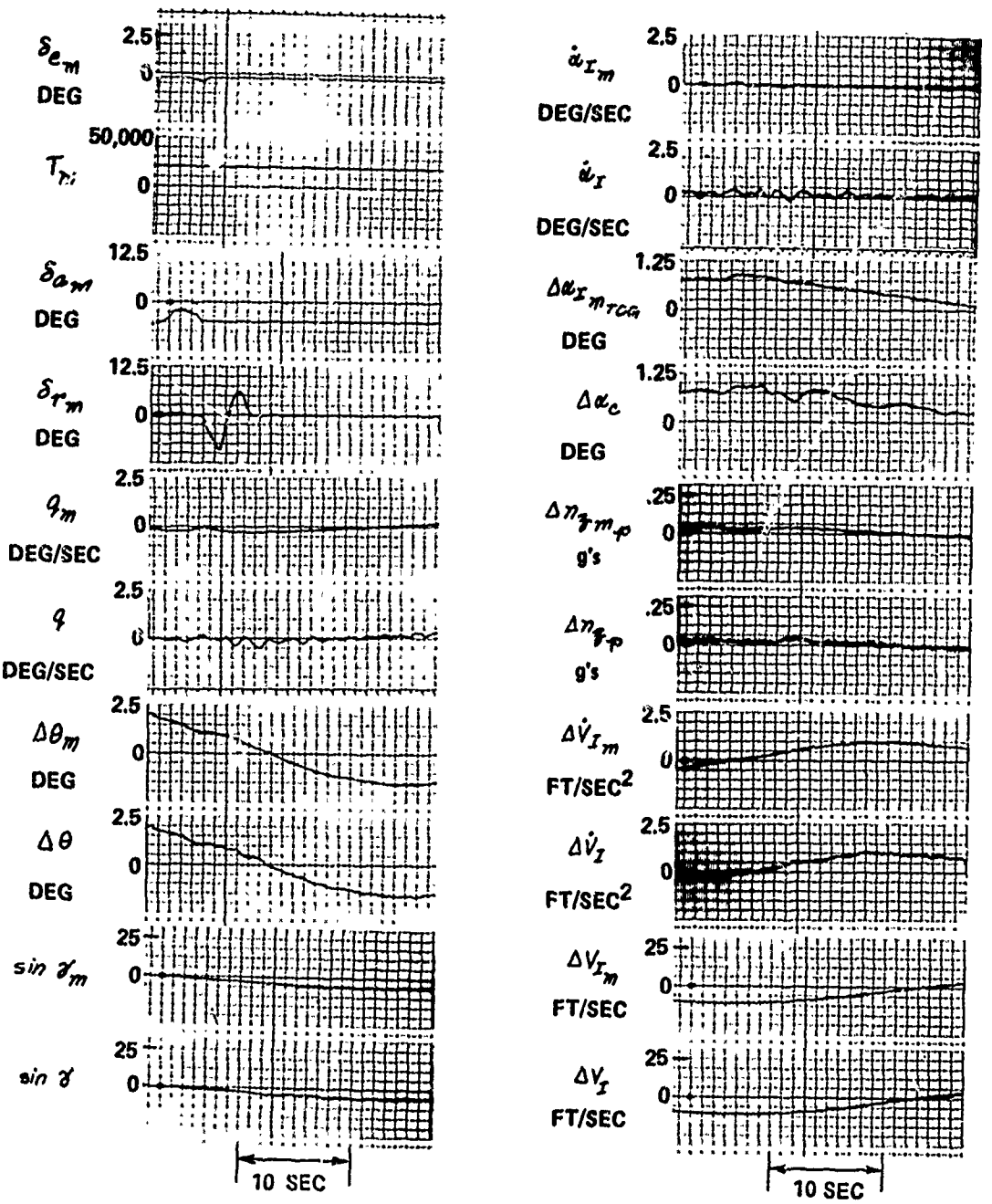

Figure 5.6 In-Flight Responses to Manual Rudder Doublet (Second Flight)

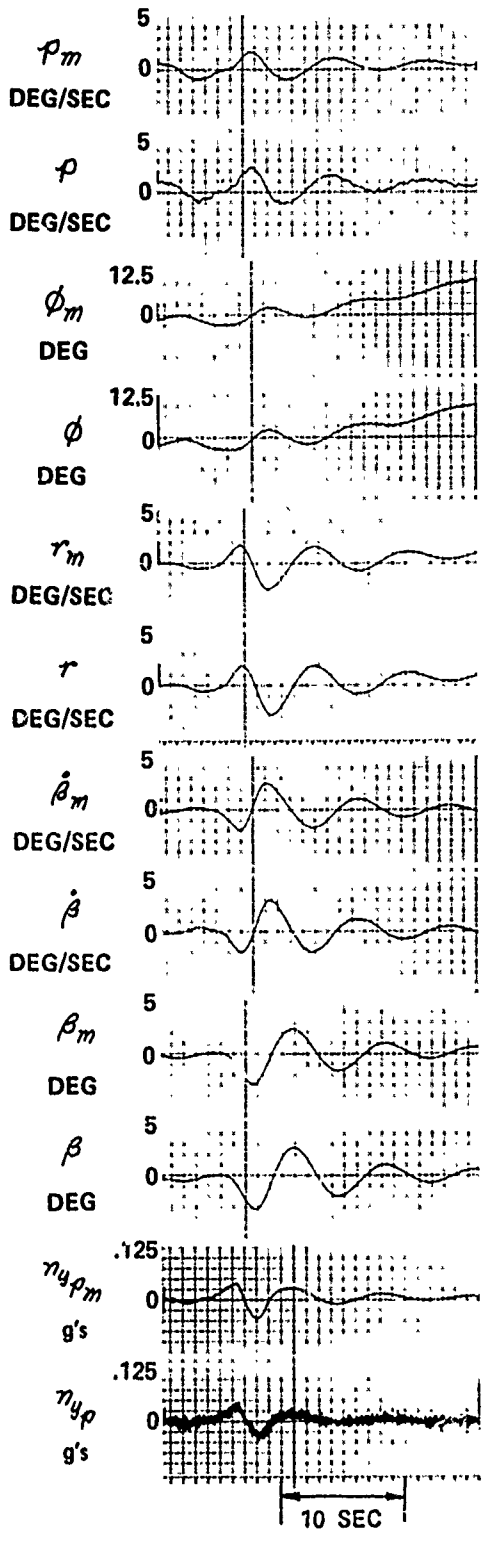

Figure 5.6 (con't) In-Flight Responses to Manual Rudder Doublet (Second Flight)

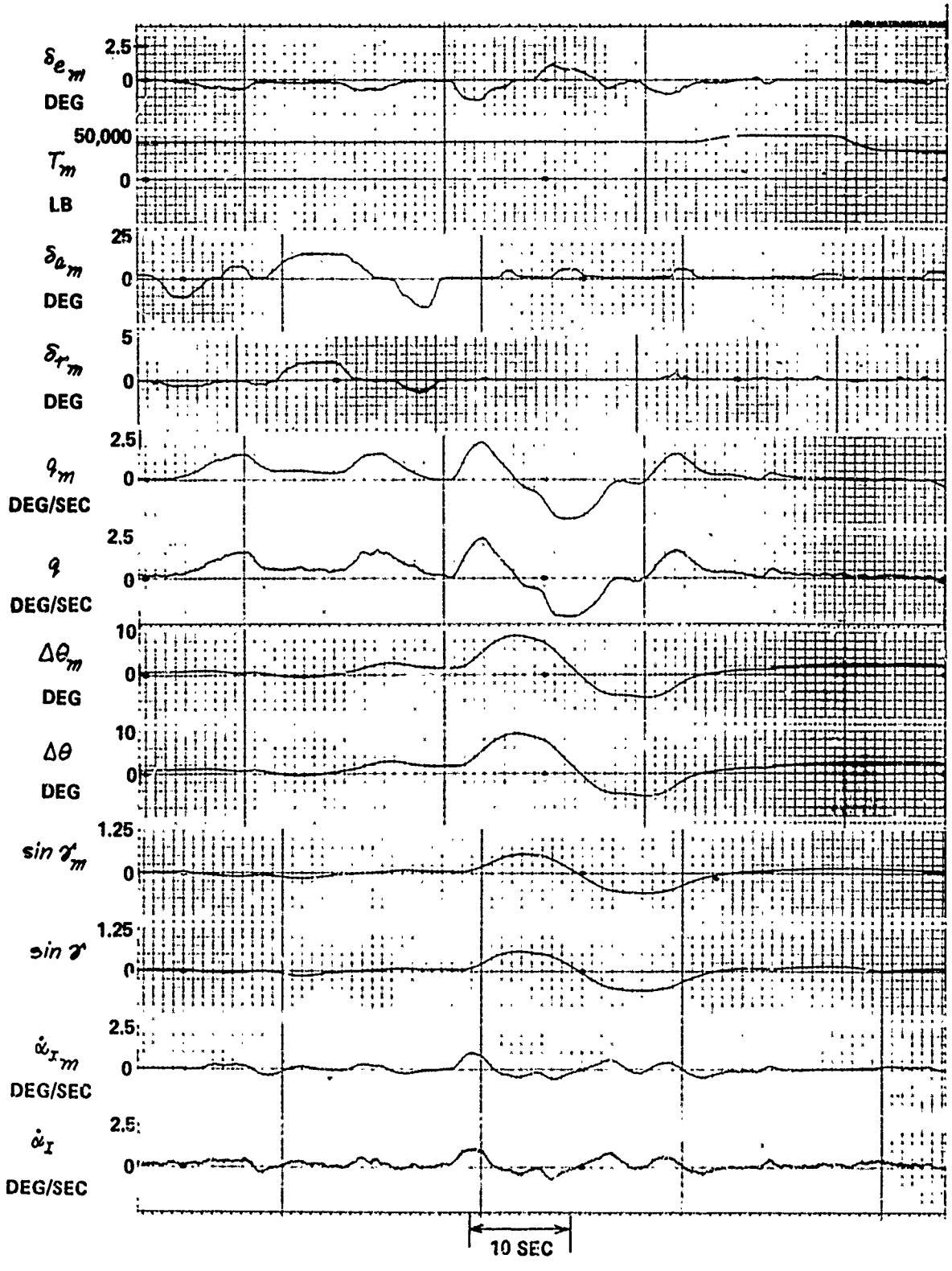

Figure 5.7 In-Flight Responses to Manual Input in Maneuvering Flight

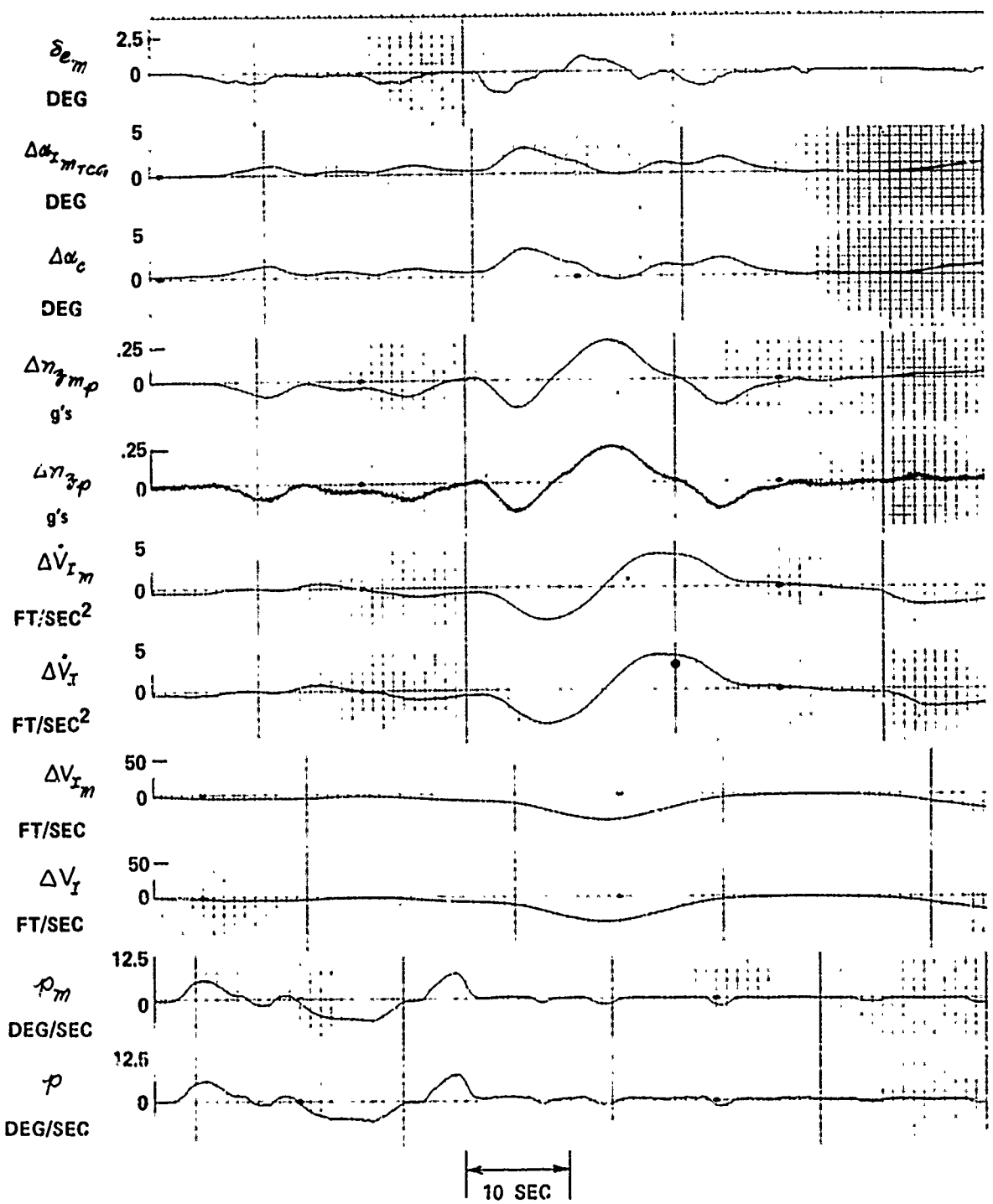

Figure 5.7 (con't) In-Flight Responses to Manual Input in Maneuvering Flight

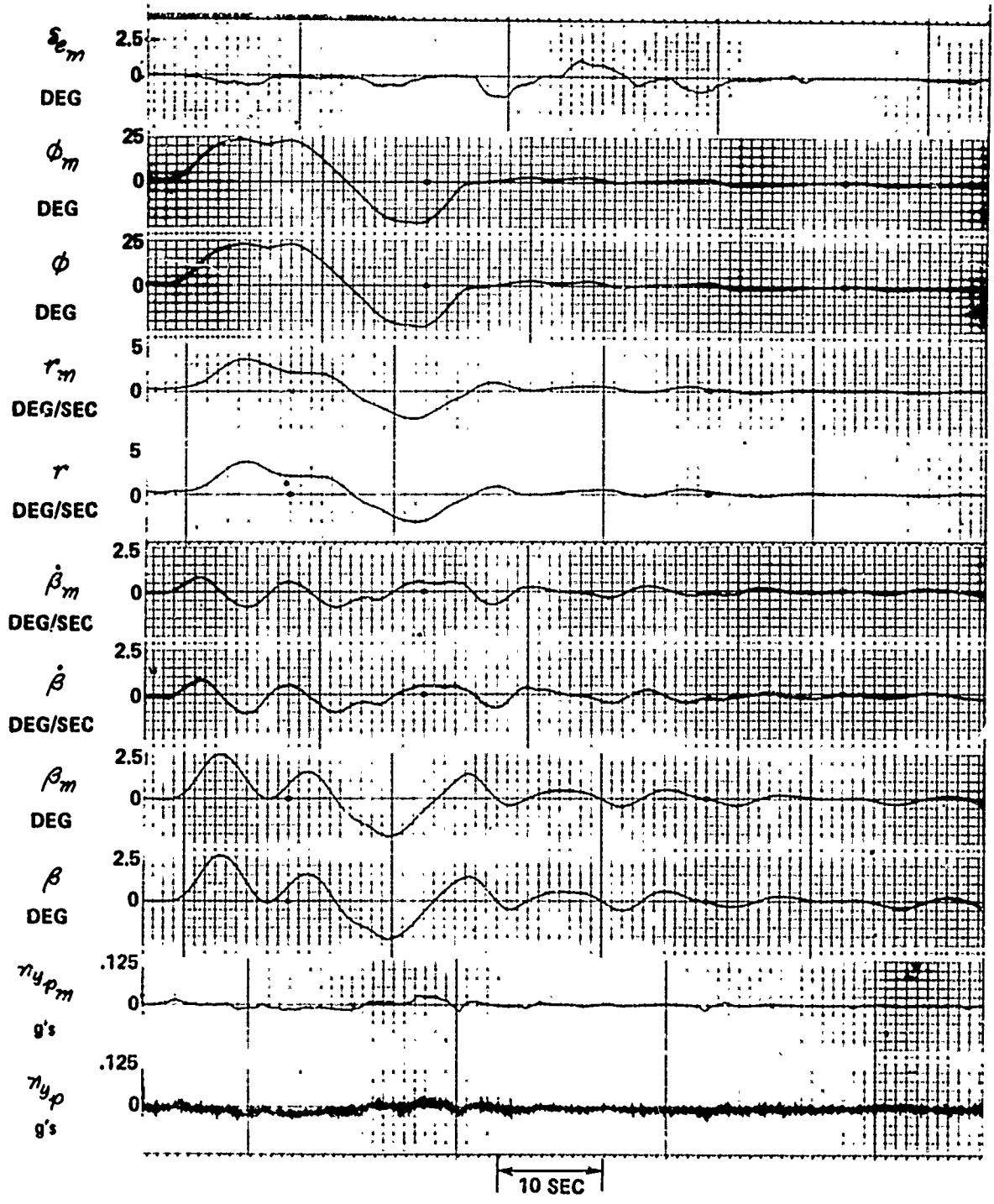

Figure 5.7 (con't) In-Flight Responses to Manual Input in Maneuvering Flight

SECTION VI

TURBULENCE ALLEVIATION AND SIMULATION

The purpose of this section is to discuss the turbulence alleviation and simulation system of the TIFS vehicle. Included is a discussion of the basic theory behind the technique used, a detailed development of the required gains, and a description of the functional operation of the system. Flight test results are also included to indicate the effectiveness of the system and point out problem areas. The capabilities and limitations of the TIFS turbulence alleviation and simulation system are not yet fully defined since there has been no system development following the flight tests. Also there have been only a few such tests. Therefore, the results reported here should be regarded as representative only of the unoptimized system.

A turbulence alleviation and simulation system is necessary to insure that the TIFS airplane responds appropriately to either existing atmospheric or artificially generated turbulence. Proper model following in the presence of atmospheric turbulence requires measurement of the turbulence field, alleviation of the TIFS responses to it and insertion of the measured turbulence into the model computer. The model following of "canned" turbulence differs only in that it is inserted into the model rather than the measured turbulence.

6.1 THE BASIC THEORY AND PRACTICAL LIMITATIONS

The block diagram given in Figure 6.1 shows the system that is used for gust measurement, alleviation and simulation. Included in this system are three sets of gains: the feedforward gains, K_m and K_{mD}, the feedback gains, K_p, and the gust compensation gain, K_v. As discussed in Reference 4, the feedforward gains are required for good model following. The function of the feedback gains is to reduce the sensitivity of the model-following system to parameter variations. In addition, the feedback gains were chosen to produce a fast, smooth regulator response with as wide a bandwidth as practical. Since a tight regulator reduces the perturbations of

the TIFS vehicle in turbulence, the presence of the feedback itself produces some gust alleviation when the feedback quantities are inertial rather than air data quantities.

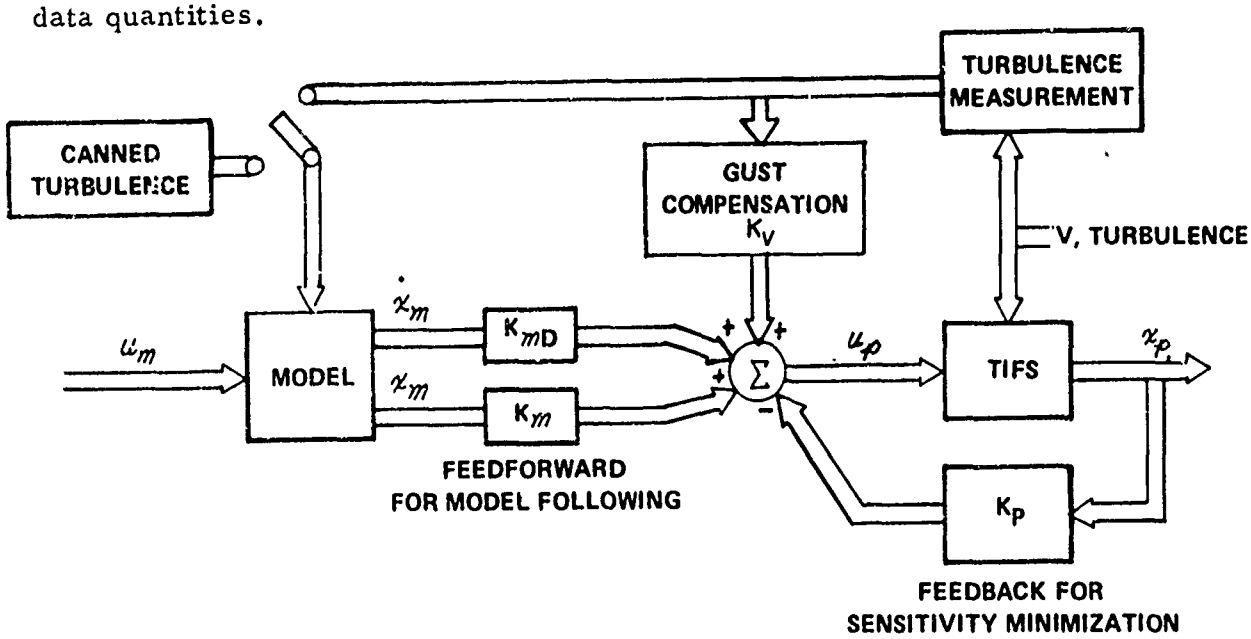

Figure 6.1 Block Diagram of TIFS Control System Including Turbulence

In addition, the gust compensator gains have the effect of reducing the vehicle perturbations even more. This compensation is designed as follows. The TIFS equations of motion are assumed to be of the form

$$\dot{x}_p = F_p x_p + G_p u_p + J_p v_p \tag{6.1}$$

The gust compensation is obtained by requiring that the excitation to the TIFS equations of motion be zero:

$$G_p u_p + J_p v_p = 0 \tag{6.2}$$

Solving this equation for u_p leads to

$$u_p = -(G_p' G_p)^{-1} G_p' J_p v_p \tag{6.3}$$

The control deflections given by this equation are those required to counteract the forces and moments imparted to the TIFS vehicle by gusts.

Several assumptions have been made in the derivation of this equation which place limitations on its validity. They are:

1. The linear, small perturbation equations of motion are assumed to be valid.

2. Independent control of all six degrees of freedom is necessary to provide exact gust alleviation.

3. Accurate knowledge of the TIFS vehicle control and turbulence effectiveness derivatives is necessary.

Furthermore, the solution given by Equation (6.3) is only a first approximation to the exact gust alleviation solution since the effects of finite actuator bandwidths have been neglected. In practice, the frequency response of the servos limits the spectrum which can be alleviated, and the rates at which the controllers can move is limited. The aircraft responses to gusts at frequencies lower than the servos bandwidth are alleviated while those at higher frequencies are not. With regard to turbulence simulation, the low frequency gust responses of the model can be matched. It may then be possible to match the higher frequency responses by modifying the input gust spectrum so that the resultant TIFS power spectrum has the desired characteristics. In this manner, it may be possible to simulate the effect of the gust excitation on some structural modes of the model.

Functionally, the gust alleviation and simulation system operates in the following manner. Vanes have been mounted on the TIFS vehicle which measure the sum of the gust and inertial angle of attack and sideslip angle. These signals are compensated for position error and angular rates. In addition, the inertial angle of attack and sideslip angle are computed using equations given in Reference 4. These inertial signals are then subtracted from the compensated vane signals to determine the gust excitations. The gust signals are then fed to the gust compensation gains. If it is desired to model-follow on the measured turbulence, these same signals are fed to the model computer; if it is desired to model-follow on canned turbulence, those signals are fed to the model computer. (See Figure 6.1)

6.2 DEVELOPMENT OF THE GUST ALLEVIATION GAINS

In this section, specific equations for the TIFS gust alleviation gains are given and numerical values for the gains presented. Consider first the longitudinal gust alleviation system. In this case the gust alleviation gains may be obtained by solving the following equations for the control deflections.

$$\begin{bmatrix} M_{\delta_e} + M_{\dot{\alpha}} Z_{\delta_e} & M_{\delta_x} + M_{\dot{\alpha}} \frac{\alpha_t}{V_t} D_{\delta_x} & M_{\delta_g} + M_{\dot{\alpha}} \left(Z_{\delta_g} + \frac{\alpha_t}{V_t} D_{\delta_g} \right) \\ 0 & D_{\delta_x} & -D_{\delta_g} \\ Z_{\delta_e} & \frac{\alpha_t}{V_t} D_{\delta_x} & \frac{\alpha_t}{V_t} D_{\delta_g} + Z_{\delta_g} \end{bmatrix} \begin{bmatrix} \delta_e \\ \delta_x \\ \delta_g \end{bmatrix}$$

$$+ \begin{bmatrix} M_\alpha + M_{\dot{\alpha}} \left(Z_\alpha + \frac{\alpha_t}{V_t} D_{\alpha_g} \right) \\ -D_{\alpha_g} \\ Z_\alpha + \frac{\alpha_t}{V_t} D_{\alpha_g} \end{bmatrix} \left[\alpha_g \right] = \begin{bmatrix} 0 \\ 0 \\ 0 \end{bmatrix} \qquad (6.4)$$

Similarly, the lateral-directional gust alleviation gains may be obtained by solving the following equations for the lateral-directional control deflections.

$$\begin{bmatrix} L_{\delta_a} & L_{\delta_r} & L_{\delta_y} \\ N_{\delta_a} & N_{\delta_r} & N_{\delta_y} \\ 0 & Y_{\delta_r} & Y_{\delta_y} \end{bmatrix} \begin{bmatrix} \delta_a \\ \delta_r \\ \delta_y \end{bmatrix} + \begin{bmatrix} L_\beta \\ N_\beta \\ Y_\beta \end{bmatrix} \left[\beta_g \right] = \begin{bmatrix} 0 \\ 0 \\ 0 \end{bmatrix} \qquad (6.5)$$

The general solution to these equations is given by Equation (6.3).

As indicated in Section V the TIFS gust alleviation gains were computed for a nominal flight condition in the landing approach island which was h = 5,000 ft, V_t = 273 fps and α_t = 4.16°. The stability and control derivatives used were the best estimates obtainable from wind tunnel data and engineering computation. Subsequently, it was found that some of the gust

alleviation gains could be removed with little effect on the resulting gust alleviation of the system. Digital simulation was used to verify these simplifications. The original gains are shown in Tables 5.1 and 5.3.

6.3 FLIGHT TEST RESULTS OF GUST ALLEVIATION

This section contains some flight test results of the TIFS gust alleviation system. A consideration of some of the problems which arose from these tests is also presented. As a general comment it can be stated that significant improvement in system performance can be anticipated when updated knowledge of the TIFS aerodynamics can be used in configuring the gust alleviation system.

Consider, first of all, Figures 6.2 and 6.3 which present results from a flight in which the longitudinal gust alleviation system was checked out. Figure 6.2 compares power spectra of the α_g input signal in each instance. As is evident, the α_g input is nearly identical and therefore the power spectra of Δn_{z_p} can be directly compared. The gust response of this variable has been noticeably alleviated up to a frequency of about 2 Hz.

Figures 6.4 through 6.6 present similar results for the lateral-directional gust alleviation system and provide a comparison between the open-loop gust responses of the TIFS and TIFS responses with the gust alleviation system engaged. Figure 6.4 shows that the β_g input spectrum in both cases is nearly identical while Figure 6.5 shows that some alleviation of the β_z gust response is achieved for frequencies up to .5 Hz. The two n_{y_p} power spectral densities are shown in Figure 6.6. These results indicate that gust alleviation does not take place but that the gust response spectrum is actually increased with the gust alleviation system engaged. This occurs up to 2 Hz, after which the two spectra are nearly identical. A possible reason for this discrepancy may be due to the fact that the side force surfaces were operated closed loop during this test. To date, the best model following has been obtained when the side force surfaces were operated

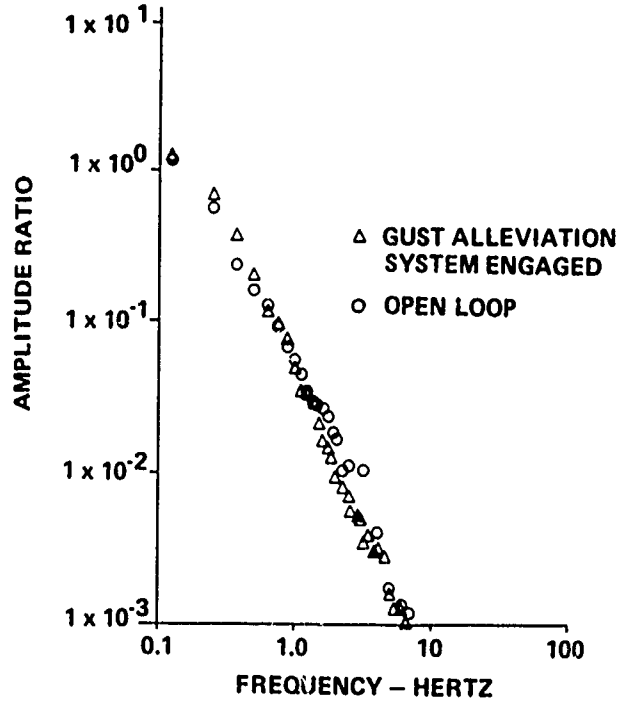

Figure 6.2 α_g Power Spectra

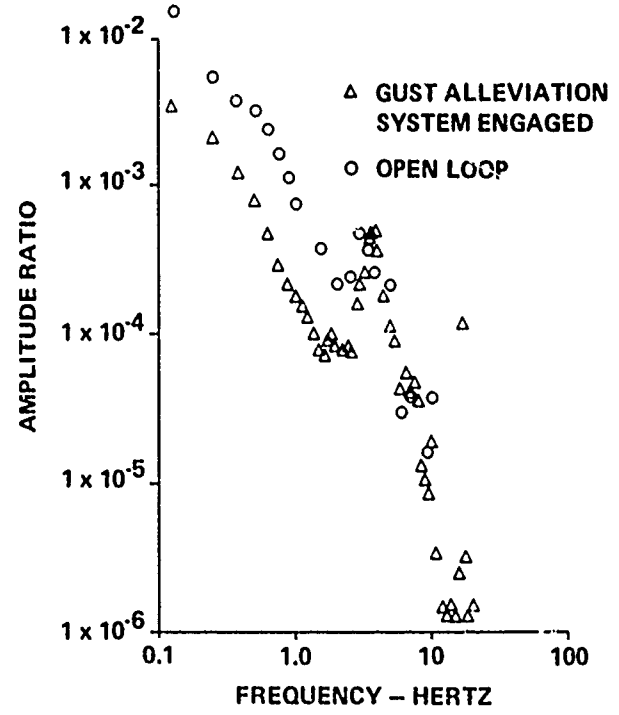

Figure 6.3 Δn_{z_p} Power Spectra

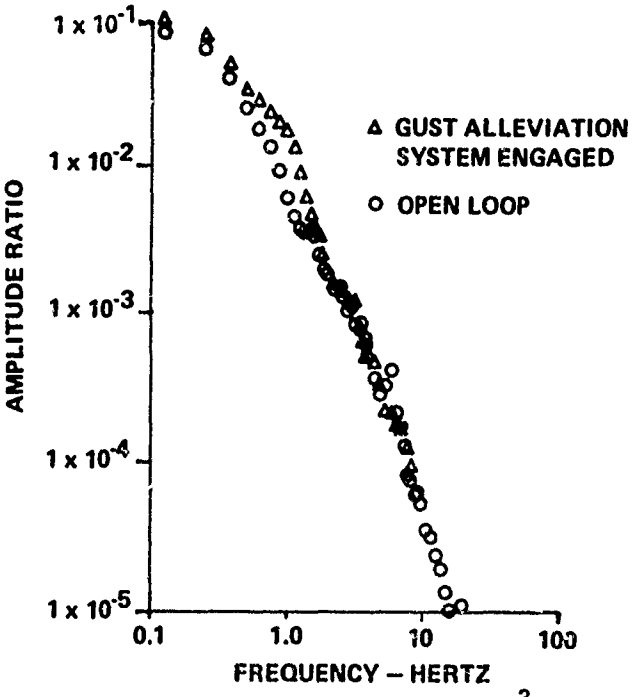

Figure 6.4 β_g Power Spectra

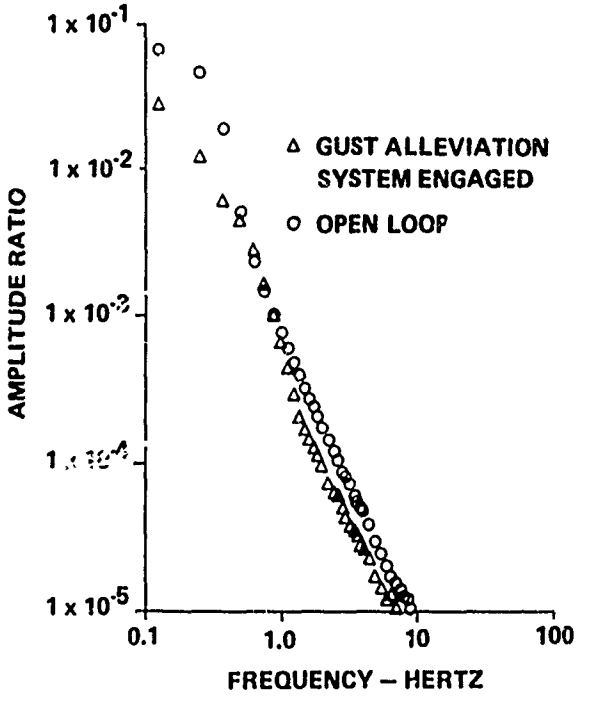

Figure 6.5 β_I Power Spectra

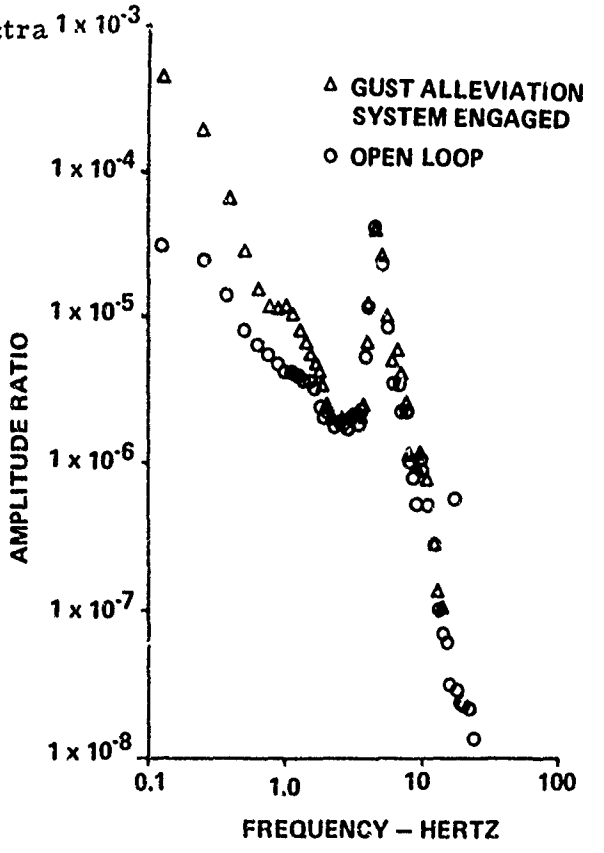

Figure 6.6 η_{ψ_p} Power Spectra

open loop and the rudder and ailerons were operated closed loop. With the side force surface loops closed, the model following in n_{y_p} is poor. For example, for a rudder doublet model input, the n_{y_p} response has a lightly damped sinusoidal response after the completion of the doublet input which is not present in n_{y_m}. It may be that the source of this error is present when the gust alleviation system is engaged, thus resulting in the poor gust alleviation.

During the initial portion of these flight tests with the gust alleviation system engaged, the variable stability system would dump a short while after engagement. This was found to be due to the excessive direct lift flap rates commanded by the gust signal. This condition was rectified by filtering the gust signal before inputting it into the gust alleviation gains. A first-order filter with a corner frequency of 6.4 Hz was tried with success. This did not inhibit the system in any way since any alleviation which took place did so at frequencies much lower than this. In addition, the servos did not have the bandwidth to alleviate frequencies at the corner frequency of the filter.

6.4 FLIGHT TEST RESULTS OF TURBULENCE SIMULATION

In addition to gust alleviation, gust simulation has also been demonstrated in flight. Figures 6.7 through 6.9 contain the results of a longitudinal gust simulation flight in which the measured turbulence was fed into the model. The α_g power spectrum is shown in Figure 6.7. Figure 6.8 shows the spectra of $\Delta\alpha_{m_{TCG}}$ and $\Delta\alpha_I$, respectively. Fairly good agreement between the two exists. The power spectra of n_{z_p} of the TIFS and model are shown in Figure 6.9. The spectra are alike up to 2 Hz, after which the Δn_{z_p} spectra has a resonance. The power spectrum of $\Delta n_{z_{m_p}}$ does not have this resonance. This discrepancy is due to the fact that no alleviation of the Δn_{z_p} spectrum occurs in the frequency range of this resonance as evidenced by Figure 6.3.

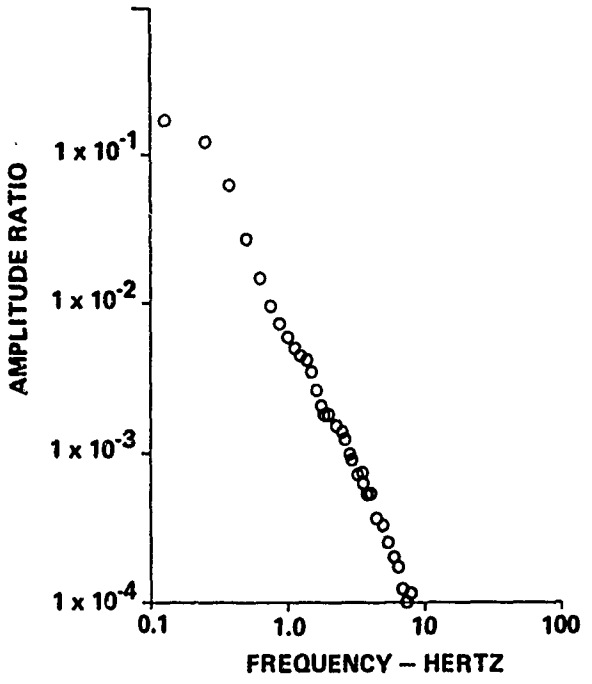

6.10

Figure 6.7 α_g Power Spectrum

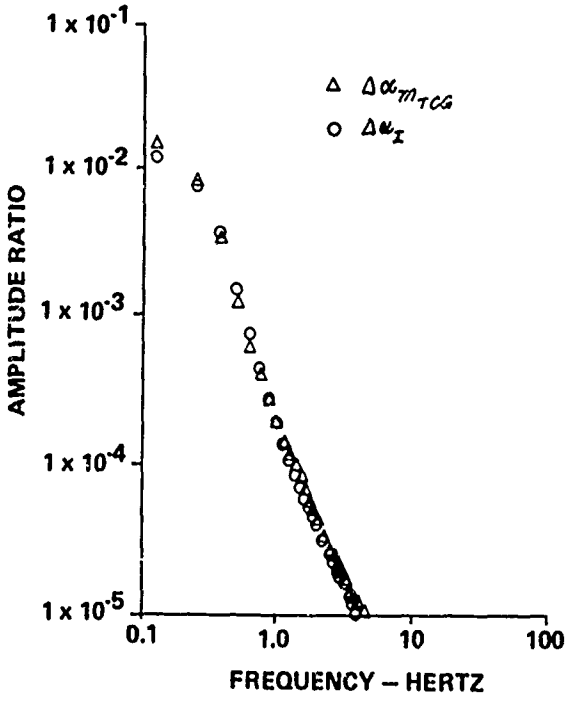

6.12

Figure 6.8 $\Delta\alpha$ Power Spectra

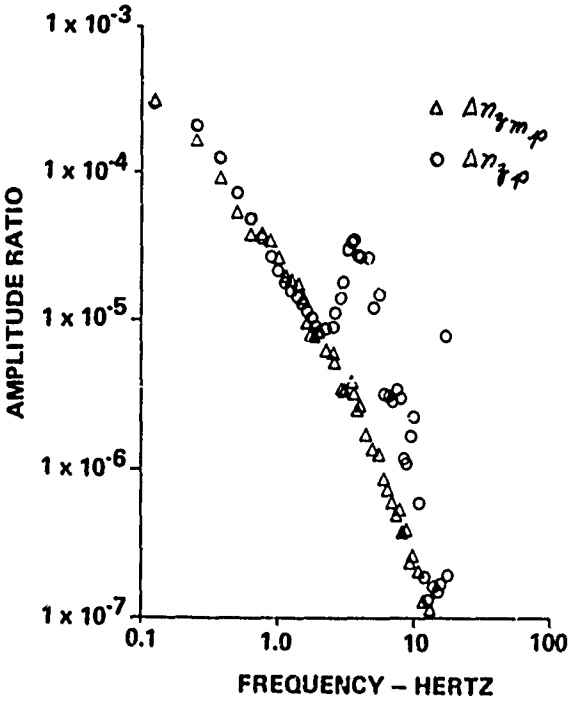

Figure 6.9 $\Delta n_{\gamma_{gp}}$ Power Spectra

Similar results are shown for the lateral-directional system in Figures 6.10 through 6.12. The β_g spectrum is shown in Figure 6.10. The spectra of β_I and $\beta_{m_{TCG}}$ are shown in Figure 6.11. The spectra exhibit fairly good agreement. The spectra of n_{y_p} and $n_{y_{m_p}}$ shown in Figure 6.12 again show a vast discrepancy. This should not be unexpected since the two spectra differed drastically in the case of gust alleviation.

The power spectra for α_g, β_g, u_g and v_g, as defined in MIL-F-8785B(ASG) (Reference 18), were also mechanized and flight tested. Reference 19 contains a development of this mechanization. During flight test it was determined that the variable stability system dumped due to the excessive control surface rates commanded by the gust. First-order filters with corner frequencies of 1.6 Hz were added to the system to overcome this fault. Power spectral results for this test have not been obtained.

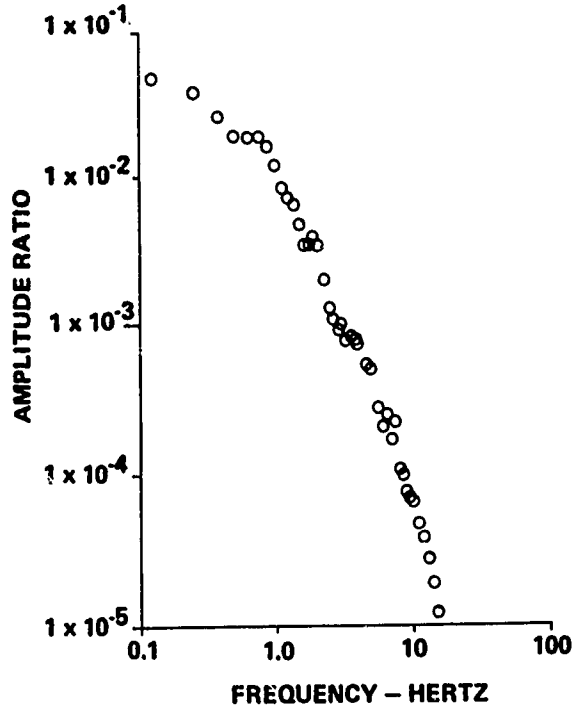

Figure 6.10 β_g Power Spectrum

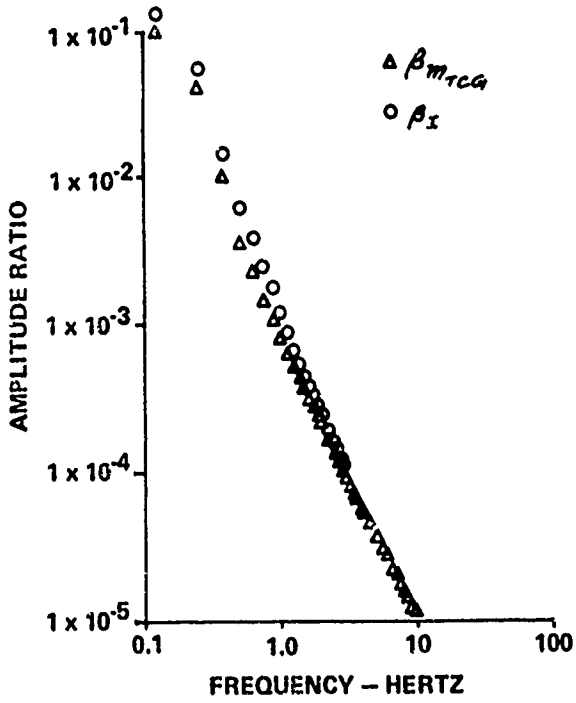

Figure 6.11 β Power Spectra

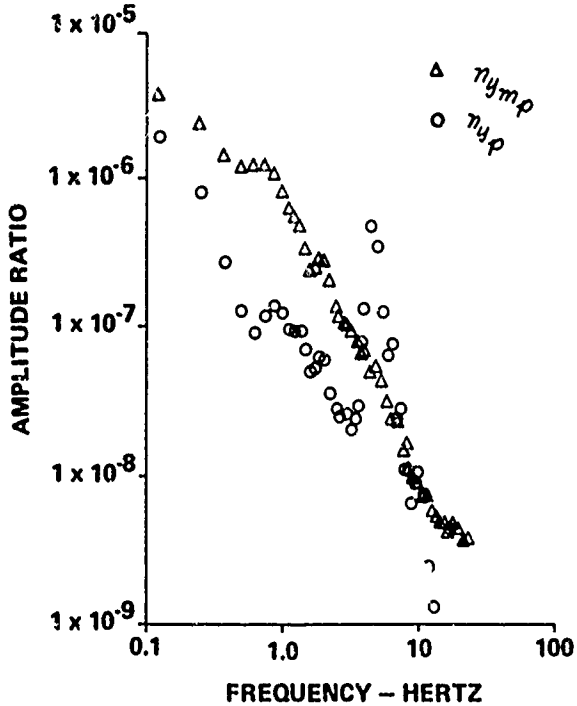

Figure 6.12 n_{yp} Power Spectra

SECTION VII

FEEL SYSTEM CAPABILITY

As indicated in the Introduction, not only can the TIFS duplicate in the evaluation cockpit the motions and environment of the simulated aircraft, but also the feel and response to the pilot's controls can be adjusted to reproduce over a broad range the exact characteristics desired. The TIFS evaluation cockpit is presently equipped with conventional controls, a wheel, column, and set of rudder pedals for each pilot and a throttle pedestal located between them. Although not currently provided, such items as a stick or side controller, landing gear and flap levers, pitch trim controls and indicators, as well as controls for yaw and roll trim can be added. The TIFS feel system provides the desired force vs. position characteristics at the controls in the cockpit by measuring the force applied to the control and commanding its position through its hydraulic actuator. The command signal to the actuator is shaped by the computer so that the feel system can provide the following characteristics at the elevator, aileron, or rudder controls of the evaluation pilot:

1. Linear adjustable force vs. position gradient.
2. Adjustable breakout force.
3. Adjustable hysteresis.
4. Adjustable split hysteresis. (Combination of breakout force and hysteresis.)
5. Adjustable deadband.
6. Adjustable natural frequency and damping ratios.
7. Possible inclusion of bobweight effects such as those due to normal acceleration and pitching acceleration.
8. Variation of the force gradient as a nonlinear function of some arbitrary variable.

The command signal to the model computer can be derived from either control force or position. In fact, except for the compliance of the physical parts, zero-displacement-for-command operation would be directly available, tantamount to an infinite force gradient. In addition, a first-order lag with a rate limit can be provided to simulate a boosted control system. The available range of these different characteristics is shown below in Table 7.1 and graphically in Figures 7.1, 7.2, and 7.3. The gearing ratios identified in the table do not necessarily reflect the maximum available with the TIFS system. They are, however, the values which we consider to be the maximum usable for an operational aircraft.

TABLE 7.1
FEEL SYSTEM CHARACTERISTICS

	Elevator	Aileron	Rudder
Force Gradient	1 to 500 lb/in.	0.1 to 10 lb/deg	4 to 4000 lb/in.
Breakout Force	0 to ± 10 lb	0 to ± 10 lb	0 to ± 20 lb
Hysteresis	0 to ± 10 lb	9 to ± 10 lb	0 to ± 20 lb
Split Hysteresis	0 to ± 20 lb	0 to ± 20 lb	0 to ± 40 lb
Deadband	0 to ± 1 in.	0 to ± 10 deg	0 to ± 0.5 in.
Natural Frequency	0 to 50 rad/sec	0 to 50 rad/sec	0 to 50 rad/sec
Damping Ratio	0 to 2.0	0 to 2.0	0 to 2.0
Maximum Force	100 lb	100 lb	200 lb
Maximum Displacement	± 5.0 in.	± 95 deg	± 3.5 in.
Maximum Gearing:			
$\frac{\text{Surf. Displ.}}{\text{Cont. Force}}$	0.5 deg/lb	1 deg/lb	0.2 deg/lb
$\frac{\text{Surf. Displ.}}{\text{Cont. Displ.}}$	10 deg/in.	1 deg/deg	20 deg/in.

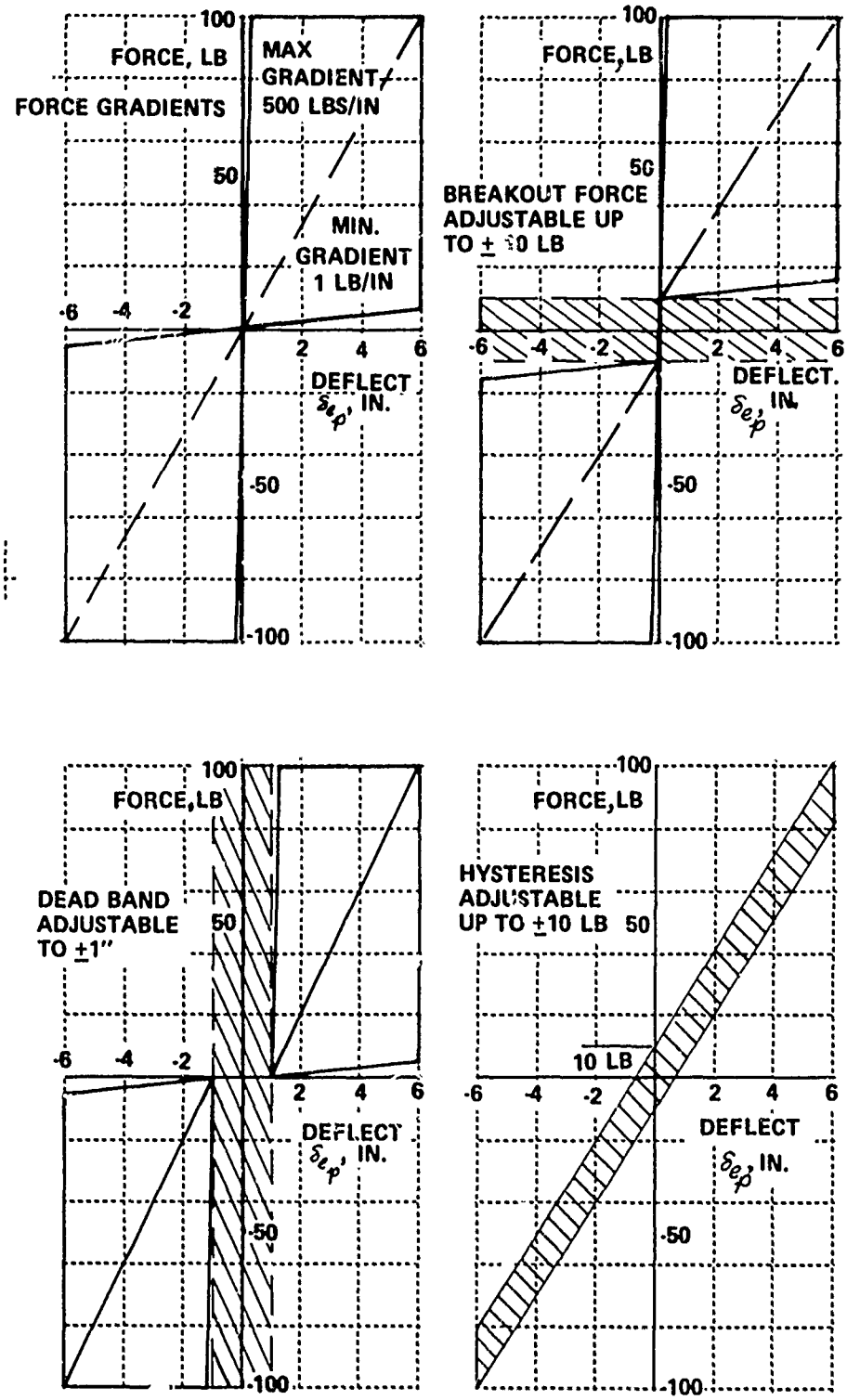

Figure 7.1 Elevator Feel Performance Capability

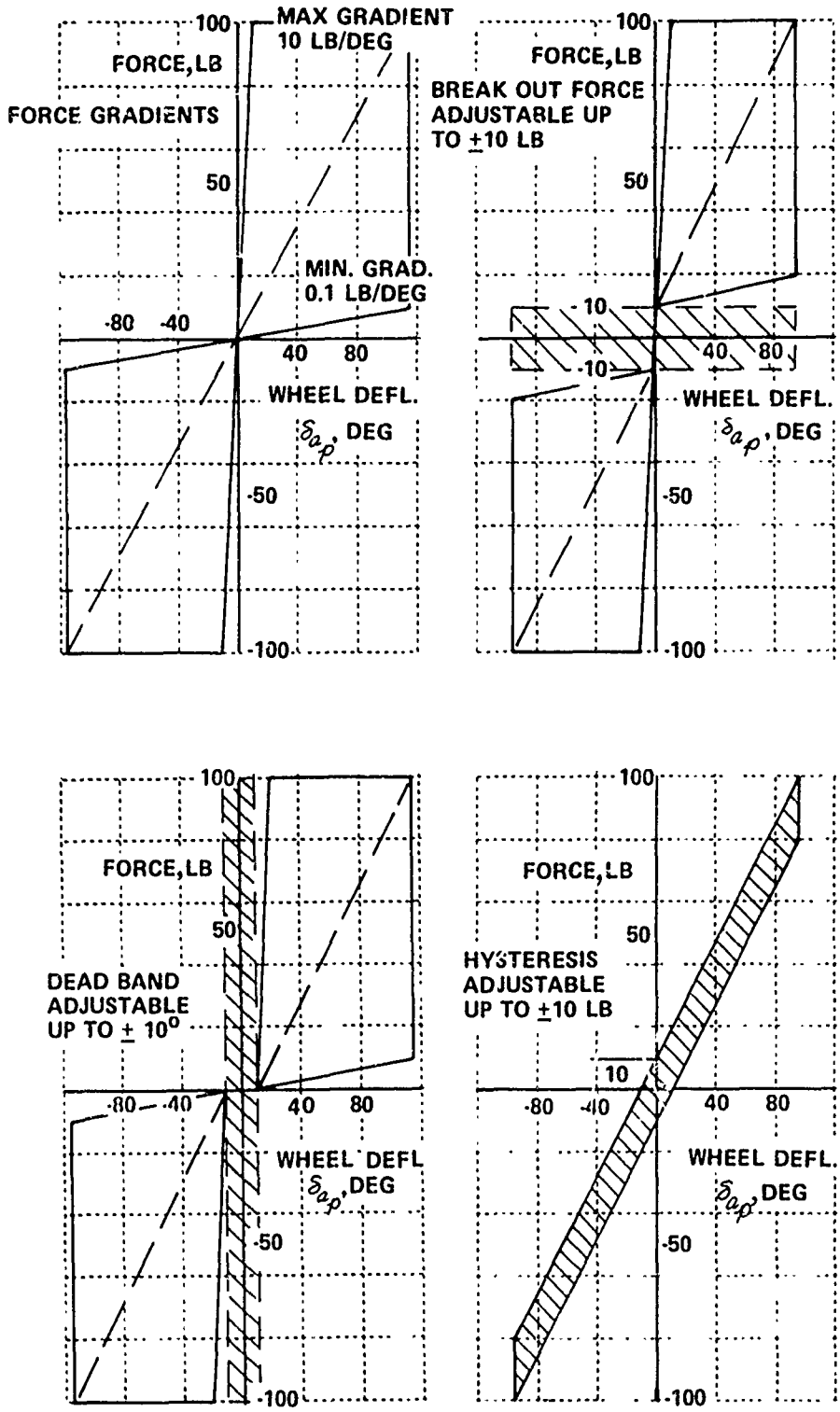

Figure 7.2 Aileron Feel Performance Capability

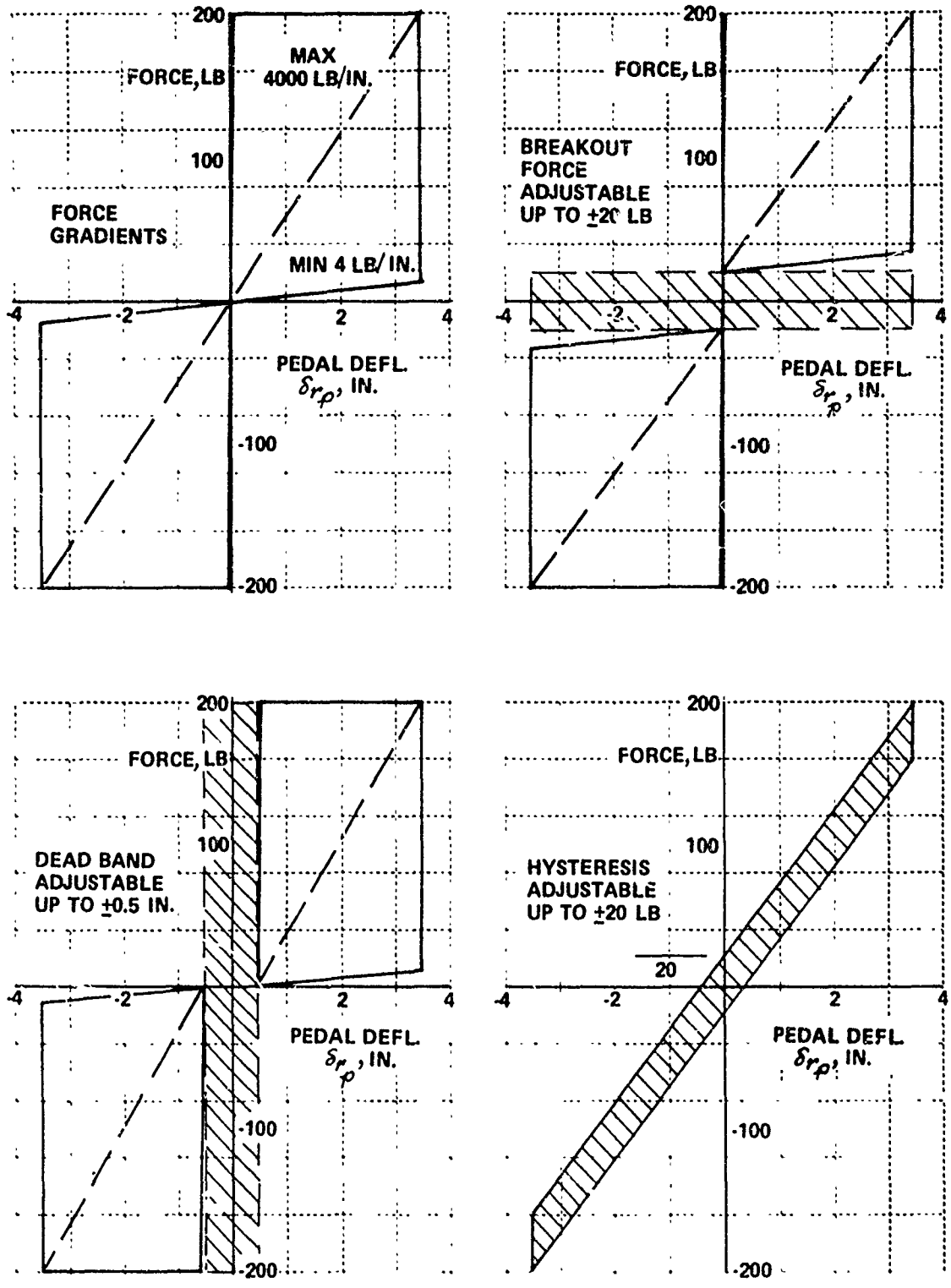

Figure 7.3 Rudder Feel Performance Capability

In addition to providing these feel characteristics, the feel system position is related to the force command by a second-order transfer function with known, independently variable natural frequency and damping the ranges of which are noted in Table 7.1. Hence a precise means is provided for controlling the dynamic feel characteristics as well as the static relationships.

A further capability is available. It is possible to simulate the various trim systems of different aircraft. The trim system provides the following rate and proportional trim capabilities:

1. Trim to the feel system position loop.
2. Trim to the feel system force loop.
3. Trim to the aircraft surface servo.

By injecting the trim into the force or position channel, it is possible to trim the feel system which in turn trims the surface. It is also possible to inject the trim signal directly into the surface to simulate a movable stabilizer trim.

The maximum trim rate for each axis of the feel system is tabulated in Table 7.2.

TABLE 7.2
MAXIMUM TRIM RATES FOR TIFS FEEL SYSTEM

Mode	Elevator	Aileron	Rudder
Position	1 in./sec	10 deg/sec	0.5 in./sec
Force	10 lb/sec	4 lb/sec	8 lb/sec
Surface	2 deg/sec	2 deg/sec	1 deg/sec

The rate trim currently available in the system could be switched to a proportional trim. Maximum proportional trim capabilities are listed in Table 7.3.

TABLE 7.3

MAXIMUM PROPORTIONAL TRIM

Mode	Elevator	Aileron	Rudder
Position	± 5 in.	± 50 deg	± 2.5 in.
Force	± 50 lb	± 20 lb	± 40 lb
Surface	± 10 deg	± 10 deg	± 5 deg

SECTION VIII

AUXILIARY SYSTEM FEATURES

Three features of the TIFS system operation in which a significant and unique capability is demonstrated have not yet been discussed. They concern safety, the physical environment of the evaluation cockpit, and the data gathering and processing system. As in the other sections of this report, these areas are outlined in terms of the capabilities provided rather than the method of their achievement since the design report and other program documentation cover those aspects thoroughly.

The primary safety feature built into TIFS is provided by the continuous monitoring of the aircraft flight control surfaces by the safety or command pilots. Since their controls are mechanically connected to the normal airplane control surfaces and engines in a conventional manner and their indicators show the positions of the direct lift flaps and side force surfaces, the safety pilots follow all the activities commanded of the TIFS. At any instant, they can take over control of the vehicle. In addition, the TIFS variable stability system has built into it a safety trip system that will disengage the variable stability system and return control of the aircraft to the safety pilots if the action commanded of a control surface would exceed the structural or other preselected limitation of the basic airframe. With regard to TIFS capabilities, it should be noted that the safety trip system can easily be connected to monitor in flight any of the several hundred signals available on the VSS computer patch panel that identify such quantities as servo amplifier signal outputs, surface positions, hinge moments, accelerations, and computed structural loads. Any value of one or preselected combination of these parameters can be used to trip the system. Since the safety trip system is responsive to surface commands, it also protects equally well against variable stability system malfunction. Further, it is fail-safe in that if electrical power is removed, the system automatically disengages. Disengagement of the variable stability system is accomplished either automatically or intentionally, by action of the safety trip system, by the safety pilots deliberately overpowering the airplane controls, or by any of the four pilots or the test engineers pushing the dump button. The safety

pilots monitor surface hinge moment and manually retrim if necessary as the simulation proceeds to keep hinge moments low and thus keep disengagement transients to a minimum.

The standard egress provisions in the C-131B cockpit and fuselage are retained in the TIFS. The front or simulation cockpit is connected to the cabin area by a tunnel. In the event that the tunnel is not usable in an emergency, there are two other exits available. An in-flight bailout door in the center of the bulkhead directly behind the evaluation pilots' seats can be removed to give access to the nose wheel well area in which handholds have been positioned to facilitate bailout. In addition, a ground emergency exit is located at the right hand side of the adapter section at the front end of the tunnel from the C-131 cabin. A parachute chest pack is stowed on the back of each of the evaluations pilots' seats for use in an emergency and a canopy breaker axe is located inside the left side of the adapter section.

The present general purpose evaluation cockpit of the TIFS was patterned after modern cockpits with side-by-side seating arrangement. It consists of a basic cockpit unit, a canopy, and an adpter section. The basic cockpit unit which constitutes the lower and major portion of the simulation cockpit contains the pilots' flight controls with artificial feel servos, seats, instrument panels, center console, flight director computer, and other ancillary equipment. The floor structure under the pilot and co-pilot seats is designed for crash landing loads as specified in paragraph 4b.260 of Civil Air Regulations, Part IVb. The general purpose canopy is not a reproduction of any existing canopy but rather a large transparent assembly inside which opaque masks can be installed as required to represent specific windshield arrangements. The four transparent acrylic plastic window units are mounted in a fiberglass reinforced framework on the sill of the basic cockpit and the upper portion of the front of the adapter section. It is the adapter section which attaches to the front face of the bulkhead at station 6.5, mounting the evaluation cockpit to the modified C-131 fuselage. A

change in the orientation of the position of the evaluation pilots with respect to the C-131H fuselage could readily be accomplished by changing the design of this adapter section.

The simulation cockpit is configured in a conventional manner. Figure 8.1 shows an evaluation pilot at the controls as well as the present instrument arrangement and an indication of the field of view available. As noted earlier, the flight controls are the normal wheel, column, and rudder pedals and a center-aisle throttle console on which currently are mounted four throttle levers and a rudder trim switch. The console also carries the push buttons for sequentially engaging the variable stability system, and, although not presently installed, provision for the addition of landing gear, speed brake, and flap levers as well as pitch and roll trim controls. Again, although the specific devices, per se, have not been designed, the modular design of the feel system components lends itself to the substitution of a stick or side controller in place of the present units. As can be seen in the picture, the flight panel in front of the pilot (which is repeated in front of the co-pilot) contains operating flight instruments. These instruments can be connected through the MF-RF patch panel to present data either from the TIFS sensors directly or that from the computed model being evaluated. The instrument panel is divided into sections to facilitate changes in the displays. The present installation, shown in more detail in Figure 8.2, consists of the basic components of the USAF PIFAX display. The following list enumerates the instruments in front of the pilot from left to right starting with the top row and working down:

Airspeed Indicator - This conventional-looking meter reads indicated airspeed.

Attitude Director Indicator - This instrument presents angle of pitch, angle of roll, turn rate, horizontal and vertical steering needles, glide slope/flight path/displacement pointer and warning flags. It is driven by a conventional flight director computer and a three-axis attitude gyro.

Figure 8.1 TIFS Simulation Cockpit

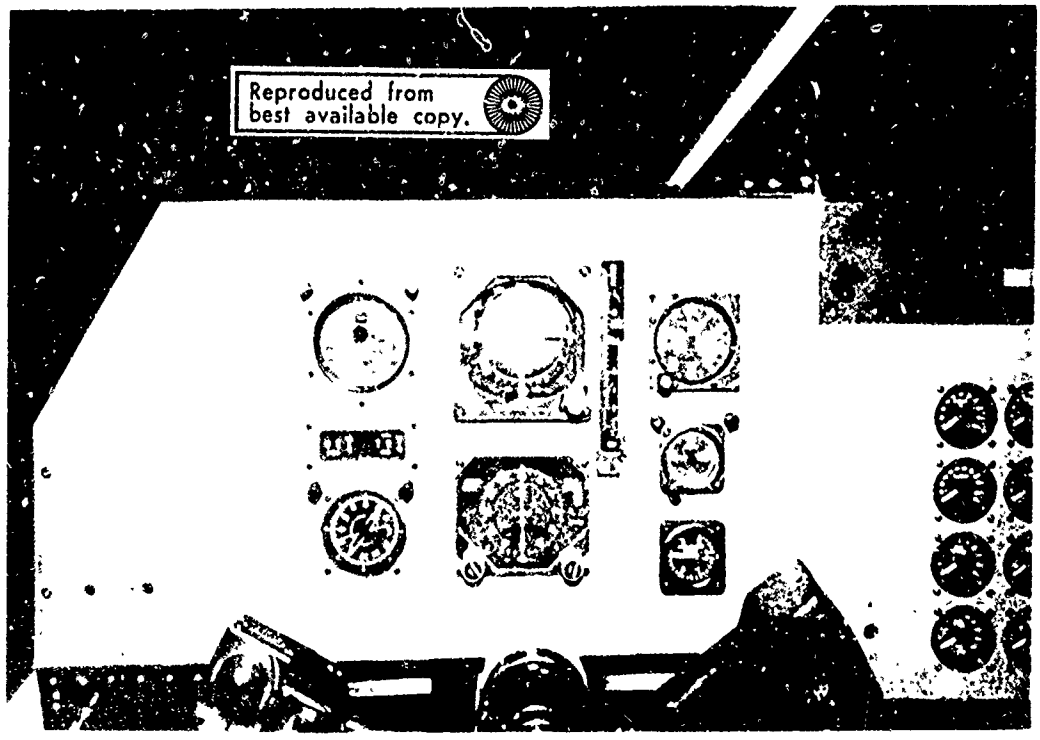

Figure 8.2 Captain's Instrument Panel in Evaluation Cockpit

Vertical Velocity Indicator - This sandwich type indicator presents vertical velocity as well as altitude for the simulated aircraft from the actual ground surface as measured by the radar altimeter.

Altimeter - The right hand instrument in the top row is the altimeter which has a presentation similar to a standard Air Force indicator.

Machmeter/True Airspeed - A machmeter and true airspeed indicator is located in the second row at the left hand side of the display. For simulating low speed maneuvers, such as landing approaches, the machmeter portion of this instrument has been altered to provide a digital readout of indicated airspeed.

Sideslip Meter - Although not shown in the picture, a meter to read the sideslip angle has been added in the middle column of instruments between the ADI and the HSI. This additional information was felt desirable for certain simulations.

Clock - A standard aircraft clock with elapsed time measuring capability is located at the right hand side of the middle row of instruments.

RMI - The radio magnetic indicator is located at the extreme left in the bottom row.

Horizontal Situation Indicator - This instrument in the center of the bottom row is used to display magnetic heading, omni, DME or TACAN, localizer, and a manual set command heading. It is a standard USAF instrument.

Accelerometer - At the right hand end of the bottom row is located an accelerometer which reads vertical accelerations at the evaluation pilots' station from minus 2 g to plus 4 g.

The center section of the instrument panel includes the mode switching controls for the flight director and the four instruments for each of four simulated engines to indicate percent thrust, percent rpm, exhaust gas temperature, and fuel flow. Currently there is no need for an engine computer as part of the simulation so these instruments are all connected to the model thrust signal. In addition to the instruments identified and shown in the picture, several indicator lights have been added to the pilot and co-pilot flight panels. These include a marker beacon light to indicate passage over a marker beacon, a touchdown light to indicate a simulated touchdown, and a green engage light which shows that the variable stability system is engaged and the evaluation pilot is in control of the aircraft. In addition to that light going out, disengagement is accompanied by an audible beeping signal on the interphone system as well as flashing lights on the center console in the evaluation cockpit, in the control or safety cockpit, and at the test engineers' stations.

Special displays such as CRT-type attitude instruments or special approach aids could be installed. The volume forward of the instrument panel and above the rudder pedal feel units is currently empty. Structurally, that area can accommodate 200 pounds of additional equipment.

The aircraft is equipped with dual VOR and dual ILS. Dual VHF and standard UHF communications are provided. The evaluation pilots can communicate through the basic aircraft's radios to the tower and approach control. The radios are controlled from the safety pilot's cockpit. A versatile intercom system is provided to allow all stations including the observers in the aft cabin to communicate. A private line is available for voice recording of evaluation pilot comments.

It was mentioned above that the instruments could be actuated either by the variable stability system computer or the TIFS sensors themselves. Hence, TIFS can directly fly by wire as well as simulating another aircraft in either the model-following or response-feedback mode. In addition, a ground computer made up of three EAI 380's is used to simulate on the ground the C-131 aerodynamics in order to facilitate the ground checkout of a specific model. When connected to the ground computer, TIFS can be operated on the ground like any other fixed-base ground simulator. The instruments and control feel will respond as if the model programmed on the TIFS were flying in the environment programmed on the ground computer. The IFR simulation capability is complete although, of course, visual cues external to the cockpit are missing.

The canopy on the TIFS simulation cockpit affords large areas of unrestricted vision. The fiberglass supporting ribs, of course, do interfere to some extent as in any windowed area but the broad clear areas available were designed to afford the maximum unrestricted vision and consequently the greatest possible variation in masking capability. A vision polar or visibility diagram for the evaluation cockpit is included as Figure 8.2. This shows the unobstructed field of view from a point located at the pilot's eye level midway between his eyes.

The in-flight aural environment of the evaluation cockpit of TIFS, a propeller driven aircraft, is of course of interest. Although no formal noise measurement program has been undertaken, some spot checks (Reference 20) have been made to obtain information that is somewhat more definitive than the usual evaluation pilot comment that he didn't notice any intruding propeller or engine noise and consequently feels the noise environment to be a reasonable simulation for a jet aircraft. These preliminary data are plotted against indicated airspeed on Figure 8.3 along with curves of aerodynamic noise reported in the handbook of noise control by C.M. Harris (Reference 21) which are included to provide a frame of reference. The outside aerodynamic noise levels are reported to be representative of a

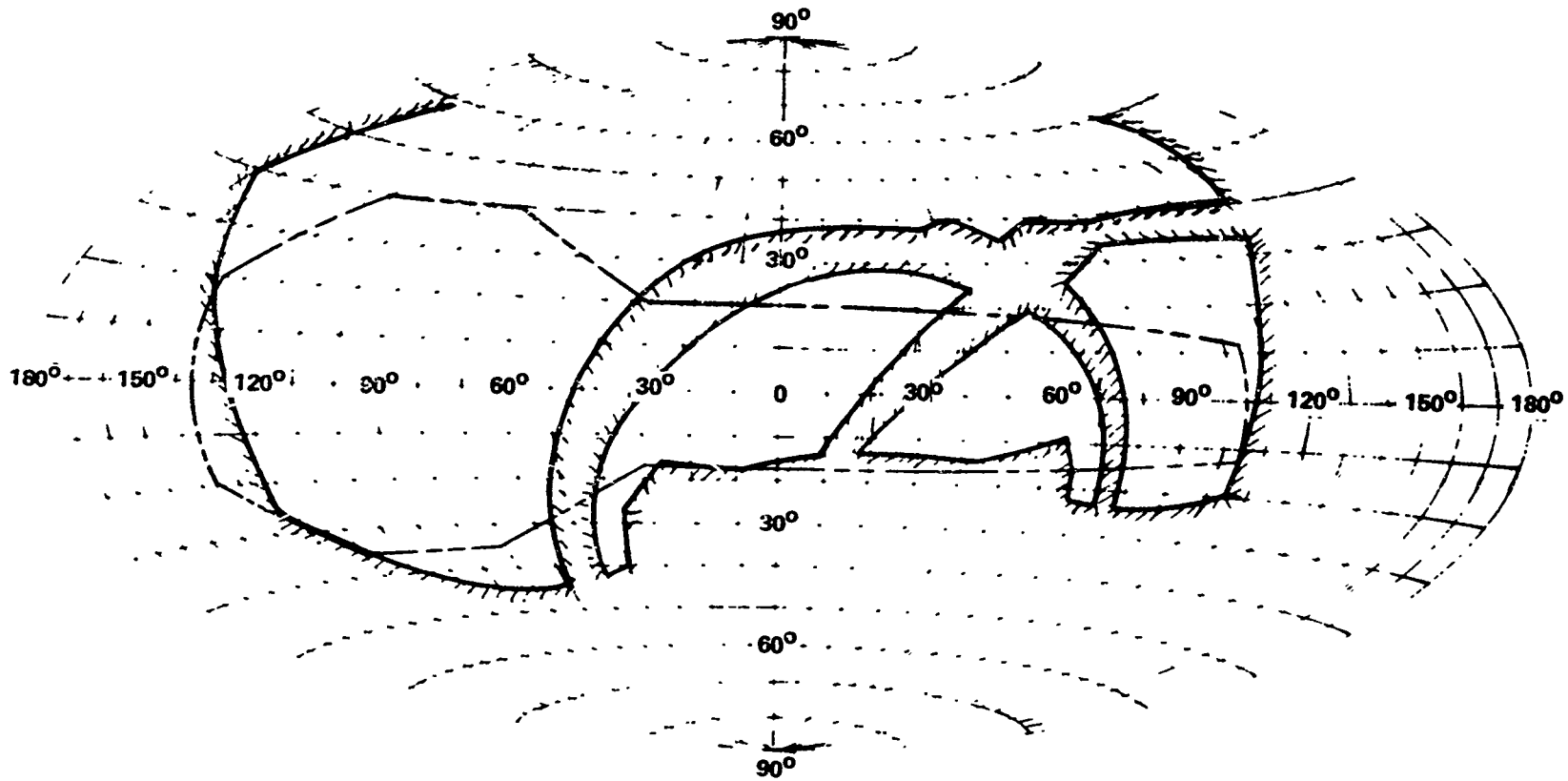

Figure 8.2 Visibility Diagram, General Purpose Canopy, TIFS Simulation Cockpit

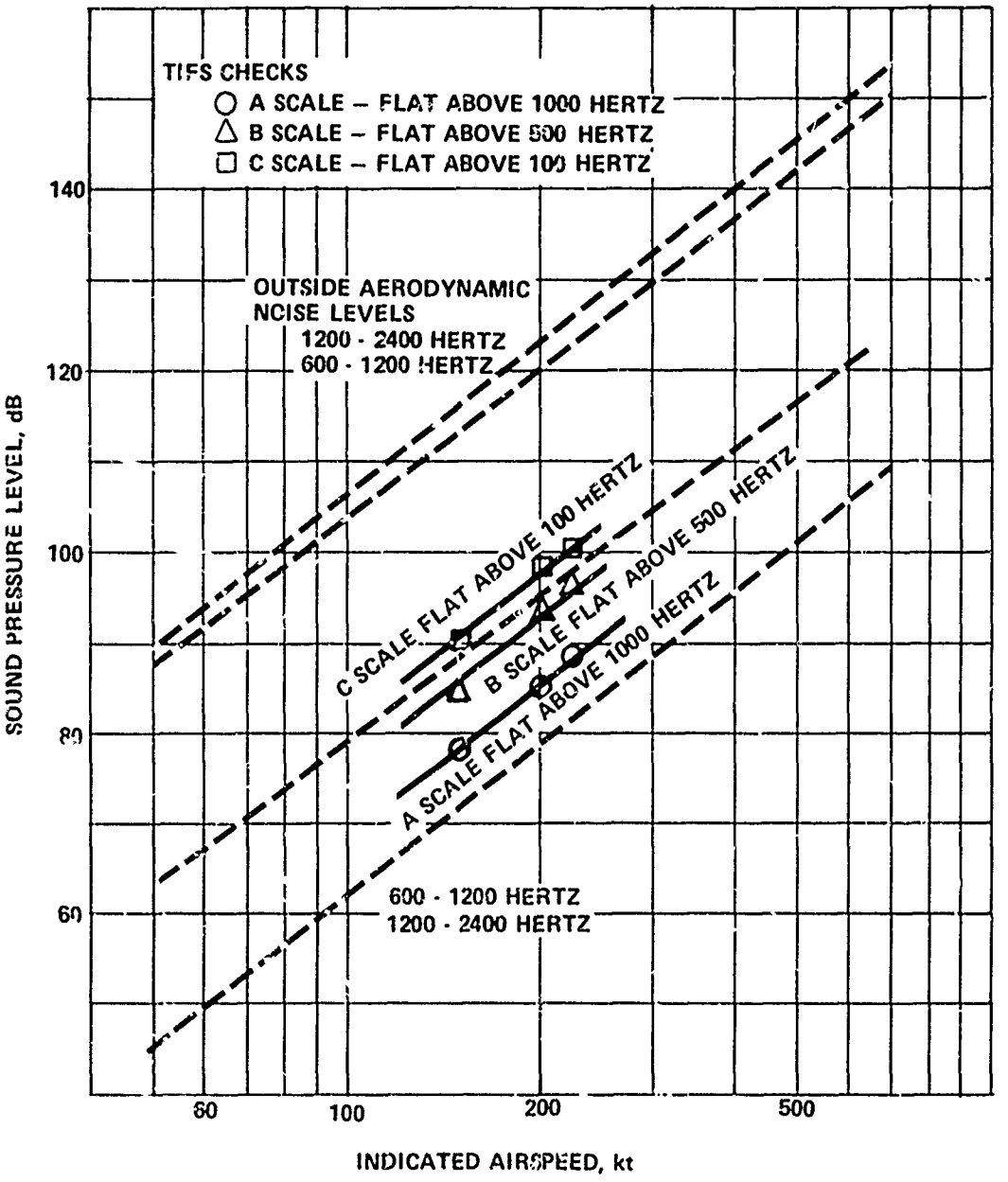

Figure 8.3 Noise Levels

number of different types of engine powered aircraft and a glider and indicate that the predominant source of noise above 600 hertz is the boundary layer. The lower broken lines show the sound levels within the cabin area attenuated by a number three sound proofing structure which weighs about .2 lb per sq ft which is felt to be representative of the maximum practical attenuation for aircraft. The TIFS data plotted with circles, triangles and squares show noise levels above a threshold frequency. The TIFS data above 500 hertz (B scale and A scale) are seen to fall in the range of the well-insulated fuselage. In fact, even the C scale data down to 100 hertz is probably comparable within the accuracy of these data. A further comparison which is perhaps more important in regard to propeller noise is available from other data in the same reference (Reference 21). In reducing the lower threshold frequency from 1000 to 500 and then 100 hertz, the sound pressure level in the fuselage of the British Comet jet transport is shown to increase by 3 dB and then an additional 8 dB; in a civilian propeller transport, these steps were 6 dB and 17 dB. Our preliminary TIFS data, by comparison, show increases of 8 dB and then 5 dB for these same frequency passband increments. Hence, it can be surmised that the noise environment in the TIFS cockpit is not dissimilar from that of the jet and does not include the appreciable rise in noise level in going from 500 Hz down to 100 Hz that is typical of propeller-driven aircraft.

A very important part of the overall TIFS capability is the data handling capability built into the system. As was indicated above, several hundred signals representative of both environmental and system conditions and their rates of change during a flight are available in the VSS for recording. Up to 58 channels of these data can be recorded during a flight test on the onboard digital tape recorder and can subsequently be played back on a ground playback unit or processed on the IBM 370/165 computer in the CAL computing center. In addition a four channel Brush recorder in the VSS allows monitoring those or other channels in flight. Selector switches provide forty possible channels for display. The total system capability has been identified in detail in the User's Manual for Digital Data Analysis (Reference 22).

The objective of the digital recording system is to achieve rapid and economical reduction of the flight data. Considerable effort has been expended in the design of the data analysis system to reduce errors so that the data reduction time would be reduced. Overnight turn-around time is, in most instances, possible. That is, where routine data reduction can be employed, the results can be available for review the morning following a flight test. The 58 channels of digital data recorded during flight on the Ampex tape recorder are compatible with the IBM system. The tape can be recorded at speeds of 50 or 100 samples of each channel per second. The system will record a 10-bit binary number plus a sign bit. The resulting recording system accuracy is approximately 2/10% or better. Each channel is filtered to avoid aliasing errors. The filter cutoff frequency changes automatically with the system record speed so that the best possible recording bandwidth is utilized.

To provide a quick look or rapid review directly after flight test, a complete ground playback system is available. It consists of an Ampex tape transport, a digital to analog converter, an 8-channel Brush recorder, and a switching system which allows any 8 of the 58 channels to be selected and played back on the strip chart in analog form.

When the flight data are processed in the CAL computer center, many analysis programs in the digital data analysis system can be used to do many different kinds of analyses. Examples include least squares programs, harmonic analyses, various plotting programs, all with options that can be made available to present the data in the desired format. These programs have been planned to provide maximum flexibility. In addition, there are available programs to compute the natural frequency and damping ratio of freely oscillating, lightly damped second-order systems or, alternately, of heavily damped modes with the maximum slope method. Throughout these programs, the goal has been to achieve maximum flexibility and adaptability with minimum chance for errors: maximum utilization of machine functions along with minimum human inputs.

SECTION IX

OTHER FACTORS AFFECTING SIMULATION CAPABILITY

As explained in Reference 4, the basic flight limitations for the C-131H apply directly to TIFS over its operating speed range. However, the addition of the new control surfaces and servo actuators does modify the basic aircraft capability by introducing different loadings. Significantly, the dive speed has been reduced to 295 knots and a reduced maneuver envelope has been adopted for simulation flight in order to admit maximum exploitation of the capabilities inherent in the TIFS variable stability system without exceeding the structural limitations of the basic airframe. To this end, as noted in Section VIII a safety trip system has been installed that can monitor loadings or conditions that cause them and disengage the variable stability system prior to its subjecting the basic airframe to harm. For instance, the direct lift flaps and side force surfaces allow operation of TIFS at horizontal and vertical attitudes in steady flight that the original aircraft could not attain. Since the time available for their exploration has been limited, conservative safety trip values or bounds have been adopted. In this section, rather than discuss the theoretical capabilities which are thoroughly covered in the reports on TIFS development (References 1, 2 and 4) the limits of the steady state flight envelopes that have so far been demonstrated in actual flight operation will be defined.

9.1 FLUTTER FLIGHT TESTS

TIFS operation up to a speed of 295 knots has been demonstrated to be flutter free either when operating as a Convair 580 with the variable stability system off and the standard flight controls being actuated by the safety pilots, or when operating on the variable stability system as the TIFS airplane with both the standard aircraft controls and the additional TIFS control surfaces being actuated through the computer controlled electrohydraulic servos but without model-following feedback loops closed. TIFS Memo No. 574 reporting the flutter tests up through 295 knots states " On the basis of the flight flutter tests that were conducted, it is concluded that both the

Convair 580 and the TIFS aircraft configurations are free from any aeroelastic instabilities throughout their range of normal flight velocities."

9.2 PROPELLER BLADE STRESS FLIGHT TESTS

A series of tests was run in which the operation of TIFS was explored at various steady state attitudes as well as with the side force surface and direct lift flaps moving at their maximum rates in an effort to assess whether the TIFS operation subjected the propellers or engines to cyclic loadings or stresses which the Detroit Diesel Allison Division of General Motors might deem excessive for their parts. The results are included in Table 9.1 taken from Reference 5 to give a comprehensive idea of the conditions investigated. The report concludes:

1) The propeller blade stresses and engine loads (prop shaft moment) are satisfactory in this installation for the flight envelope tested.

2) Static ground operation above 1000 horsepower and with wind velocities greater than nine knots will be conducted with aircraft headed into the wind. This does not apply during takeoff or transient taxi conditions.

The range of steady state attitudes explored is shown in Figure 9.1. The solid line is the angle of attack for 1 g level flight of the clean trimmed aircraft with side force surfaces and flaps at zero deflection. It is essentially the same curve as that exhibited by the C-131H or 580. The dashed curves above and below that line identify test conditions with the direct lift flaps deflected in accordance with the schedule identified in Figure 9.2. With these flaps up (negative DLF deflection), the angle of attack is higher than the standard aircraft and conversely with the flaps down (positive flap deflections), the angle of attack is lower. In addition, as indicated on Figure 9.2, the Fowler flaps can be lowered below 220 knots just as on the standard

Table 9-1

A/F TIFS PROPELLER BLADE VIBRATION SURVEY

ETR 71D71 TABLE I
MAXIMUM MANEUVERS FLOWN USING VARIABLE STABILITY CONTROL SURFACES

KIAS AT 10,000 FT	STEADY STATE OPERATION						40° SEC ACTUATION RATE			
	POSITIVE SIDESLIP (1)	NEGATIVE SIDESLIP (1)	POSITIVE SIDESLIP PLUS SFS (degs)	POSITIVE SIDESLIP PLUS SFS (degs)	+ DLF AND G's(2) (TED degs and g's)	- DLF AND G's(2) (TEU degs (and g's)	SFS		DLF	
							TEL degs	TER degs	TED degs	TEU degs
140	10°	10°	12 & 15 TEL 5 & 15 TER	11 & 15 TEL 11 & 15 TER	35 & 0.5 35 & 1.0 35 & 1.5	-30 & 0.5 -30 & 1.0 -30 & 1.5	20	20	35	30
200	6°	6°	6 & 10 TEL 4 & 15 TER	4 & 10 TEL 6 & 15 TER	30 & 0.5 35 & 1.0 30 & 1.8	-23 & 0.5 -23 & 1.0 -23 & 2.0	15	15	35	20
240	3.5°	4°	4 & 8 TEL 3 & 10 TEL	3 & 8 TEL 4 & 10 TER	6 & 0.5 17 & 1.0 6 & 1.5	-13 & 0.5 -13 & 1.0 -13 & 2.0	7.5	7.5	20	15
260	3°	3°	3.5 & 7 TEL 2 & 10 TER	2 & 7 TEL 2.5 & 10 TER	1 & 0.5 7 & 1.0 1 & 1.5	-12 & 0.5 -12 & 1.0 -12 & 2.0	5	5	15	15

(1) – RUDDER ONLY, WITH AILERON FOR WINGS LEVEL
(2) – G's AT A/C C.G.
SFS – SIDE FORCE SURFACES
TEL – TRAIL EDGE LEFT
TER – TRAILING EDGE RIGHT
DLF – DIRECT LIFT FLAPS

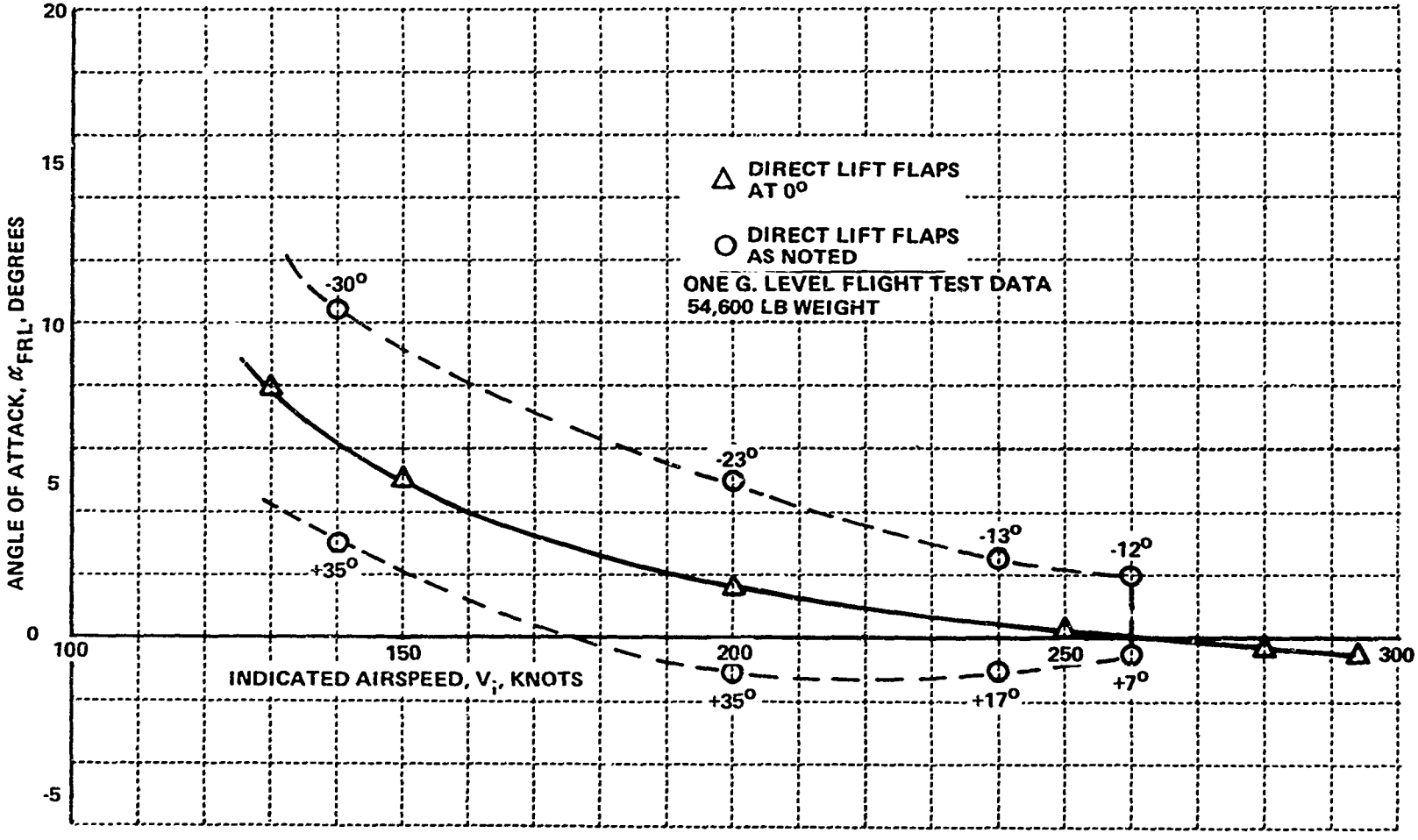

Figure 9.1 TIFS Attitude Envelope

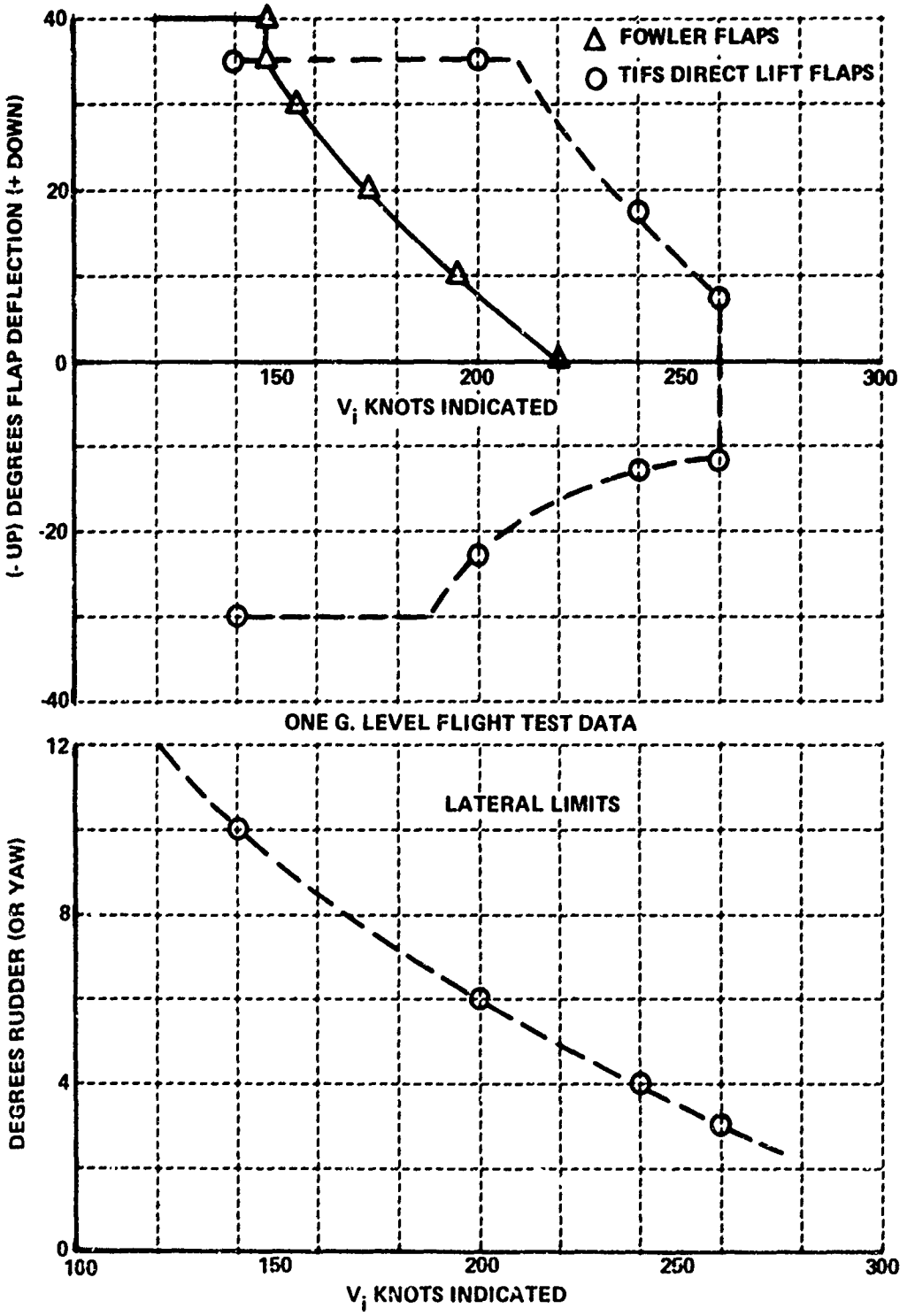

Figure 9.2 TIFS Flap Limits

580 which would make operation at even lower angle of attack available in that speed range. In addition, as noted in Table 9.1, the TIFS aircraft was subjected to g loadings from minus .05 to positive 1.5 or 2 at these various test conditions.

The lower curve on Figure 9.2 shows the lateral limits of operation which have been investigated. These data are practically the same whether right or left and, in addition, are produced by rudder deflections of the same magnitude and direction when the side force surfaces are trimmed at zero. Side force surface deflection is restricted only to the degree that stall should be avoided.

9.3 GROUND VIBRATION TESTS

The ground vibration tests conducted in the spring of 1971 are reported in TIFS Memo No. 569. The significant modes for structural mode simulation and gust simulation work are the lowest frequency modes for symmetrical wing and empennage excitation. These are summarized in Table 9.2. TIFS Memo No. 569 compares the measured modes with the calculated modes used for flutter prediction and the measured modes on the C-131H.

9.4 WEIGHTS AND ENDURANCE

To cover the increased weight of the aircraft, a loads analysis was performed in the spring of 1971 for a 49,000 zero fuel weight aircraft. Wing loads are reported in an addendum to TIFS Memo No. 491 and fuselage loads are reported in an addendum to TIFS Memo No. 423. This work now clears the TIFS for a maximum zero fuel weight of 49,000 lb, a maximum takeoff of 54,600 lb and a maximum landing weight of 50,600 lb. The fuel loading of 5,600 lb implied in these figures allows approximately a two-hour flight with normal reserves.

TABLE 9.2

Lowest Frequency Structural Modes
(Ref. TIFS Memo No. 569)

	Mode Description	Frequency Hertz	Damping Ratio
	Symmetrical		
1.	Wing Bending	3.35	.10
2.	Wing Coupled Bending With Engine Nacelle Motion	4.90	.04
3.	Wing-Fuselage Bending	6.60	.06
	Antisymmetrical		
1.	Wing Bending-Torsion	4.20	.07
2.	Fuselage Torsion and Stabilizer Bending	4.65	.11
3.	Wing-Fuselage Bending and Torsion	4.80	.15

9.5 ELECTRICAL POWER

The electrical system in the TIFS airplane has been designed to adequately supply its operational needs. The primary electrical power sources include a 395 ampere (continuous) 30 volt D.C. generator and two 40 KVA 400 cycle 120/208 volt alternators. The latest loads analysis in TIFS Memo No. 493 defines the present C-131 and VSS power use (page 11 for D.C. and pages 12 and 13 for A.C.) TIFS operations in normal daytime, non-icing conditions requires 290 amps D.C. and 20 KVA of A.C. (~8 KVA from the left alternator and 12 from the right). Consequently, although specific requirements for night landing approaches (landing lights) or use of

de-icing equipment during simulation would use up a significant portion of the indicated spare electrical capacity, for normal daylight simulations in TIFS this unused electrical capability could be made available for operating additional equipment that might be desirable in the conduct of particular programs. Since phase is important for the VSS power used for signals and signal processing and the present equipment is run from the left hand alternator, the growth capability is 32 KVA for that type of system function. For additions for which phase is not critical the total excess capacity or 60 KVA would be available.

In February of 1971, two 200 amp TRU's using 6 KVA each at rated load were installed to provide for A.C. power in the event of failure of the single D.C. generator mounted on the left engine. These two TRU's are run from the right hand engine alternator. Therefore the TIFS aircraft can be operated with complete reliability in night, IFR, and icing conditions (the worst case) and therefore can be ferried to remote base operation points with schedule reliability.

REFERENCES

1. Flight Research Department Staff: Total In-Flight Simulator (TIFS) - Preliminary Design Report. AFFDL-TR-71-119, August 1971.

2. Newell, F.D. : The C-131H TIFS: A Preliminary Study of its Capabilities and Usefulness for Simulation and Handling Qualities. CAL Report No. TB-2376-F-2, March 1970.

3. Fabian, G.J. : Installation, Operation and Maintenance Instructions for the Total In-Flight Simulator (TIFS). CAL Report No. TB-2376-F-3, June 1971.

4. Flight Research Department Staff: Total In-Flight Simulator (TIFS) - Final Report. AFFDL-TR-71-77, August 1971.

5. Faulkner, W. R. : TIFS Propeller Blade Stress Survey. CAL Report No. TB-3020-F-1, September 1971.

6. Etkin, B. : Dynamics of Flight. John Wiley and Sons, Inc., New York, New York, 1965.

7. Connelly, M.E. : Simulation of Aircraft. MIT Servomechanisms Laboratory Report 7591-R-1, 15 February 1958.

8. Wasserman, R. et al. : In-Flight Investigation of an Unaugmented Class III Airplane in the Landing Approach Task, Phase I - Lateral-Directional Study. AFFDL-TR-71-164, Vol. I, January 1972.

9. Wasserman, R. et al. : In-Flight Investigation for an Unaugmented Class III Airplane in the Landing Approach Task, Phase II - Longitudinal Study. AFFDL-TR-71-164, Vol. II, January 1972.

10. Motyka, P.R., Rynaski, E.G., and Reynolds, P.A. : Theory and Flight Verification of the TIFS Model-Following System. AIAA Paper 71-961, August 1971.

11. Motyka, P.R. : Variable Stability Control Concepts for a Fighter In-Flight Simulator. CAL Report No. IB-2895-F-1, December 1970.

12. Chen, R. T. N. : Control Equations for CTIFS Nonlinear Simulation. CAL CTIFS Memo No. 143, 14 February 1969.

13. Miele, A. : Flight Mechanics, Vol. I - Theory of Flight Paths. Addison-Wesley Publishing Co., Inc. Reading Mass., 1962.

14. Ledder, H.J. : AF/TIFS Lift, Drag and Performance Data Obtained From Flight Test. CAL TIFS Memo No. 553, February 1971.

15. Zukaitis, K.E. : Additional Low Speed Wind Tunnel Tests of a .092 Scale Model of the Cornell Aeronautical Laboratory Total In-Flight Simulator (TIFS). General Dynamics/Convair Report No. CVAL 471-A, Vol. I & II, 27 November 1967.

16. Riedler, A.D. et al.: Aerodynamic Data, Flight Criteria, and Unit Load Distributions for Structural Design of the Model 340 Airplane Turboprop Configuration. General Dynamics/Convair Report No. ZU-340-001, 31 August 1951.

17. Newton, G.C., Jr., et al. : Analytical Design of Linear Feedback Controls. John Wiley and Sons, Inc., New York, 1957.

18. Military Specification - Flying Qualities of Piloted Airplanes. MIL-F-8785B(ASG), August 1969.

19. Sir cuse, R.E.: Turbulence Simulation. CAL TIFS Memo No. 567, June 1971.

20. Breuhaus, W.O.: Noise Measurement in TIFS. CAL TIFS Memo No. 610, August 1971.

21. Harris, C.M.: Handbook of Noise Control. McGraw-Hill Book Company, New York, 1957.

22. Dolbin, B.H., Jr. and Trautman, R.W.: Users Manual for Digital Data Analysis. CAL CTIFS Memo No. 135, T-33 TM No. 55, April 1969.